UTILIZING COMMERCIAL SOIL SENSING TECHNOLOGY FOR AGRONOMIC DECISIONS

A Dissertation

Presented to

The Faculty of the Graduate School

at the University of Missouri

In Partial Fulfillment

Of the Requirements for the Degree

Doctor of Philosophy

By

LANCE S. CONWAY

Dr. Newell Kitchen

Dr. Stephen Anderson

Dr. Kenneth Sudduth

Dissertation Supervisors

MAY, 2022

The undersigned, appointed by the dean of the Graduate School, have examined the dissertation entitled

UTILIZING COMMERCIAL SOIL SENSING TECHNOLOGY

FOR AGRONOMIC DECISIONS

Presented by Lance S. Conway,

A candidate for the degree of Doctor of Philosophy, Natural Resources, and hereby certify that, in their opinion, it is worthy of acceptance.

Dr. Newell Kitchen

Dr. Stephen Anderson

Dr. Kenneth Sudduth

Dr. Kristen Veum

Dr. Brent Myers

ACKNOWLEDGEMENTS

I would like to sincerely thank my advisors, Drs. Newell Kitchen, Stephen Anderson, and Kenneth Sudduth for their guidance throughout this research project. Their drive and passion for their work has kept me motivated and made my graduate experience extremely enjoyable. Their profound and diverse experience has been an excellent resource throughout my PhD experience. I also thank my committee members, Drs. Kristen Veum and Brent Myers, for their help and direction throughout my graduate research. I thank Dr. Mac Bean for introducing me to Dr. Kitchen in 2014, which eventually led to an undergraduate, MS, and PhD position with the USDA Cropping Systems and Water Quality Unit. The early experiences gained with the research group led to my interest in precision agriculture. Ultimately, my PhD research direction was a culmination of experiences gained from 2014 to 2018. I appreciate the collaboration with Chin Nee Vong, which allowed for a unique evaluation of precision seeding technology. I appreciate the effort put forth by Kurt Holiman, Scott Drummond, Matt Volkmann, Curtis Ransom, Jeff Svedin, and James Fischer for all of their help to collect, analyze, and interpret data. I thank God for the many blessings I have received to make this possible. I am forever indebted to my parents, Steve and Lori, for their support and for motivating me to attend graduate school. Last but certainly not least, I thank my wife Mary, and our two daughters, Nora Mae and Hannah, for their unending love and support. This research was funded by the USDA-ARS.

TABLE OF CONTENTS

LIST OF TABLES

Chapter 2: Repeatability of Commercially Available Visible and Near Infrared Proximal Soil Sensors

Chapter 3: Improving Soil Organic Matter Estimation with Planter-based Optical Reflectance Sensing Approaches

Chapter 4: Predicting Corn Emergence Rate with Topographic Features and on-the-go Furrow Sensing Technology

LIST OF FIGURES

Chapter 1: Literature Review and Sensor System Overview

Chapter 2: Repeatability of Commercially Available Visible and Near Infrared Proximal Soil Sensors

Chapter 3: Improving Soil Organic Matter Estimation with Planter-based Optical Reflectance Sensing Approaches

Chapter 4: Predicting Corn Emergence Rate with Topographic Features and on-the-go Furrow Sensing Technology

APPENDIX A: Supplemental Material for Chapter 2

DISSERTATION ABSTRACT

Planters with mounted proximal soil sensing systems can densely quantify seed zone soil variability. Technology now allows for real-time sensor information to control multiple row-unit functions on-the-go (e.g., planting depth). These and other developing sensor-based control systems have the potential to greatly improve correctness when planting, and therefore row-crop performance. For sensor-based control to be widely adopted, practitioners must understand the precision and utility of the systems. Therefore, research was conducted to: (i) determine how well commercially available sensors can estimate soil organic matter (OM) and whether sensor output was repeatable among sensing dates; (ii) evaluate OM prediction accuracy across selected soils and soil volumetric water contents with both a commercially-available, planter-mounted sensor, and machine learning techniques applied to multiple combinations of soil reflectance bands within the visible and near infrared spectrum; and (iii) investigate if planter and other proximal soil sensor data, in combination with topographic features, could predict field-scale corn emergence rate at varying planting depths. Results found that commercial sensors could estimate general trends in spatial variability of OM, but that some inconsistencies were associated with a "global" calibration that appeared susceptible to temporal variations in soil water content. In the controlled environment, results for sensor estimation of OM were similar to the field study. Further, results showed that spectral information within the entire range used by the commercial systems evaluated was required to consistently predict OM at varying volumetric water contents. Lastly, the

field-scale agronomic analysis found that inherent soil and landscape variability drove the emergence rate response at the site. However, planter metrics were still useful

DISSERTATION INTRODUCTION

In the past decade, technology has allowed for the incorporation of proximal soil sensor systems onto commercial row-crop equipment. Primarily through optical visible and near-infrared (VNIR) reflectance, these systems can estimate important agronomic soil properties *in situ*, such as soil moisture and organic carbon or matter (OC/OM). Sensing these and other properties on-the-go during grain-crop planting may improve planter performance and seedling emergence uniformity, an outcome that has been shown to optimize yield potential.

Although relatively new to production-scale agricultural equipment, sensing techniques, such as VNIR spectroscopy, have been evaluated for soil physical and chemical property estimation across a range of environments both in laboratory and field settings, and to a lesser extent, through stand alone on-the-go sensing. The recent integration of proximal sensing of the seed furrow and/or rooting zone into commercial row-crop implements allows for spatial quantification of these soil properties. If properly equipped, commercial planters with these sensors also have the capability to control planting depth, insecticide, fertilizer, seeding rate, and seed hybrid or variety on-the-go. However, challenges from environmental factors such as ambient light, soil moisture, texture, and residue can all impact reflectance and subsequently, soil sensor estimations. Further, factors such as dust, soil smearing, and variable distance between the sensor and the soil can all introduce error.

Although promising, little is known about the performance and consistency of these sensors across a range of environmental and management conditions. Therefore, the

first objective of this research project explored the field-scale accuracy, precision, and repeatability of the sensors at estimating soil OM (Chapter 2). Additionally, the second objective was to evaluate the ability of a commercially available sensor system to estimate OM under varying soil water contents in a controlled environment, as well as how to improve OM estimates from visible and near-infrared spectra using advanced analytical techniques (Chapter 3). Lastly, the third objective was to determine the extent these sensor metrics can be used in making agronomic decisions at planting for optimum crop performance (Chapter 4).

CHAPTER 1: LITERATURE REVIEW AND SENSOR SYSTEM OVERVIEW

Introduction

Recent technology has allowed for the integration of soil sensors, utilizing diffuse reflectance spectroscopy in the visible and near-infrared reflectance (VNIR) region, into commercially available equipment. These sensor platforms can prediction important agronomic soil properties *in situ* that are critical for crop production, such as soil water and organic carbon or matter (OC/OM). In some scenarios, the predictions can be in real-time, allowing for the potential to vary crop inputs and/or make on-the-go adjustments to row-crop production equipment (i.e., seeding depth). In order to use VNIR for real-time control or to estimate OC stocks, it is important for practitioners to recognize the capabilities and the limitations of VNIR sensing technology. Extensive laboratory research has illustrated the capabilities of VNIR to estimate soil properties (i.e., soil water and OM) across a range of soils and environments (Brown et al., 2006; Rienzi et al., 2014; Zhou et al., 2020), illustrating strong opportunity for VNIR proximal sensing platforms. However, sensor accuracy has been found to decrease in circumstances where field-moist soils were evaluated, as opposed to dry and ground soil (Minasny et al., 2010; Bricklemeyer and Brown 2010). This has been largely attributed to the complex response of soil reflectance to varying volumetric water contents and interactions with other soil properties that affect spectral features (Lee et al., 2009; Rienzi et al., 2014). Additionally, sensitivity to moisture has been found to vary within the VNIR region, with greater sensitivity found in longer wavelengths (>1400 nm; Lobell and Asner, 2002).

Sensing these and other properties on-the-go during grain-crop planting may improve planter performance and seedling emergence uniformity, an outcome that has

been shown to help optimize yield (Carter et al., 1992; Nafziger et al, 2009). The recent integration of proximal sensing of the row-crop seed zone and/or the seed furrow into commercial row-crop planters allows for spatial quantification of agronomically important soil properties. Commercial planters equipped with these sensors also have the capability to control planting depth, insecticide, fertilizer, seeding rate, and seed hybrid or variety on the go. Although promising, little is known about the performance and consistency of these sensors across a range of environmental and management conditions.

Visible and Near-infrared Reflectance Spectroscopy

In order to collect soil spectra, emission from a subset or continuum of frequencies (e.g., 400 to 2500 nm) are directed towards a soil sample. Depending on the soil components, radiation will cause molecular bonds to bend or stretch (vibrate). These molecules will absorb light at different levels, allowing for a characteristic spectrum to be used for analytical purposes (Stenberg et al., 2010; Miller, 2010). The wavelength where absorption occurs depends on the chemical matrix and environmental factors, such as neighboring functional groups, which allows for the detection of molecules that contain similar types of bonds (Stenberg et al., 2010). When near infrared radiation interactions with soil, the overtones and combinations of fundamental vibrations in the mid-infrared region are detected. The present study focused on primarily on the estimation soil OC/OM, as well as the influence of soil water content and texture on prediction accuracy.

Organic Carbon

A large number of studies have evaluated using VNIR for soil OC estimation. The ability to estimate OC is possible because the fundamental vibrations of organic molecules occur in the mid-IR and their overtones occur in the Vis-NIR region. These

occurrences are due to stretching and bending of N-H, C-H, and C-O bonds. In the visible spectrum, wavelengths near 410, 520, 540, 550, and 570 nm have all been found useful when predicting OC (Daniel et al., 2004; Brown et al., 2006; Viscarra-Rossel et al., 2006). In the NIR region, wavelengths near 960, 1100, and 1400 nm have been identified as sensitive to different levels of OC (Palacio-Orueta and Ustin, 1998; Daniel et al., 2004). Additional wavelengths (>1400 nm) have also been found useful, although out of the range used by commercially available sensors. Some examples are 1600 and 2200 nm, which have been found significant for OC prediction by several researchers (Cho et al., 2018, Zhou et al., 2022, Rienzi et al., 2014), and have been attributed to aliphatic compounds. Studies utilizing continuous spectra that includes longer wavelengths (1500-2500 nm) have illustrated strong OC predictive capability, with RMSE below 3.1 g kg^{-1} (Dunn et al., 2002; Sepherd and Walsh, 2002). However, these results were achieved with air-dried soils. In comparison, accuracies have been found to degrade when field-moist soils were evaluated (Minasny et al., 2010; Bricklemeyer and Brown, 2010). This has been largely attributed to the complex response of soil reflectance to varying soil water contents and interactions with other soil properties that affect spectral features (Lee et al., 2009; Rienzi et al., 2014). Additionally, sensitivity to moisture has been found to vary within the VNIR region, with greater sensitivity found at longer wavelengths (>1400 nm; Lobell and Asner, 2002).

Soil texture has also been found to influence OC prediction accuracy. In general, RMSE of OC predictions decreases with increasing clay content (Stenberg et al., 2002). This has been attributed to the scattering of light by coarser-textured soils, resulting in an overestimation of OC. Another hypothesis for this trend is that OM is the stronger

absorbent in the soil matrix, and therefore dominates the spectra (Clark, 1999). Collectively, research has illustrated that soil texture can influence OC prediction.

Specific wavelength assignments are difficult, however, as other organic and inorganic molecules may also influence absorption in useful regions. Although results have been poor when using the visible region alone, performance has improved when including the visible region and NIR for calibration (Fystro, 2002). However, this method can still be influenced by other soil properties such as texture, moisture, and mineralogy (Hummel et al., 2001).

Accuracies are generally found to decrease when calibrations are conducted across a wide geographic range or when few wavelength bands are used (Ladoni et al., 2009). Reduction in accuracy often occurs because reflectance values are influenced by moisture, texture, mineralogy, parent material, and SOM (Hummel et al., 2001).

Soil Water Content

The ability for VNIR to detect soil moisture occurs because of strong water absorption in the NIR region due to O-H stretching and bending (Hunt, 1977). However, because porosity and the refractive index of soils vary, a standard relationship between reflectance and soil water content (volumetric or gravimetric) cannot be established (Whalley et al., 1991). Water exposed on surfaces as well as free water filling pore spaces generally decreases reflection. Wavelength assignments for these relationships are typically at or near 1400 or 1900 nm (Viscarra Rossel et al., 2005). Between these wavelengths, 1900 nm has been found to be the best at quantifying soil water content (Baumgardner et al., 1985) because 1400 nm coincides with hydroxyl ions. Weaker absorption occurs near 970, 1200, and 1780 nm (Baumgardner et al., 1985). Research has

shown that the use of only 1 or 2 wavebands has resulted in reduced accuracy of soil moisture predictions when compared to 4 or more wavebands (Hummel et al., 2001; Bullock et al., 2004).

Although the influence of soil water content in soil spectra is clear, published RMSE values are surprisingly high when compared to properties such as OC (Hummel et al., 2001; Christy, 2008). In relative terms, the RMSE are only as good as OC, which has a more subtle impact on spectral reflectance when compared to soil water content. In some cases, the erosion of accuracy may be caused by on-the-go measurements (Mouazen et al., 2006). For example, Hummel et al., (2001) found under-estimation occurred on the wettest soils due to the potential presence of a layer of water on the sample, possibly causing specular reflectance.

Spectral Pre-Processing

Several spectral smoothing techniques have been employed to reduce signal noise. These can include averaging, moving averages, or Savitsky-Golay transformations (Savitzky and Golay, 1964). Subsequent pre-treatment and processing techniques have also been explored to improve predictive capability across a wide range of soils or soil water contents. These transformations have included standard normal variate, first or second derivative, detrending, and/or mean centering (Minasny et al., 2011; Cho et al., 2017; Zhou et al., 2022). Because derivates generally increase noise, they are often used in conjunction with one of the aforementioned smoothing approaches.

The best pre-treatment or combination of pre-treatment techniques is soil or dataset-specific. However, the first and second derivatives are most widely used. They allow for a baseline correction and can enhance subtle signals (Stenberg et al., 2010). Not

surprisingly, this technique has been found effective on soils with varying water contents, and is helpful due to the significant and non-linear effect of soil water on reflectance (Lobell and Asner, 2002). Research has shown this technique effective, with similar prediction accuracies among varying soil water contents (Rienzi et al., 2014)

Machine Learning

In many analyses, VNIR-based OM predictions have been derived from statistical methods such as principal component regression (PCR) or partial least squares regression (PLSR) techniques (Sudduth and Hummel, 1993; Brown et al., 2006). However, recent advancements in statistical and machine learning have allowed for new approaches, such as decision trees, support vector machine regression (SVMR), and artificial neural networks. Several researchers have found similar or improved performance from the advanced techniques compared to traditional methodology on dry, ground soil (Viscarra Rossel and Behrens, 2010; Mouazen et al., 2010). Results reported by Morellos et al. (2016) on field-moist soils determined that Cubist and SVMR approaches outperformed PCR and PLSR modelling in one field in Premslin, Germany. Although these past studies are encouraging, more research is needed to understand how these modeling techniques could be applied to on-the-go sensors across varying soils and soil water contents.

Proximal Sensing

In the past decade, technology has allowed for the incorporation of proximal soil sensor systems onto commercial row-crop equipment. These systems can estimate, through optical visible and near-infrared reflectance (VNIR) sensing, important agronomic soil properties *in situ*, such as soil moisture and organic carbon or matter (OC/OM). Although relatively new to production-scale agricultural equipment, VNIR

spectroscopy for soil physical and chemical property estimation has been evaluated across a range of environments through stand alone on-the-go sensing (Nawar and Mouazen, 2019; Christy, 2008). Using VNIR can be practical due to the cost of instrumentation when compared to laboratory analyses, ability to integrate into necessary field operations, and potential to estimate multiple soil properties from a single sensing operation. However, challenges from environmental factors such as ambient light, soil moisture, texture, and residue can all impact reflectance and result in low-quality *in situ* soil sensor data (Stenberg et al., 2010). Further, factors such as dust, soil smearing, and variable distance between the sensor and the soil can introduce measurement error (Sudduth and Hummel, 1993). These factors require careful sensor system design and engineering for reproducible data.

In the late 1980s, several prototype VNIR on-the-go and in-situ spectrometers were developed (Shonk et al., 1991; Sudduth and Hummel, 1993). Evaluation of more recently developed systems has demonstrated the accuracy of OC estimations using on-the-go sensing (Christy, 2008; Bricklemyer and Brown, 2010; Nawar and Mouazen, 2019). Most of these studies used full-spectrum sensing, spectral pre-processing techniques, and calibration procedures to develop spatial OC estimates. One example was research conducted by Nawar and Mouazen (2019) which aimed to compare real-time and to laboratory sensing of OC. Their study also evaluated several calibration methods that ranged from regional to field specific. The results showed that, in two of the three calibration techniques, real-time sensing predictions of OC were comparable to laboratory results. Additionally, including regional data in the calibration method resulted in an improved OC estimation (coefficient of determination (R^2) = 0.74) when compared

to the single field technique (R^2 = 0.65). These results suggest that accuracies from real-time sensing can be comparable to analyses performed in a laboratory setting. Additionally, they suggest that including regional information prior to sensing could improve real-time estimations of OC.

A similar study was performed in central Kansas, USA across 8 fields within two counties, covering nearly 300 ha (Christy, 2008). This study utilized a shank-mounted spectrometer with a sensing range from 920 to 1718 nm attached to a tractor-mounted toolbar. Several cross-validation schemes were evaluated, and predictions of gravimetric water content and OM varied with each method. Performance was poorest when an entire field ("one-field-out") was excluded from the training dataset. This method resulted in cross-validation R^2 values of 0.40 and 0.67 for soil moisture and OM, respectively. The highest accuracies were observed when the "leave-one-out" method was used, where a single sample was omitted at each training iteration. This method used the entire dataset for training and validation, where one sample was removed for prediction at each iteration. The cross-validation R^2 values were 0.67 and 0.80 for soil moisture and OM, respectively. The "one-field-out" results would be most representative of real-time sensor estimation with no field-specific calibration. Therefore, this research illustrates the limitations of real-time sensors that have the capability to guide on-the-go control of planter functions.

Sensor and Control Systems

Active Hydraulic Downforce

During planting operations, the row-unit depth-gauge wheels roll on the soil surface to establish planting depth, and subsequently apply a load to the soil surface

(Hanna et al., 2010). This impact is the remaining load after the downforce systems have applied enough force to engage the disk openers to the target planting depth, and is referred to as gauge wheel load (GWL). In general, downforce systems aim to apply downforce that allows enough GWL for disk openers to penetrate the soil to the desired planting depth, while not causing excessive compaction to the seed zone. The latest active downforce systems sense GWL and subsequently transfer the correct amount of force from the planter toolbar to the row-unit in order to maintain a certain GWL (e.g., 445 N). Assuming there is enough weight on the toolbar, this value remains relatively static with only the amount of force varying within the field.

Commercially available active hydraulic downforce systems originally became available in 2016. Since then, research has evaluated the ability of these and static systems to be a surrogate for estimation soil properties (Brune et al., 2018), as well as the impact of downforce on row-crop emergence and yield (Badua et al., 2021; Drewry et al., 2021; Poncet et al., 2019). Results from Brune et al. (2018) found that planter row-unit downforce was correlated to soil physical properties, such as shear strength, penetration resistance, and bulk density. However, correlations were not strong between downforce and OM or clay content. Therefore, other sensor systems (i.e., VNIR spectroscopy) are likely better alternatives for estimating these soil properties.

Relationships between downforce and corn emergence have been mixed. In some cases, no response of corn emergence to downforce was observed (Poncet et al., 2019). Conversely, other studies have found differences among varying GWL. Specifically, results from Hanna et al. (2010) found that the rate of corn emergence was greater in wet conditions and low GWL. These results suggest that the optimum GWL is likely to vary

with soil moisture levels. However, current systems only target a single GWL, and simply vary the amount of applied force throughout a field. Therefore, potential exists to implement other sensor metrics (i.e., soil moisture) to determine a soil-specific target GWL.

Implement-Mounted Sensors

Since 2018, two commercially available implement-mounted optical sensing systems have been released. These included the Veris iScan (Veris Technologies, Salina, KS, USA) and Precision Planting SmartFirmer (Precision Planting, Tremont, IL, USA). The iScan is designed to mount on common toolbars, such as a row-crop planter or equipment. It includes soil-engaging sensors that measured apparent soil electrical conductivity (EC_a; 0-61 cm), volumetric soil water content (through capacitance), temperature, and reflectance at two wavelength bands centered at 660 (20 nm width) and 940 nm (30 nm width). The moisture and optical sensing components of the iScan are positioned to press against the bottom of the slot created by the runner (Lund and Maxton, 2019). Prior to sensing, the soil ECa, optical and capacitance sensors are calibrated following procedures provided by Veris Technologies. The data are logged at 1 Hz to Veris Technologies Soil Viewer real-time mapping software.

The SmartFimers are designed to mount to a planter row-unit behind the seed tube, replacing traditional seed firming devices. They can be instrumented on all or a subset of row units. Data collected with the SmartFirmer is recorded at 1 Hz with a Precision Planting second or third generation 20|20 monitor. Data layers from the SmartFirmer consist of Furrow Moisture (%), Temperature (°C), OM (%), Cleanness (%), and Uniformity (%). These metrics, aside from Temperature, are derived from the

optical portion of the sensor that measures reflectance from five wavelength bands in the VNIR region (peak wavebands: 468, 592, 858, 1198, and 1468 nm). The waveband widths vary from 20 nm at shorter wavelengths (i.e, 468 nm) to 50 nm at longer wavelengths (i.e., 1468 nm).

Early Corn Stand and Emergence Uniformity

Factors Affecting Emergence

Research has found that corn seedling emergence is highly dependent upon seed-to-soil contact, soil moisture, aeration, and soil temperature (Alessi and Power, 1971; Gupta et al., 1988, Elmore et al., 2014). Additionally, studies have found optimum corn germination to occur at soil temperatures greater than 20 C, at field capacity, and with good seed-to-soil contact (Schneider and Gupta, 1985). Generally, operators of row-crop seeding equipment target a planting depth, downforce, row-closing, and residue management strategy that optimizes these parameters. Across landscapes, however, spatial variability in seed zone soil properties often exist due to variations in soil texture, crop residues, and landscape position.

Seeding Depth

Agronomic research has evaluated the impact of seeding depth on corn emergence, emergence rate, and yield across landscapes. Studies have aimed to determine whether the optimum planting depth should vary with soil type. Results from these studies are mixed, but have collectively illustrated that the optimal corn planting depth can vary from 2.5 to 7.6 cm based upon soil texture, moisture, temperature, and other factors (Stewart et al., 2021; Coronel et al., 2018; Thomison et al., 2013; Cox and Cherney, 2015; Thomason et al., 2008). In general, however, research agrees that

planting at depths less than 3.8 cm can negatively affect corn emergence due to poor seed-to-soil contact and susceptibility of the seed to moisture and temperature flux. Additionally, poor nodal root development at shallow planting depths can result in yield loss and lodging susceptibility (Elmore and Abendroth, 2007). Further research is needed to determine whether within-field soil moisture or estimations of seed-to-soil contact can give insight to growers to determine the optimum seeding depth for uniform emergence.

In an effort to improve seeding management across variable landscapes, precision agriculture research has explored varying seeding depths within a given field based upon changes in soil moisture (René-Laforest et al., 2015). Soil moisture estimated through a capacitance sensor was used as the guiding parameter because of the influence of soil moisture on germination, as well as the access to on-the-go soil moisture sensors. This recent study illustrated that varying planting depth within a field has potential to improve corn root development and yield. The improvement was attributed to planting shallower in relatively wet conditions, and deeper in relatively dry conditions. Further research is needed to apply these results to more local environments in the U.S. Midwest. In addition to sensor technologies, topographic features can give insight into soil water availability, movement, and accumulation across landscapes (Pachepsky et al., 2001). High-resolution elevation is now available through digital elevation models, as well as from machine data collected during field operations.

Overview of Precision Planting Sensor Systems

Background

In 2018, Precision Planting released a seed firmer (similar to a Keeton seed firmer) with an integrated optical and thermopile sensor located on the side of the firmer

(Fig. 1; Koch et al., 2018). The electro-optical portion of the sensor suite consists of emitters and detectors that collect reflectance from five different wavebands of light ranging from the visible spectrum (467 and 592 nm) to the NIR region (850, 1200, and 1465 nm). This technology is commonly referred to as VNIR reflectance, and can be used to estimate soil physical and chemical properties.

In 2018, the optical portion of the sensor produced output data layers consisting of furrow moisture (%), organic matter (OM; %), cleanness (%), and uniformity (%). All metrics, except for organic matter, were collected on a row-by-row basis at 5 Hz with no inter-row interpolation. Exported data, however, were averaged across SmartFirmers on the planter at a frequency of 1 Hz for data collected with a 2nd generation 20|20 Seedsense monitor (.DAT file format). Organic matter estimations were interpolated across SmartFirmers, resulting in some smoothing of the data across the planter row units (Koch et al., 2018). Like the other metrics, a single value for OM was recorded at 1 Hz. In 2019, Precision Planting added cation exchange capacity (CEC; meq/100 g) to the SmartFirmer's suite of measurements. Additionally, data collected with 3rd Generation 20|20 monitors can be exported on a row-by-row basis (.2020 file format). Like the previous monitor, data are recorded at 1 Hz.

Precision Planting SmartFirmer

The SmartFirmer system utilizes several metrics to help guide planter row-unit management, either in real-time or manually by the operator. The following describes each metric, as well as the description of each by the manufacturer (Precision Planting, 2019).

Furrow Moisture

The percent of water weight that a corn seed is projected to absorb in a 3 day time period. It is recommended to keep this value above 30% for adequate moisture conditions

- Can be used to control planting depth real-time with SmartDepth system.

Organic Matter

The portion of the soil that consists of plant material in various stages of decomposition. SmartFirmer measurement of OM includes all of this except for visible crop residue.

- Can be used to control population, hybrid/variety, fertilizer rates, and insecticide rates.

Cation Exchange Capacity

The soil's capacity to hold and exchange cations. This represents the ability for soil to hold onto fertilizers and liming agents, the higher the number indicates a higher holding capacity"].

Clean Furrow

A measure of the crop residue in the furrow. (Precision Planting, 2019). Acceptable = 90%; Goal=95%. Used to guide residue management decisions (row cleaners, tillage, etc.).

Uniform Furrow

Any variation in the furrow (light, cloddiness, moisture changes). Can indicate row unit mechanical problems, tillage patterns, opportunity to adjust row cleaners, windrowed residue, etc.; Goal = above 95%.

Furrow Temperature

Real time temperature at seeding depth; Goal = above 50 F. This metric is estimated with a thermopile sensor for temperature measurements.

Precision Planting DeltaForce

Planter opening discs require a certain amount of force to create a seed trench down to the desired planting depth (Hanna, 2016; Fig. 2). This can vary from 222 to over 1779 N depending on soil conditions, speed, moisture, tillage practice, opening disc wear, etc (Sharda et al., 2016). The force to create the trench comes from the deadweight mass of the row unit (890-1556 N), plus the additional force transferred from the frame to the parallel arms through spring, pneumatic, or hydraulic mechanisms. If additional force is leftover after the seed trench has been created, the leftover force gets transferred to the gauge wheel. This is referred to as gauge wheel load (GWL).

In 2013 Precision Planting released DeltaForce, an automated hydraulic row-unit downforce system (Sauder et al., 2013). DeltaForce senses GWL and adjusts downforce on each row to maintain a target GWL (e.g., 444 N). The system was an improvement on the previous pneumatic systems because adjustments were made at each row rather than across the planter toolbar. Additionally, the hydraulic reaction time (1-2 sec) was much quicker than the slower (10-15) sec response of pneumatic systems. The hydraulic system also allowed for lifting of the row unit under wet or soft conditions.

The two main components of the system are the instrumented load sensing pin for sensing GWL, and the hydraulic cylinder for applying lift or downforce (Fig. 3). The load pin measures GWL at 200 Hz, resulting in two metrics displayed to the operator: Downforce (lb_f) and Margin (lb_f). The load pin sensor contains a strain gauge and is located where gauge wheel depth adjusting arm pivots. The pin has two inner and two outer lobes. Force is transferred from the gauge wheel arm to the depth adjustment (inner lobes), while the weight of the shank is pushing down and is carried on to the two outer

lobes. This applies a bending stress to the pin, and allows the strain gauge to estimate total weight carried by the gauge wheels. It is important to note that downforce data contains a low signal to noise ratio and that large amounts of smoothing are required for practical interpretation (Hanna et al., 2010; Badua et al., 2018).

Load pin readings are used for calculating the amount of additional lift or downforce required to maintain a target GWL. The force adjustments at each cylinder are controlled by an electronic solenoid. The system can go from maximum lift force (2000 N) to maximum applied force (2670 N) in 2 seconds. Currently, applied downforce is displayed and mapped on the 20|20 monitor, but does not exist in the exported data.

Downforce Related Metrics

Downforce: Gauge wheel load (N) measured from load pin. Measured at 200 Hz and recorded at 1 Hz.

Margin: The minimum downforce value recorded from the load pin in a 3 sec period. Normal condition target = 444 (N)

Ground Contact: The percentage of time that there is some weight (> 1 lb_f) carried on the gauge wheel (measured with load pin). Target is 100%.

Applied Downforce: The amount force applied to the row unit by the cylinder. Calculated from the command pressure sent to each hydraulic cylinder.

Good Ride: Measures vertical movement of the row unit from an accelerometer within each row unit's module. It is defined as the percent of time that the row unit ride is sufficient enough to not interfere with seed spacing

Bibliography

Alessi, J. and Power, J.F., 1971. Corn emergence in relation to soil temperature and seeding depth. Agron. J. 63: 717-719.

Badua, S. A., Sharda, A., Strasser, R., & Ciampitti, I. 2021. Ground speed and planter downforce influence on corn seed spacing and depth. Precision Agriculture 22: 1154-1170.

Baumgardner, M. F., Silva, L. F., Biehl, L. L., and Stoner, E. R. 1985. Reflectance properties of soils. Advances in Agrony. 38: 2–44.

Brown, D.J., K.D. Shepherd, M.G. Walsh, M.D. Mays, and T.G. Reinsch. 2006. Global soil characterization with VNIR diffuse reflectance spectroscopy. Geoderma 132: 273-290.

Bricklemyer, R. S., and D.J. Brown. 2010. On-the-go VisNIR: Potential and limitations for mapping soil clay and organic carbon. Computers and Electronics in Agriculture, 701: 209-216. https://doi.org/10.1016/j.compag.2009.10.006

Brune, P.F., B.J. Ryan, F. Technow, and D.B. Myers, 2018. Relating planter downforce and soil strength. Soil and Tillage Research, 184, pp.243-252.

Bullock, P. R., X. Li, L. and Leonardi. 2004. Near-infrared spectroscopy for soil water determination in small soil volumes. Can. J. Soil. Sci. 84:333–338.

Cho, Y., Sheridan, A.H., Sudduth, K.A. and Veum, K.S., 2017. Comparison of field and laboratory VNIR spectroscopy for profile soil property estimation. Trans. of the ASABE. 60:1503-1510. https://doi.org/10.13031/trans.12299

Christy, C. D. 2008. Real-time measurement of soil attributes using on-the-go near infrared reflectance spectroscopy. Comp and Elec in Agric. 61:10-19. https://doi.org/10.1016/j.compag.2007.02.010

Clark, R. N. 1999. Spectroscopy of rocks and minerals and principles of spectroscopy. In ‘‘Remote Sensing for the Earth Sciences’’ (A. N. Rencz, Ed.), pp. 3–58. John Wiley & Sons, Chichester, UK.

Coronel, E. G., C.A. Alesso, G.A. Bollero, K.L. Armstrong, and N.F. Martin. 2020. Field-specific yield response to variable seeding depth of corn in the Midwest. Agrosystems, Geosciences & Environment, 3:e20034. https://doi.org/10.1002/agg2.20034

Cox, W. J., and J.H. Cherney. 2015. Field-scale studies show site-specific corn population and yield responses to seeding depths. Agronomy J. 107: 2475–2481. https://doi.org/10.2134/agronj15.0308

Daniel, K. W., N.K. Tripathi, and K. Honda. 2003. Artificial neural network analysis of laboratory and in situ spectra for the estimation of macronutrients in soils of Lop Buri (Thailand). Aust. J. Soil Res. 41, 47–59

Dunn, B. W., H.G. Beecher, G.D. Batten, and S. Ciavarella. 2002. The potential of near-infrared reflectance spectroscopy for soil analysis—A case study from the Riverine Plain of south- eastern Australia. Aust. J. Exp. Agric. 42, 607–614.Drewry et al., 2021

Elmore, R. W. and L. J. Abendroth. 2007. Allelopathy: a cause for yield penalties in corn following corn? Integrated crop management newsletter. Iowa State University. 25 Oct 2010.

Fystro, G., 2002. The prediction of C and N content and their potential mineralisation in heterogeneous soil samples using Vis–NIR spectroscopy and comparative methods. Plant and soil. 246: 139-149.

Gupta, S.C., E.C. Schneider, and W.B. Swan. 1988. Planting depth and tillage interactions on corn emergence. Soil Sci. Soc. Am. J. 52:1120–1127.

Hanna, H. M., B.L. Steward, and L. Aldinger. 2010. Soil loading effects of planter depth-gauge wheels on early corn growth. Applied Engineering in Agriculture. 26: 551–556

Hanna, H. M. 2016. Making sure planter technology accomplishes the basics.

Hummel, J. W., K.A. Sudduth, and S.E. Hollinger. 2001. Soil moisture and organic matter prediction of surface and subsurface soils using an NIR soil sensor. Comput. Electron. Agric. 32: 149–165.

Hunt, G. R. 1977. Spectral signatures of particulate minerals in visible and near-infrared. Trans. Am. Geophys. Union 58: 553

Koch, D., M. Strnad, M. Morgan, and B. McMahon. 2018. Systems, Methods, and Apparatus for Soil and Seed Monitoring. US 20180168094A1

Ladoni, M., H.A. Bahrami, S.K. Alavipanah, and A.A. Norouzi. 2010. Estimating soil organic carbon from soil reflectance: a review. Precision Agriculture, 11:82-99.

Lee, K.S., D.H. Lee, K.A. Sudduth, S.O. Chung, N.R. Kitchen, S.T. and Drummond. 2009. Wavelength identification and diffuse reflectance estimation for surface and profile soil properties. Trans. of the ASABE. 52:683-695.

Lobell, D.B., and G.P. Asner. 2002. Moisture effects on soil reflectance. Soil Sci. Soc. of Amer. J. 66: 722-727.

Lund, E., and C. Maxton. Comparing organic matter estimations using two farm implement mounted proximal sensing technologies. In: Proceedings of the 5th Global Workshop on Proximal Soil Sensing, May 28-31, 2019, Columbia, Missouri. p 35-40.

Miller, C. E. 2001. Chemical principles of near-infrared technology. In ‘‘Near-Infrared Technology in the Agricultural and Food Industries’’ (P. Williams and K. Norris, Eds.), pp. 19–37. The American Association of Cereal Chemists Inc., St. Paul, MN

Minasny, B., A.B. McBratney, V. Bellon-Maurel, J.M. Roger, A. Gobrecht, L. Ferrand, and S. Joalland. 2011. Removing the effect of soil moisture from NIR diffuse reflectance spectra for the prediction of soil organic carbon. Geoderma. 167:118–124. doi:10.1016/j.geoderma.2011.09.008

Mouazen, A.M., B. Kuang, J. De Baerdemaeker, and H. Ramon. 2010. Comparison among principal component, partial least squares and back propagation neural network analyses for accuracy of measurement of selected soil properties with visible and near infrared spectroscopy. Geoderma, 158:23-31. https://doi.org/10.1016/j.geoderma.2010.03.001

Morellos, A., X.E. Pantazi, D. Moshou, T. Alexandridis, R. Whetton, G. Tziotzios, J. Wiebensohn, R. Bill, and A.M. Mouazen. "Machine learning based prediction of soil total nitrogen, organic carbon and moisture content by using VIS-NIR spectroscopy." Biosystems Engineering 152: 104-116.

Nawar, S., and A.M. Mouazen. 2019. On-line vis-NIR spectroscopy prediction of soil organic carbon using machine learning. Soil and Tillage Research. 190:120-127. https://doi.org/10.1016/j.still.2019.03.006

Nafziger, E. D., P.R. Carter, and E.E. Graham. 1991. Response of corn to uneven emergence. Crop Science, 31, 811–815. https://doi.org/10. 2135/cropsci1991.0011183X003100030053x

Pachepsky, Y. A., D.J. Timlin, and W.J. Rawls. 2001. Soil water retention as related to topographic variables. Soil Science Society of America Journal, 65: 1787–1795. https://doi.org/10.2136/sssaj2001. 1787

Palacios-Orueta, A., and S.L. Ustin. 1998. Remote sensing of soil properties in the Santa Monica Mountains I. Spectral analysis. Remote sensing of Environment, 65: 170-183.

Poncet, A. M., J.P. Fulton, T.P. McDonald, T. Knappenberger, and J.N. Shaw. 2019. Corn emergence and yield response to row-unit depth and downforce for varying field conditions. Applied engineering in Agriculture. 35:399–408.

René-Laforest, F. F. 2015. Real-time variable control technologies for precision agriculture. (Master’s thesis, McGill University, Montreal, QC, Canada). Retrieved from https://escholarship.mcgill.ca/concern/ theses/fx719q20j

Rienzi, E. A., B. Mijatovic, T.G. Mueller, C.J. Matocha, F.J. Sikora, and A. Castrignanò. 2014. Prediction of soil organic carbon under varying moisture levels using reflectance spectroscopy. Soil Science Society of America Journal. 78: 958-967.

Savitzky, A., and M. Golay. 1964. Smoothing and differentiation of data by simplified least squares procedures. Anal. Chem. 36, 1627–1639.

Sharda, A., Badua, S., Flippo, D., Griffin, T.W. and Ciampitti, I., 2016. Real-time gauge wheel load variability on planter with downforce control during field operation. In Proceedings of the 13th International Conference on Precision Agriculture.

Shepherd, K. D., and M.G. Walsh. 2002. Development of reflectance spectral libraries for characterization of soil properties. Soil Sci. Soc. Am. J. 66: 988–998.

Stenberg, B. 2010. Effects of soil sample pretreatments and standardised rewetting as interacted with sand classes on Vis-NIR predictions of clay and soil organic carbon. Geoderma. doi:10.1016/j.geoderma.2010.04.008

Stenberg, B., A. Jonsson, and T. Börjesson. 2002. Near infrared technology for soil analysis with implications for precision agriculture. In Near infrared spectroscopy: Proceedings of the 10th international conference, kyongju s. korea. nir publications, chichester, UK (pp. 279-284).

Shonk, J. L., Gaultney, L. D., Schulze, D. G., & Van Scoyoc, G. E. (1991). Spectroscopic sensing of soil organic matter content. Transactions of the ASAE, 34(5), 1978-1984.

Stewart, S., N.R. Kitchen, M.A. Yost, L.S. Conway, and P. Carter. 2021. Planting depth and within-field soil variability impacts on corn stand establishment and yield. Agrosystems, Geosciences & Environment 4:e20186.

Sudduth, K.A. and J.W. Hummel. 1993. Soil organic matter, CEC, and moisture sensing with a portable NIR spectrophotometer. Transactions of the ASAE. 36:1571-1582.

Thomison, P., A. Geyer, and R. Minyo. 2013. Taking a second look at planting depths for corn (C.O.R.N. Newsletter July 2013). Ohio State University Extension. https://agcrops.osu.edu/newsletters/2013/ 07#3

Thomason, W. E., S.B. Philips, M.M. Alley, P.H. Davis, M.A. Lewis, and S.M. Johnson. 2008. In-row subsoil tillage and planting depth influence corn plant population and yield on sandy- textured MidAtlantic Coastal Plain soils. Crop Management, 7: 1–12. https://doi. org/10.1094/CM-2008-0519-01-RS

Viscarra Rossel, R. A., McGlynn, R. N., and McBratney, A. B. 2006. Determing the composition of mineral-organic mixes using UV-vis-NIR diffuse reflectance spectroscopy. Geoderma 137: 70–82.

Viscarra Rossel, R.A., and T. Behrens. 2010. Using data mining to model and interpret soil diffuse reflectance spectra. Geoderma. 158:46–54. doi:10.1016/j. geoderma.2009.12.025

Whalley, W. R., P.B. Leedsharrison, and G.E. Bowman. 1991. Estimation of soil-moisture status using near-infrared reflectance. Hydrol. Process. 5:321–327.

Zhou, P., K.A. Sudduth, K.S. Veum, and M. Li. 2022. Extraction of reflectance features for estimation of surface, subsurface, and profile soil properties. Comp. and Elec. In Agric. 196: 106845. https://doi.org/10.1016/j.compag.2022.106845

Figures

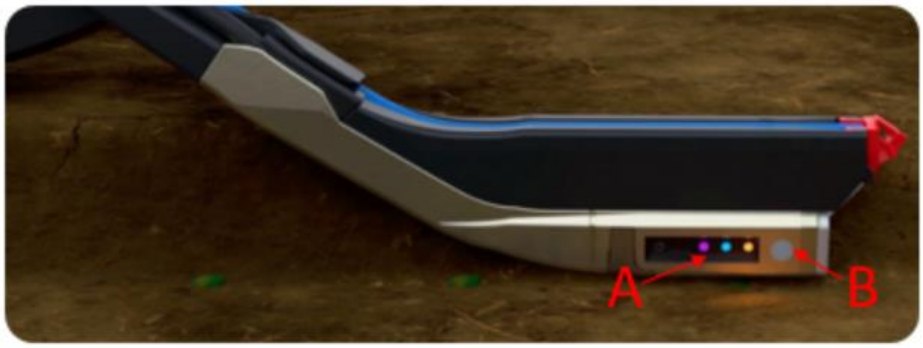

Fig. 1. Precision Planting SmartFirmer labeled with optical sensor (A) and temperature sensor (B).

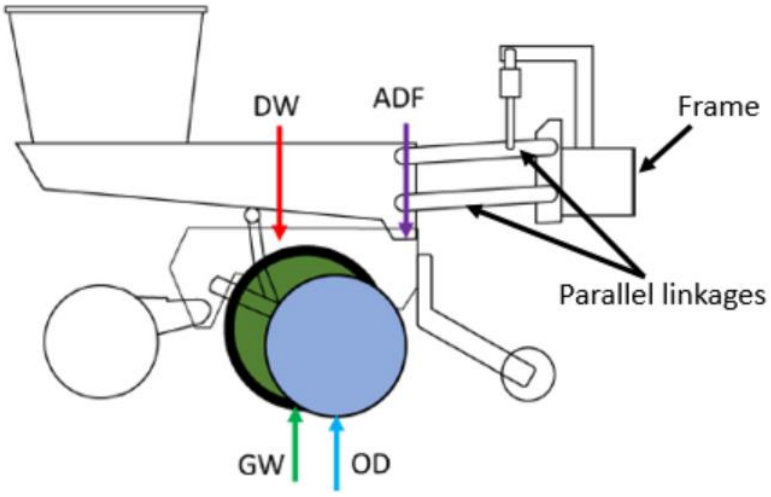

Fig. 2. Diagram of a typical planter row unit, with select mechanical forces identified (adapted from Brune et al., 2018). DW = Dead weight; ADF = Applied downforce; GW = Gauge wheel; OD = Opening Disc.

Fig. 3. Precision Planting's load sensing pin (A) and downforce cylinder used with the DeltaForce System.

CHAPTER 2: REPEATABILITY OF COMMERCIALLY AVAILABLE VISIBLE AND NEAR INFRARED PROXIMAL SOIL SENSORS

Abstract

Integration of reflectance sensors into commercial planter or tillage components have allowed for dense quantification of spatial soil variability. However, little is known about sensor performance and reproducibility. Therefore, research was conducted in Missouri in 2019 to determine (i) how well sensors can estimate soil organic matter (OM) and (ii) whether sensor output could be repeatable among sensing dates. Soil sensor data were collected across three weeks on an alluvial soil with the Precision Planting SmartFirmer and Veris iScan. Output layers used in analyses included OM and Furrow Moisture from the SmartFirmer, as well as OM, reflectance, and soil apparent electrical conductivity from the iScan. Ground-truthing soil samples were collected at 0-50 mm on the first date to determine OM and on all dates to determine soil gravimetric water content. Results showed OM estimations by the iScan, which included the manufacturer's specified field-specific calibration, were reproducible among the three sensing dates, with coefficient of determination (R^2) ranging from 0.95 to 0.97. Similarly, root mean square error (RMSE) values were between 1.60 and 2.41 g kg^{-1}. SmartFirmer results showed OM was overestimated in areas of low OM, and underestimated in areas of high OM when compared to laboratory-measured data (R^2 = 0.34; RMSE = 6.90 g kg^{-1}). Additionally, variability existed in OM estimations between dates in areas that were lower in laboratory-measured OM, soil moisture, and clay content. These results suggest real-time estimations of OM may be subject to variability, and local information is likely necessary for consistent soil reflectance-based OM estimations.

Introduction

In the past decade, technology has allowed for the incorporation of proximal soil sensor systems onto commercial row-crop equipment. Through optical visible and near-infrared reflectance (VNIR), these systems can estimate important agronomic soil properties *in situ*, such as soil moisture and organic carbon or matter (OC/OM). Although relatively new to production-scale agricultural equipment, VNIR spectroscopy for soil physical and chemical property estimation has been evaluated across a range of environments both in laboratory settings (Rienzi et al., 2014) and, to a lesser extent, through stand alone on-the-go sensing (Nawar and Mouazen, 2019). Using VNIR can be practical due the ability to integrate into necessary field operations, and potential to estimate multiple soil properties from a single sensing operation. Further, the systems are inexpensive when compared to the equipment they are integrated into (i.e., row-crop seeder). However, challenges from environmental factors such as ambient light, soil moisture, texture, and residue can all impact reflectance and result in low-quality *in situ* soil sensor data (Stenberg et al., 2010). Further, factors such as dust, soil smearing, and variable distance between the sensor and the soil can introduce measurement error (Sudduth and Hummel, 1993). These factors require careful sensor system design and engineering for reproducible data.

In the late 1980s, several prototype VNIR on-the-go in situ spectrometers were developed (Shonk et al., 1991; Sudduth and Hummel, 1993). Evaluation of more recently developed systems has demonstrated the accuracy of OC estimations using on-the-go sensing (Christy, 2008; Bricklemyer and Brown, 2010; Nawar and Mouazen, 2019). Most of these studies used full-spectrum sensing, spectral pre-processing techniques, and

calibration procedures to develop spatial OC estimates. One example was research conducted by Nawar and Mouazen (2019) which aimed to evaluate how real-time compared to laboratory sensing of OC. Their study also evaluated several calibration methods that ranged from regional to field specific. The results showed that, in two of the three calibration techniques, real-time sensing predictions of OC were comparable to laboratory results. Additionally, including regional data in the calibration method resulted in an improved OC estimation (coefficient of determination (R^2) = 0.74) when compared to the single field technique (R^2 = 0.65). These results suggest that accuracies from real-time sensing can be comparable to analyses performed in a laboratory setting. Additionally, they suggest that including regional information prior to sensing could improve real-time estimations of OC.

A similar study was performed in central Kansas, USA across 8 fields within two counties, covering nearly 300 ha (Christy, 2008). This study utilized a shank-mounted spectrometer with a sensing range from 920 to 1718 nm attached to a tractor-mounted toolbar. Several cross-validation schemes were evaluated, and predictions of gravimetric water content and OM varied with each method. Performance was poorest when an entire field ("one-field-out") was excluded from the training dataset. This method resulted in cross-validation R^2 values of 0.40 and 0.67 for soil moisture and OM, respectively. The greatest accuracies were observed when the "leave-one-out" method was used, where a single sample was omitted at each training iteration. This method used the entire dataset for training and validation, where one sample was removed for prediction at each iteration. The cross-validation R^2 values were 0.67 and 0.80 for soil moisture and OM, respectively. The "one-field-out" results would be most representative of real-time sensor

estimation with no field-specific calibration. Therefore, this research illustrates the limitations of real-time sensors that have the capability to guide on-the-go applications of seed or soil amendments, but do not have field-specific data for calibration.

Reproducibility at a given location under varying environments should also be considered when assessing performance of proximal soil sensors. Soil moisture is a dynamic factor, and changes could influence repeatability of reflectance, and thus OC or OM estimations. Laboratory research has been conducted to evaluate the effect of soil moisture on the prediction of OC (Sudduth and Hummel, 1991; Nocita et al., 2012; Rienzi et al., 2014). In all studies, results showed the influence of soil moisture on reflectance of a given soil to be nonlinear. This factor makes accounting for moisture challenging. Therefore, different forms of spectral pre-processing were performed in the studies to account for the influence of moisture on reflectance, and subsequently OC prediction. Although specific moisture contents varied between studies, results were consistent in that OC prediction was not equal across moisture contents. For example, Rienzi et al. (2014) found prediction R^2 to vary from 0.64 to 0.88 and RMSE to vary from 4.02 to 7.13 g kg^{-1} among soil moisture contents. Generally, prediction accuracies decreased with increasing moisture content. These and other similar studies suggest that accounting for moisture when proximally sensing OC or OM on-the-go will be required for reproducible results.

In addition to varying moistures, clay type and amount have also been found to influence reflectance (Viscarra Rossel et al., 2009). In general, studies have found the accuracy of OC prediction decreases with increasing sand content (Stenberg; 2010; Stenberg et al., 2010). This research found OC to be overestimated by VNIR in very

sandy soils due to the smaller surface area of the sand particles, which resulted in OM dominating the spectra. Interestingly, similar work found that clay content could have a positive or negative effect on OC prediction accuracy, dependent upon soil sample condition. When air-dry samples were used, clay content had a negative effect on accuracy, with the opposite occurring with rewetted samples (Stenberg et al., 2010).

Collectively, previous research conducted utilizing VNIR reflectance suggests that the interaction of OM, clay, and moisture creates a challenging environment for consistent VNIR estimates of soil properties. How this challenge is met in commercially available proximal soil sensor systems is not well understood over diverse environments, but understanding is needed if these sensors are to be used with confidence in agronomic decision making. Therefore, research was conducted to evaluate OM estimations produced by two commercially available sensor systems, as well as the influence of soil moisture and texture on the repeatability of OM estimations by these systems.

Materials and Methods

Site Information

Research was conducted in September and October of 2019 near Claysville, MO (lat. 38.6582, long. -92.2436). The site was located on an alluvial soil directly adjacent to the Missouri River. The soil was classified as a Peers silty clay loam (fine-silty, mixed, superactive, mesic Fluvaquentic Hapludolls). However, textural analysis (methodology below) showed portions of the field were classified as a sandy loam, suggesting the Peers silty clay loam did not encompass the entire site. The area used in the study consisted of 5 ha and was chosen because it included a stark contrast in both soil texture and OM. Surface soil ranged in clay content from 47.2 to 326 g kg^{-1}, and OM varied from 12.8 to

37.1 g kg^{-1}. Historically corn (*Zea mays* L.), soybean (*Glycine Max* [L.]), and wheat (*Triticum*) had been grown on the field, with tillage occurring prior to corn planting and following corn harvest. In the spring of 2019, flooding inhibited planting of a grain crop and the land was fallowed. Prior to sensor data collection, the site was tilled two times at a depth of 100 to 150 mm with a 6 m wide disk.

Data collection occurred at three dates in 2019 (Sep 17, 24, and Oct 1), hereafter referred to as date 1, 2, and 3, respectively. Prior to date 1, rainfall had not occurred in nine days, resulting in the driest of the three dates. On Sep 22 13 mm of precipitation was received, which resulted in the wettest conditions for the Sep 24 sensing event. Additional precipitation (14 mm) occurred on Sep 28 prior to the final sensing date. Collectively, average gravimetric water content values based upon soil samples collected at the site were 16.1, 19.5, and 19.2 g 100 g^{-1}, respectively. Details about soil sample collection can be found below. Lastly, ambient air temperatures at the time of sensing were between 24 and 28 °C at all three dates.

Proximal Sensing Data Collection

Proximal soil sensor data were collected on all three dates with two commercially available sensor systems. The first was the Precision Planting SmartFirmer (Precision Planting, Tremont, IL, USA). The SmartFimer is designed to mount to a planter row-unit behind the seed tube, replacing traditional seed firming devices. For this study, they were instrumented on each row of a 4-row planter. All data from the SmartFirmer were recorded at 1 Hz with a Precision Planting Seedsense monitor. Data layers from the SmartFirmer consisted of Furrow Moisture (%), Temperature (°C), OM (%), Cleanness (%), and Uniformity (%). All OM values were converted from percent to mass basis (g

kg^{-1}) for ease of comparison among soil sensors and laboratory data. These metrics, aside from Temperature, were derived from the optical portion of the sensor that measures reflectance from five wavelength bands in the VNIR region (468, 592, 858, 1198, and 1468 nm).

The two metrics used in our investigation were Furrow Moisture and OM. Furrow Moisture is defined by Precision Planting as the percent of water weight a corn seed is projected to imbibe over a three-day period (Precision Planting, 2018). As such, it is an index of water availability and is not equivalent to volumetric or gravimetric water content. Furrow Moisture was estimated by each SmartFirmer, but data were logged as an average across the four sensors. The manufacturer's calibration relating OM to reflectance was based on OM data derived from the loss on ignition test (Nelson and Sommers, 1996; Precision Planting, 2018). SmartFirmer OM was also estimated by row, but values were derived through an interpolation method using data from other row units (Strnad, 2018). This method allowed for leveling of sensor output across the planter, each of which measured distinct values. These OM estimates were also averaged across rows in the export. Therefore, OM data used in the study were an average across the four rows of the interpolated measurements.

The planter used in the study had MaxEmerge XP (Deere & Co., Moline, IL, USA) row units and an automated hydraulic downforce system (Precision Planting DeltaForce®). The hydraulic downforce system automatically adjusted row unit downforce or uplift to maintain a target gauge wheel load of 445 N. This improved the consistency of disk-opener operating depth (set to 50 mm) across the site. The lens of the

SmartFirmer pressed against the sidewall, approximately 6 mm above the bottom of the slot created by the disk-openers.

The other sensing platform used in the study was the Veris iScan (Veris Technologies, Salina, KS, USA). This system is designed to mount on common toolbars, such as a row-crop planter or tillage implement. For our study, the iScan was attached to the middle of a pull-type toolbar, directly behind the centerline of the tractor. It included soil-engaging sensors that measured apparent soil electrical conductivity (EC_a; 0.61 m), volumetric soil water content (through capacitance), temperature, and reflectance at two wavelength bands (660 and 940 nm). The moisture and optical sensing components of the iScan are positioned to press against the bottom of the slot created by the runner (Lund and Maxton, 2019). The operating depth of these sensors was set to 50 mm. Prior to all data collection events, the soil EC_a, optical, and capacitance sensors were calibrated following procedures provided by Veris Technologies. Data were logged at 1 Hz to Veris Technologies Soil Viewer real-time mapping software.

The metrics from the iScan used in this study consisted of soil EC_a, moisture, visible reflectance (660 nm), infrared reflectance (940 nm), and OM. The OM estimates were derived from optical sensor reflectance, through a calibration process that included laboratory-measured samples and is further described below.

The 4-row planter and toolbar-mounted iScan were both pulled by a John Deere 6110R (Deere & Co., Moline, IL, USA) equipped with automated machine guidance. The steering was controlled through John Deere's integrated automatic steering system (AutoTrac) and utilized StarFire 2 differential correction, providing ±100 mm pass-to-pass accuracy. Data were all collected at an operating speed of 2.2 m s^{-1}. Data collection

with the 4-row planter occurred first at each date, immediately followed by the iScan. At date 1, the transect spacing for the planter and the iScan were 3 and 6 m, respectively. At dates 2 and 3, a 6 m transect spacing was used for both systems. At date 2, the transects used for the automated guidance were shifted 100 mm north of the transect used on date 1. The transects were shifted 100 mm south of the original transects on date 3. The tractor and toolbar-mounted iScan followed the same transect as the tractor and planter at all three dates, centered between rows 2 and 3, so that the iScan was not running in soil disturbed by the planter.

Manual Sample Data Collection

Soil samples were collected after the first sensing date (n=13) and were targeted based upon the OM maps created by the SmartFirmer. Areas of high, medium, and low OM were chosen targeted for the sampling locations. At each georeferenced location, six 25 mm diameter soil cores were taken within 1 m of the location and split into 0 to 50 and 50 to 150 mm depth increments, and then combined to represent the location. For OM analyses in this study, only data from the 0-50 mm depth were used to maintain consistency with the optical sensor operating depth. Soil samples were analyzed for soil physical properties and OC at the University of Missouri's Soil Health and Assessment Center following established procedures (Nelson and Sommers, 1996). The OC estimates were developed through the loss on ignition test, and were multiplied by a constant of 1.72 to convert to OM.

Soil moisture samples were collected during or immediately following the sensing operation for all three dates. The first set of samples (n=13) were georeferenced and based upon SmartFirmer Furrow Moisture and iScan soil moisture. Subsequent samples

were taken at the same locations on dates 2 and 3. One soil sample was collected from each location at each date from 0 to 50 mm with a 50 mm inner diameter core. For gravimetric water content calculations, sample moist weights were recorded immediately after sampling and dry weights after drying for 48 hours at 105 °C.

Sensor Data Pre-Processing, Calibration, and Analysis

Data collected with the iScan were filtered to ensure adequate quality, where global field outliers were removed if data were greater than two standard deviations from the mean of the entire field. To determine OM, laboratory (loss on ignition) results from four soil sampling locations, selected based upon reflectance values from the two wavelength bands emitted by the iScan, were obtained and submitted to Veris Technologies, who developed the calibration of reflectance to OM. Areas ranging from high to low reflectance were chosen to capture the range in soil variability at the site. Due to consistencies in the spatial structure of reflectance over dates, the same four sample locations were used for all three dates.

All planter sensor data from 20|20 Seedsense monitor that contained a downforce margin of <1 N were removed due to uncertainty of operating depth. The SmartFirmer system processes the reflectance data into a real-time estimated OM, and no further adjustments were performed. As previously mentioned, these OM estimates were interpolated values calculated from a combination of all four SmartFirmer sensors present on the planter.

SmartFirmer and iScan data from all three dates were merged with laboratory measured data collected through manual sampling using ArcGIS (Esri, Redlands, CO, USA). The merged dataset consisted of the point (manually sampled) measurements and

all sensor data within a 4.5 m radius of the sample location. This resulted in a total of 3 to 5 sensor data points, which were subsequently averaged and used in the statistical analysis. Linear regression models were examined using R Studio (RStudio Team, 2021) to evaluate the relationship of SmartFirmer or iScan metrics to results from laboratory measured soil samples. Independent variables were SmartFirmer or iScan OM. Likewise, the dependent variables were laboratory-measured OM. Regression models were considered significant at $P \leq 0.05$ and were compared using R^2 and RMSE.

For an evaluation of sensor metric repeatability over the entire investigation area, both SmartFirmer and iScan point data were converted to a 6 m grid using Ag Leader's Spatial Management Software (SMS; Ag Leader, Ames, IA). Inverse distance weighting was used due to the spatially dense nature of the dataset (Wilson et al., 2005). The maximum sampling distance used for interpolation was 9 m, and 0.6 was used as the distance or weight ratio. Data from both sensor systems at all three dates were merged to a common grid to allow for statistical analysis of changes in moisture and OM over dates. Collectively, these data allowed for a statistical analysis of spatial and temporal changes in moisture and OM for each system. Linear regression was used following the aforementioned procedures in R Studio, where the independent variable was SmartFirmer Furrow Moisture, iScan soil moisture, or laboratory measured OM, and the dependent variable was sensor-based OM or the coefficient of variation (CV) of sensor-based OM.

Soil apparent electrical conductivity (EC_a) has been utilized as a source for estimating within-field spatial variability of soil texture (Sudduth et al., 2005). Therefore, soil EC_a from the Veris iScan was used to develop a soil clay content map of the study site using the laboratory measured samples (0-150 mm) in conjunction with soil EC_a.

Similar to methodology presented above, all soil EC_a data within 5 m of each sampling location were spatially merged using ArcGIS. Subsequently, a regression model was developed (using aforementioned procedures) where laboratory measured clay content was the dependent variable, and soil EC_a was the independent variable. After the model was developed, the regression equation was applied to the entire field of EC_a measurements so estimated clay content could be analyzed across the site.

Results and Discussion

Veris iSCAN

Soil Texture

Soil EC_a showed strong spatial structure across the study site, where the highest EC_a was observed in the northwest portion of the field, and lowest EC_a observed in the southeast portion. A transitional zone of medium EC_a existed in the center of the field, dissecting the site from northeast to southwest. Since a strong positive linear relationship was found between clay content and soil EC_a at the soil sampling locations ($R^2 = 0.90$), soil EC_a could be meaningfully transformed to estimate clay content across the field (Fig. 1). This soil EC_a derived clay content map illustrated greater clay content on the northern and western-most portions of the field (>250 g kg^{-1}). In contrast, the eastern and southern-most portions were lower in clay content (<100 g kg^{-1}). This ability to predict soil texture was consistent with previous research estimating soil texture with soil EC_a on alluvial soils in Missouri, USA (Kitchen et al., 1996).

Soil Reflectance and Organic Matter

Reflectance across the site at 660 nm (visible) averaged 162, 165, and 164 decimal counts for dates 1, 2, and 3, respectively. Likewise, reflectance at 940 nm (IR)

averaged 439, 442, 435 decimal counts for dates 1, 2, and 3, respectively (Fig. 2). Interestingly, date 2 had the greatest mean reflectance at both wavelengths despite the highest moisture content. This may have been due to slight differences in sensor and soil engagement between the dates. Spatial variation in soil reflectance at both wavelength bands was clearly defined, with greater reflectance on the eastern portion, lower reflectance on the western portion, and a transitional area in the middle of the field (Fig. 2). Further, the spatial structure and relative trends were consistent between all three sensing dates. In general, reflectance values were lower in areas with greater clay content. Although increasing sand content has been found to decrease reflectance, greater soil moisture was likely the driving factor that resulted in lower reflectance on the finer textured soil (Cierniewski and Kusnierek, 2010). The map illustrating the difference in reflectance between dates showed that the decrease in reflectance was greatest on the coarser textured soil from dates 1 to 2. This was likely due to water being adsorbed by the finer textured soil for those portions of the field following the rain event between sensing dates. Contrary, the coarser textured area of the field likely had more water present on soil particles which lowered the reflectivity (Twomey et al., 1986). Similar to dates 1 and 2, reflectance also varied spatially between dates 2 and 3. The inverse occurred when compared to date 1 to 2, with reflectance increasing on the eastern portion of the field. The increase may have been caused by slightly drier soil conditions at date 3 than date 2. However, the cause of the decrease in reflectance on the western portion of the field is unknown.

Mean OM varied little between the three sensing dates and averaged 24.0 g kg^{-1} across sensing dates. The OM maps created were based upon reflectance, and therefore

followed the same spatial structure (Fig. 2; Fig. 3). Areas of greater reflectance (east portion) were estimated by the linear model developed by Veris Technologies to have a lower OM when compared to the western portion. This relationship was observed across all three sensing dates. Additionally, areas of high OM corresponded with areas of high estimated soil moisture content (Fig. 3). Together, these layers help illustrate the spatial trends between soil properties across the field. Areas of greater clay content (Fig. 1) also exhibited greater OM and soil moisture across all three dates. Also, a positive and linear response between sensor-based OM and laboratory-measured OM were observed at each of the dates (Fig 4; Table 1). The R^2 values were very high ($\geq$0.95) and RMSE were low ($\leq$2.41 g kg^{-1}). These accuracies were as good or better than other similar published laboratory or field studies (Christy, 2008; Kweon and Maxton, 2013; Rienzi et al., 2013; Nawar and Mouazen 2019). This was attributed to the inclusion of calibration samples, strong contrast in OM at the site, and the relatively small study area. Collectively, these results illustrate that the sensor system could consistently and accurately estimate OM at this highly-variable site, despite changes in average reflectance between sensing dates. Further, these results suggest that a local calibration for each sensing date resulted in repeatable spatial representation of soil OM at varying soil moisture levels.

Precision Planting SmartFirmer

Soil Organic Matter

Over the three sampling dates, some inconsistencies were observed in OM estimates. At the first date, sensor OM averaged 26.1 g kg^{-1} across the study site, ranging from around 20 to 36 g kg^{-1}. Additionally, clear spatial variation in sensor-estimated OM was observed within the field (Fig. 5). Estimates were greater on the northwestern portion

when compared to the central and eastern portions. In general, OM followed similar spatial structure to clay content, where the greatest OM coincided with areas of greater clay content (Fig 1 and 5). At the second date, average sensor OM across the site increased slightly when compared to date 1 (27.1 g kg^{-1}), and the range was smaller (22.5-34.5 g kg^{-1}). Similar to date 1, OM estimates were greatest on the western portion of the field. However, the lowest OM estimates (~23 g kg^{-1}) were observed throughout the center of the field. Further, sensor OM increased on the eastern portion where previous estimates at date 1 were lowest. At the last sensing date, mean OM across the site was 26.2 g kg^{-1}. Average sensor OM was similar to the first date, although the range in OM was smaller (23-33 g kg^{-1}). Therefore, areas of very low and very high OM were not as low or as high as date 1. Spatial patterns on the western portion were similar to dates 1 and 2. However, OM estimates were low in both the central and eastern portions of the field.

Across dates, results showed a positive relationship of SmartFirmer OM to laboratory measured OM (Table 2). This illustrated that the sensor system could, at this site, detect general trends of high and low OM (R^2=0.52). However, the slope of the of the regression equation was not close to 1 (0.23), and the intercept was 20.8 g kg^{-1}. This response suggested that areas of low OM were consistently overestimated by the system, while areas of greater OM were underestimated. Similar linear responses have also been reported by similar research (Wijewardane and Morgan, 2016; Rienzi et al., 2013; Bricklemyer and Brown , 2010). The overall accuracy of the model was slightly poorer when compared to data published by Christy et al. (2008), who simulated real-time NIR-based OC estimates through their “one-field-out” validation procedure. Their R^2 and

RMSE values were 0.67 and 5.2 g kg^{-1}, respectively. However, their work highlighted that this method was the least accurate when compared to models that included field-specific calibration.

Among dates, responses were similar at the first and third sensing date, where a positive linear response between laboratory measured and sensor-estimated OM was observed (Fig 6; Table 2). At the second date, however, no response was observed and the average OM across the site was 27.8 g kg^{-1}. Collectively, OM estimations were consistent across the three dates in areas of the field with OM >20 g kg^{-1}. However, estimations in areas of lower OM were more variable. These areas with the greatest variation, or greatest CV, in OM coincided with the coarser textured portion of the field (Fig. 7), and can be visualized through the CV of OM among dates (Fig. 7; Fig. 8). Thus, it was hypothesized that the coarser texture alone or in combination with soil moisture influenced the OM estimation by the SmartFirmer. Research has shown that OM prediction error generally increases as clay content decreases (Stenberg et al., 2002).

Soil Moisture and Texture Influence on OM

SmartFirmer Furrow Moisture averaged 44.2, 57.8, and 54.0% across the site at dates 1, 2, and 3, respectively. These values follow similar trends to the aforementioned gravimetric water content collected at the three dates. In general, Furrow Moisture was greater on the west half of the field when compared to the east (Fig. 5). Although average Furrow Moisture at the site increased from date 1 to date 2, the increase (~12-20%) was more dramatic on the coarser textured (eastern) portion of the field. On the finer textured soil (western portion), Furrow Moisture increase was <12%. This suggests that the rainfall event that occurred between the two sensing dates had a greater influence on

Furrow Moisture estimation in the coarser textured than the finer textured soil. From date 2 to 3, Furrow Moisture decreases were greatest in the north-central portion of the field. The spatial structure was less defined, indicating that the moisture variations were not as variable between dates 2 and 3.

Across the study site, changes in OM were related to changes in Furrow Moisture between dates 1 and 2, as well as dates 2 and 3 (Fig. 9). This suggests that soil moisture may have influenced the SmartFirmer estimation of OM. From sensing date 2 to date 3, the range of the change in OM was lower than date 1 to 2. Additionally, OM decreased as Furrow Moisture increased across the study site. Differing responses among soil textures were observed from date 1 to 2, where OM increased as Furrow Moisture increased in areas of lower clay content. Conversely, the opposite occurred in the finer textured soil, and the response was more similar to date 2 to 3. These results from date 1 to 2 suggest that both soil texture and soil moisture affected the OM estimation by the SmartFirmer. The direct cause of this is unknown, but could have been due to the difference between the wetting and drying effects and/or sensor-to-soil engagement between sensing dates.

Conclusions

Research conducted with two commercial sensor systems showed that spatial variability in soil OM could be captured by both at our study site. However, this study also demonstrated some of the challenges associated with the reproducibility of OM estimates based upon real-time VNIR reflectance sensing. Specifically, the results showed that inconsistencies could occur due to temporal variations in soil moisture and spatial variability in soil texture. Therefore, our results showed that real-time estimations using a single “global” calibration were subject to variability and not as consistent as

systems employing a field-specific calibration that includes laboratory-measured results. This highlights an example tradeoff between superior accuracy and the ability to use sensor data for real-time control. Practitioners should consider the accuracy required to make useful input management decisions. Further research is also needed to determine whether accuracy could be improved with calibration information (e.g., soil survey map) to make region or field-specific estimations in real-time.

Bibliography

Bricklemyer, R. S., & Brown, D. J. (2010). On-the-go VisNIR: Potential and limitations for mapping soil clay and organic carbon. *Computers and Electronics in Agriculture*, *70*(1), 209-216. https://doi.org/10.1016/j.compag.2009.10.006

Christy, C. D. (2008). Real-time measurement of soil attributes using on-the-go near infrared reflectance spectroscopy. *Computers and electronics in agriculture*, *61*(1), 10-19. https://doi.org/10.1016/j.compag.2007.02.010

Cierniewski, J., & Kuśnierek, K. (2010). Influence of several size properties on soil surface reflectance. *Quaestiones Geographicae. 29*:13-25. https://doi.org/10.2478/v10117-010-0002-9

Gee, G. W., & Or, D. (2002). 2.4 Particle-size analysis. Methods of soil analysis. Part, 4(598), 255-293.

Kitchen, N. R., Sudduth, K. A., & Drummond, S. T. (1996). Mapping of sand deposition from 1993 midwest floods with electromagnetic induction measurements. *Journal of Soil and Water Conservation*, *51*(4), 336-340.

Kweon, G., & Maxton, C. (2013). Soil organic matter sensing with an on-the-go optical sensor. *Biosystems engineering*, *115*(1), 66-81.

Lund, E., & Maxton, C. Comparing Organic Matter Estimations Using Two Farm Implement Mounted Proximal Sensing Technologies. *PSS 2019*, 35.

Nawar, S., & Mouazen, A. M. (2019). On-line vis-NIR spectroscopy prediction of soil organic carbon using machine learning. *Soil and Tillage Research*, *190*, 120-127. https://doi.org/10.1016/j.still.2019.03.006

Nelson, D. W., & Sommers, L. E. (1996). Total carbon, organic carbon, and organic matter. *Methods of soil analysis: Part 3 Chemical methods*, *5*, 961-1010.

Nocita, M., A. Stevens, C. Noon, & van Wesemael, B. (2013). Prediction of soil organic carbon for different levels of soil moisture using Vis-NIR spectroscopy. *Geoderma 199*:37–42. https://doi.org/10.1016/j.geoderma.2012.07.020

Precision Planting. (2018). SmartFirmer: Setup & Operation for Gen 2 20/20 Display. Retrieved from https://s3.amazonaws.com/pp3-products/file-1585250294/SmartFirmer%20Operators%20Guide%20-%20Gen3%20(955714).pdf

Rienzi, E. A., Mijatovic, B., Mueller, T. G., Matocha, C. J., Sikora, F. J., & Castrignanò, A. (2014). Prediction of soil organic carbon under varying moisture levels using reflectance spectroscopy. *Soil Science Society of America Journal, 78*(3), 958-967. https://doi:10.2136/sssaj2013.09.0408

Shibusawa, S. (2001). Soil mapping using the real-time soil spectrophotometer. In *Precision Agriculture'01, Proc., 3rd Euro. Conf. Precision Agriculture, Agro Montpellier* (pp. 485-490).

Shonk, J. L., Gaultney, L. D., Schulze, D. G., & Van Scoyoc, G. E. (1991). Spectroscopic sensing of soil organic matter content. *Transactions of the ASAE, 34*(5), 1978-1984.

Wilson, R. C., Freeland, R. S., Wilkerson, J. B., & Hart, W. E. (2005). Interpolation and data collection error sources for electromagnetic induction-soil electrical conductivity mapping. *Applied engineering in agriculture, 21*(2), 277-283.

Stenberg, B., Jonsson, A., & Börjesson, T. (2002). Near infrared technology for soil analysis with implications for precision agriculture. In *Near infrared spectroscopy: Proceedings of the 10th international conference, kyongju s. korea. nir publications, chichester, UK* (pp. 279-284).

Stenberg, B. (2010). Effects of soil sample pretreatments and standardised rewetting as interacted with sand classes on Vis-NIR predictions of clay and soil organic carbon. *Geoderma, 158*:15-22.

Stenberg, B., R.A. Rossel, A.M. Mouazen, and J. Wetterlind. (2010). Visible and near infrared spectroscopy in soil science. *Advances in Agronomy, 107*:163-215. https://doi.org/10.1016/S0065-2113(10)07005-7

Strnad, M. (2018). Method for Leveling Sensor Readings Across an Implement. (International Publication Number: WO 2018/200870). U.S. Patent and Trademark Office.

Sudduth, K. A., & Hummel, J. W. (1991). Evaluation of reflectance methods for soil organic matter sensing. *Transactions of the ASAE, 34*(4), 1900-1909.

Sudduth, K. A., & Hummel, J. W. (1993). Portable, near-infrared spectrophotometer for rapid soil analysis. *Transactions of the ASAE, 36*(1), 185-193.

Sudduth, K.A., Kitchen, N.R., Wiebold, W.J., Batchelor, W.D., Bollero, G.A., Bullock, D.G., Clay, D.E., Palm, H.L., Pierce, F.J., Schuler, R.T. & Thelen, K.D. (2005). Relating apparent electrical conductivity to soil properties across the north-central USA. *Computers and electronics in agriculture*, *46*(1-3), 263-283. https://doi.org/10.1016/j.compag.2004.11.010

Twomey, S. A., Bohren, C. F., & Mergenthaler, J. L. (1986). Reflectance and albedo differences between wet and dry surfaces. *Applied optics*, *25*(3), 431-437.

Viscarra Rossel, R.A., & Lark, R.M. (2009). Improved analysis and modelling of soil diffuse reflectance spectra using wavelets. *European Journal of Soil Science. 60*: 453– 464. https://doi.org/10.1111/j.1365-2389.2009.01121.x

Wijewardane, N. K., Ge, Y., & Morgan, C. L. S. (2016). Prediction of soil organic and inorganic carbon at different moisture contents with dry ground VNIR: a comparative study of different approaches. *European Journal of Soil Science*, *67*(5), 605-615. https://doi: 10.1111/ejss.12362

Wu, C.Y., A.R. Jacobson, M. Laba, & Baveye P.C. (2009). Alleviating moisture content effects on the visible near-infrared diffuse reflectance sensing of soils. *Journal of Soil Science. 174(8):*456–465. https://doi:10.1097/SS.0b013e3181b21491

Tables

Table 1. Linear regression parameters describing Veris iScan soil organic matter (OM) response to laboratory measured OM at all three sensing dates at the study site near Claysville, MO.

	Intercept	*Slope*	R^2	*RMSE (g kg^{-1})*
Date 1 (17 Sep 2019)	1.58	0.88	0.95	2.41
Date 2 (24 Sep 2019)	1.33	0.90	0.97	1.98
Date 3 (1 Oct 2019)	0.73	0.97	0.97	1.60
All Dates	1.21	0.92	0.96	2.02

Table 2. Linear regression parameters describing SmartFirmer soil organic matter (OM) response to laboratory measured OM at all three sensing dates at the study site near Claysville, MO.

	Intercept	*Slope*	R^2†	*RMSE (g kg^{-1})*
Date 1 (17 Sep 2019)	17.5	0.34	0.82	5.82
Date 2 (24 Sep 2019)	27.8	-	-	-
Date 3 (1 Oct 2019)	20.1	0.25	0.81	6.52
All Dates	20.8	0.23	0.52	6.90

†R^2 values are not shown for nonsignificant regression models.

Figures

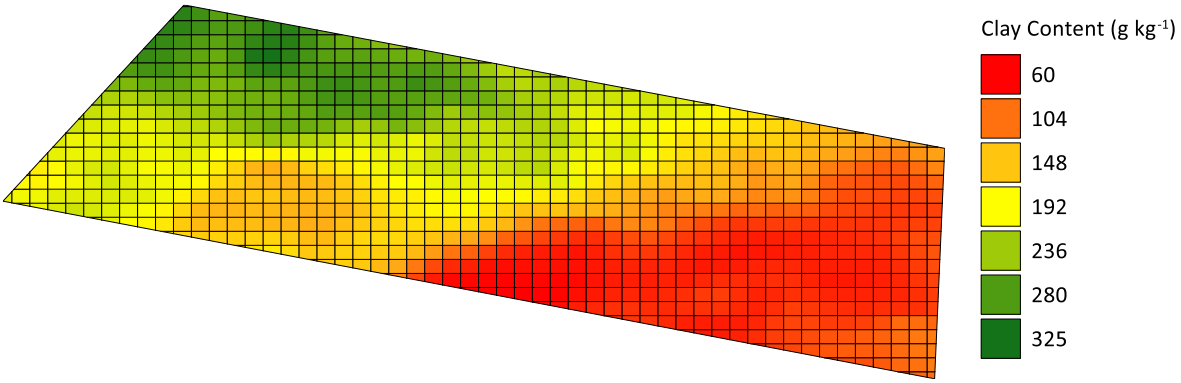

Fig. 1. Modeled clay content based upon soil apparent electrical conductivity and laboratory-measured soil samples at the study site in Claysville, MO.

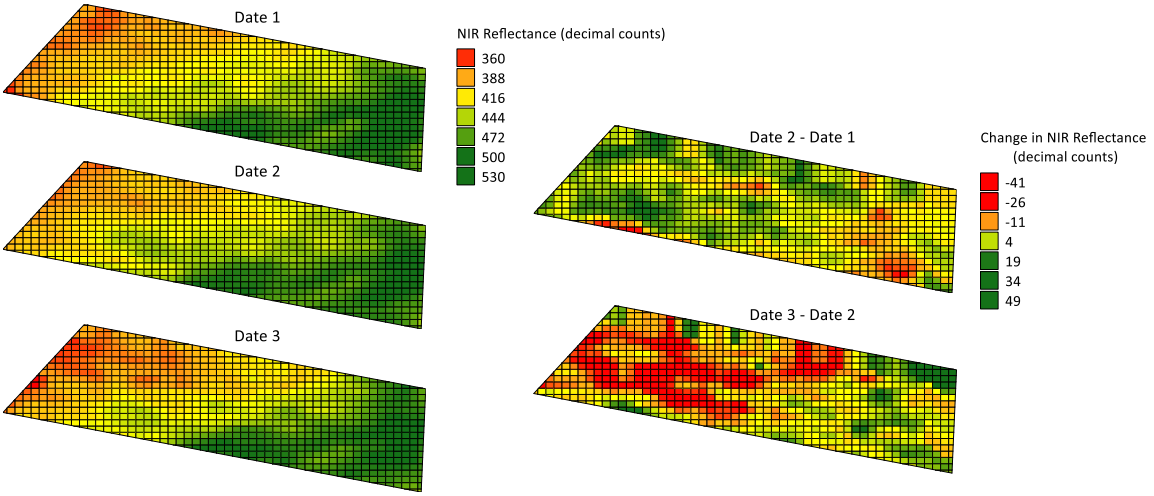

Fig. 2. Near-Infrared Reflectance (left; NIR) from the Veris iScan at all sensing dates, and NIR change from Dates 1 to 2, and Dates 2 to 3 at the study site in Claysville, MO.

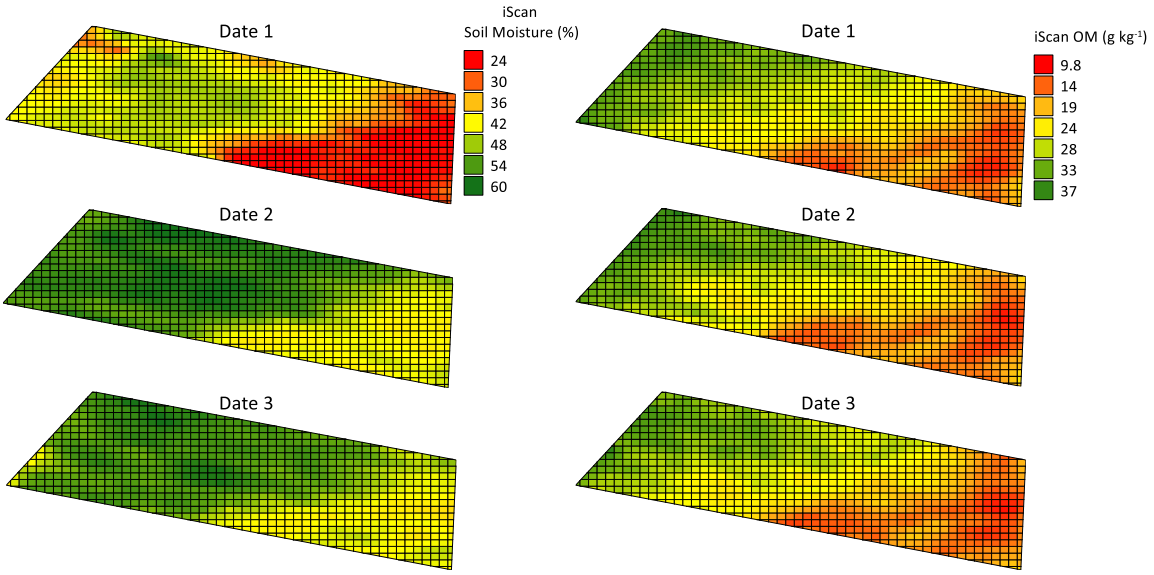

Fig. 3. Soil moisture (left) and soil organic matter (OM) estimates from the Veris iScan on sensing dates 1, 2, and 3 at the study site in Claysville, MO.

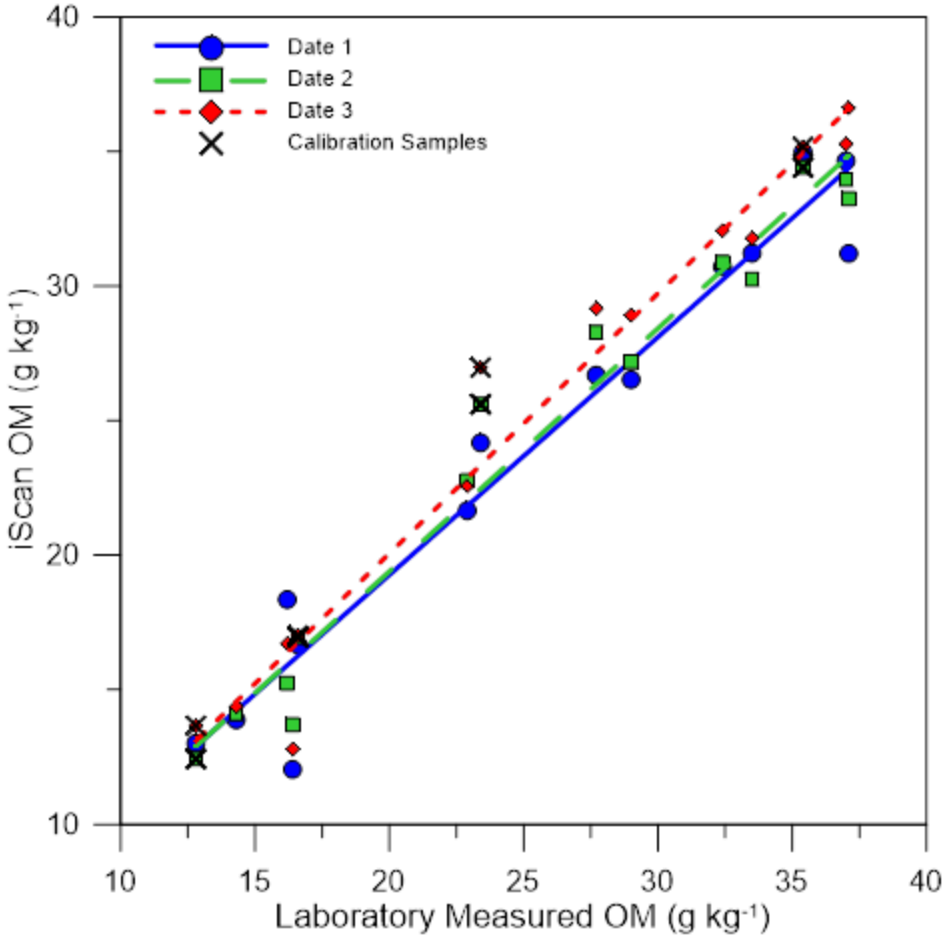

Fig.4. Veris iScan soil organic matter (OM) in relation to laboratory measured OM at the study site in Claysville, MO.

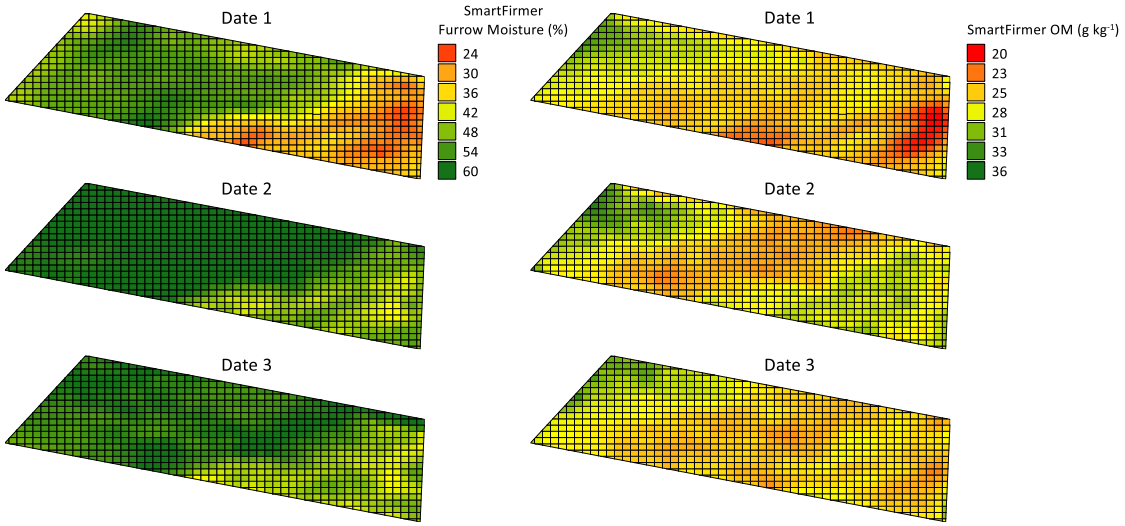

Fig.5. Precision Planting SmartFirmer Furrow Moisture (left) and soil organic matter (OM; right) at all three sensing dates at the study site in Claysville, MO.

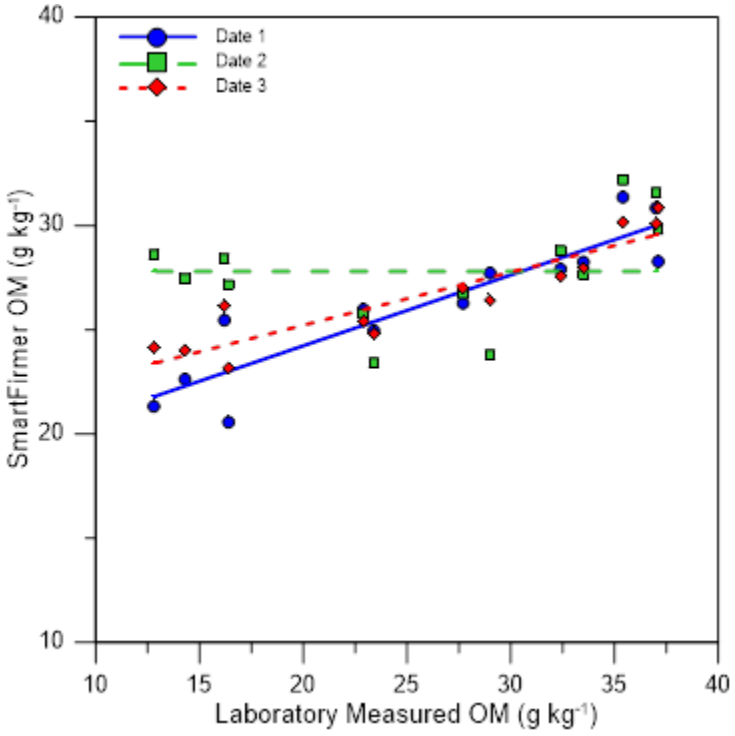

Fig.6. Precision Planting SmartFirmer soil organic matter (OM) in relation to laboratory measured OM at the study site in Claysville, MO.

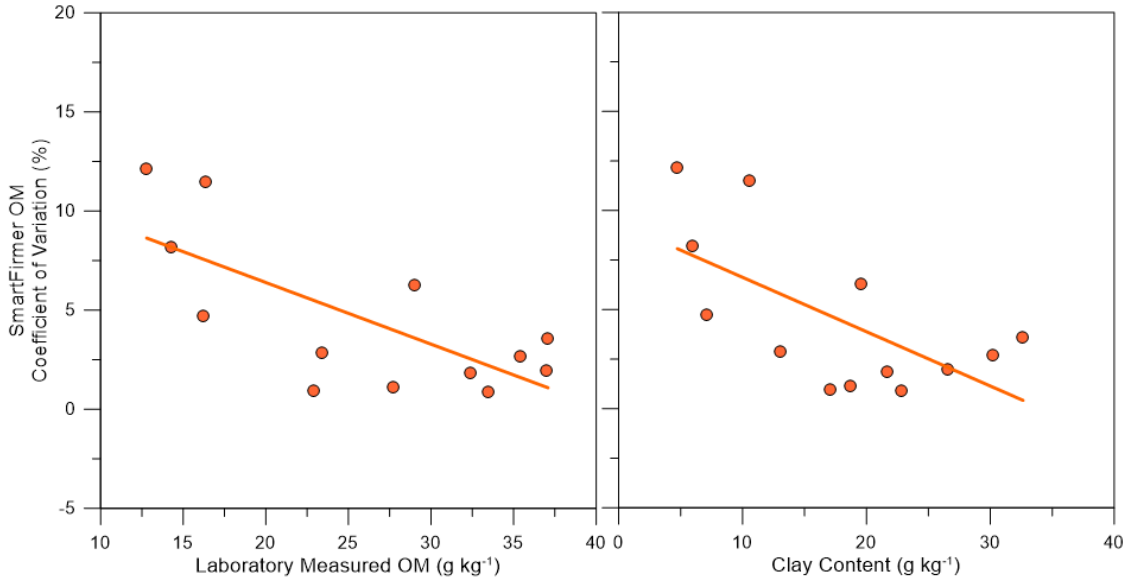

Fig. 7. SmartFirmer organic matter (OM) across-date coefficient of variation (CV) in relation to laboratory-measured OM (left) and clay content (right) at the study site in Claysville, MO.

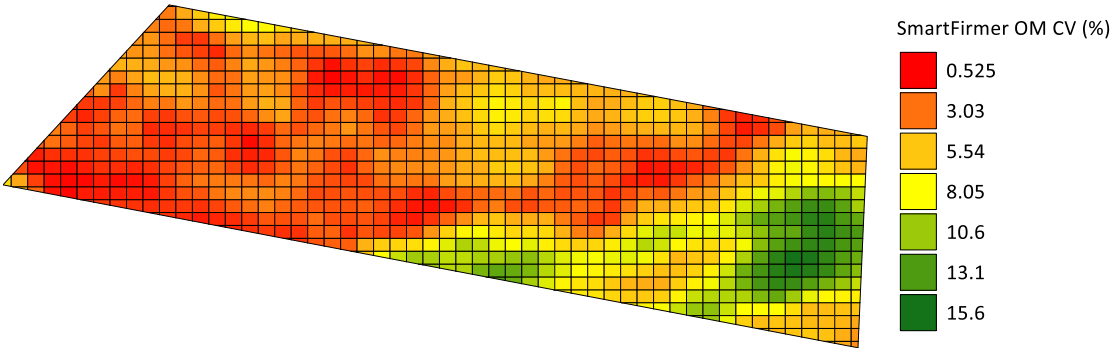

Fig.8. Precision Planting SmartFirmer soil organic matter (OM) coefficient of variation (CV) across the three sensing dates at the study site in Claysville, MO.

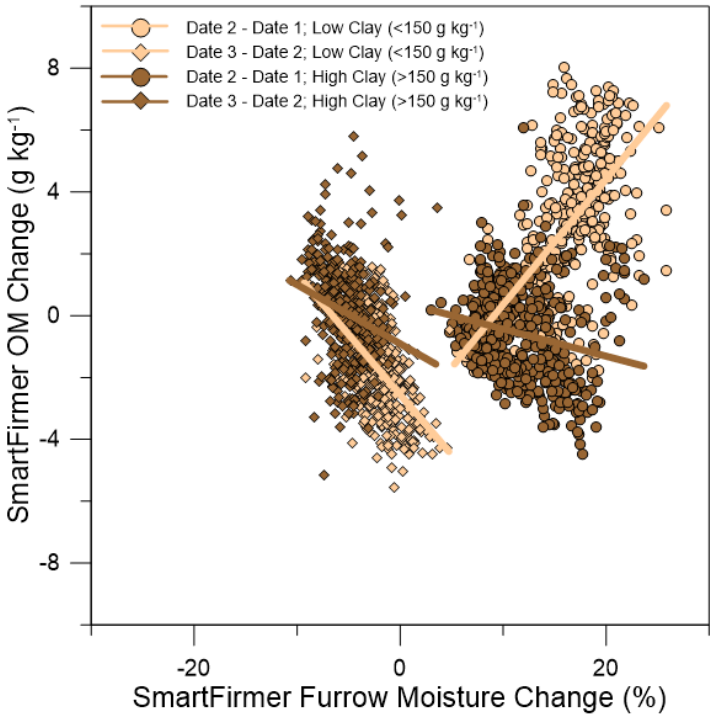

Fig. 9. Precision Planting SmartFirmer soil organic matter change (OM) in relation to the change in SmartFirmer Furrow Moisture at the study site near Claysville, MO.

CHAPTER 3: IMPROVING SOIL ORGANIC MATTER ESTIMATION WITH PLANTER-BASED OPTICAL REFLECTANCE SENSING APPROACHES

Abstract

Proximal soil sensing technologies have the ability to densely quantify soil organic matter (OM) variability utilizing visible and near infrared (VNIR) reflectance technology. However, issues such as soil texture, soil water content, and sensor-to-soil engagement can all affect OM prediction accuracy. Therefore, research was conducted to determine OM prediction accuracy across selected soils and soil volumetric water contents (VWC) with (i) a commercially-available, planter-mounted sensor and (ii) machine learning techniques applied to multiple combinations of soil reflectance bands within the VNIR spectrum. A total of 90 soils collected across several counties in Missouri and Illinois, USA were used in the modeling procedures for the study. Data were collected at three selected VWC with the Precision Planting SmartFirmer and a benchtop spectrometer. Spectral pre-processing and machine learning techniques were utilized for prediction of OM in all modeling approaches. Results found that SmartFirmer OM predictions were affected by soil VWC with OM predictions decreasing with increasing VWC. Additionally, accuracies degraded with increasing VWC (RMSE = 10.2-13.8 g kg^{-1}). Findings from three modeling approaches showed that a continuous spectrum (i.e., 400-1500 nm) greatly improved performance (RMSE = 5.25 g kg^{-1}) over the targeted wavebands used by the SmartFirmer. Furthermore, including the entire VNIR region (400-2500 nm) resulted in the best predictive capability (RMSE = 1.42 g kg^{-1}). However, because a full-spectrum approach may not be practical due to economic and computational expense, utilizing continuous reflectance from 400 to 1500 nm in conjunction with spectral pre-processing and machine learning may be an acceptable

method for estimating OM. These findings contribute to the development and improvement of commercially available proximal soil sensors that may be used to monitor soil carbon stocks, assess changes in soil health, or for other precision agriculture applications.

Introduction

Recent technology has allowed for the integration of soil sensors utilizing diffuse reflectance spectroscopy in the visible and near-infrared reflectance (VNIR) region into commercially available equipment. These sensor platforms can predict important agronomic soil properties that are critical for row crop production *in situ*, such as soil water and organic carbon or matter (OC/OM). In some scenarios, the predictions can be available in real-time, allowing for the potential to vary crop inputs and/or make on-the-go adjustments to row-crop production equipment (i.e., seeding depth). In order to use VNIR for real-time control or to estimate OC stocks, it is important for practitioners to recognize the capabilities and the limitations of VNIR sensing technology. Extensive laboratory research has illustrated the capabilities of VNIR sensing to estimate soil properties (i.e., soil water and OM) across a range of soils and environments (Brown et al., 2006; Rienzi et al., 2014; Zhou et al., 2022), illustrating strong opportunity for VNIR proximal sensing platforms. However, sensor accuracy has been found to decrease in circumstances where field-moist soils were evaluated, as opposed to dry and ground soil (Minasny et al., 2010; Bricklemeyer and Brown 2010). This has been largely attributed to the complex response of soil reflectance to varying VWC and interactions with other soil properties that affect spectral features (Lee et al., 2009; Rienzi et al., 2014). Additionally,

sensitivity to moisture has been found to vary within the VNIR region, with greater sensitivity found in longer wavelengths (>1400 nm; Lobell and Asner, 2002).

Several approaches have been evaluated to increase OM prediction accuracy for soils varying in soil water contents. Generally, adjustments have been made through one or more reflectance preprocessing techniques, such as standard normal variate (SNV), first or second derivative, detrending, and/or mean centering (Minasny et al., 2011; Cho et al., 2017; Zhou et al., 2022). Some of these techniques, such as the first derivative, require full spectrum sensing. However, current commercially-available, implement-mounted systems, such as Precision Planting's SmartFirmer (Precision Planting, Tremont, IL) or the Veris iScan (Veris Technologies, Salina, KS), target specific wavelength bands (e.g., 660 (±20) and 940 (±30) nm). The discrete waveband approach subsequently limits the application of some preprocessing techniques, such as derivatives, that have been found to aid in accounting for soil water. Thus, some platforms employing discrete waveband sensing require laboratory-measured OM from each field to develop a field-specific calibration (Lund and Maxton, 2019). This approach has been found accurate and repeatable across sensing dates where soil moisture varies (Chapter 1). However, it requires manual input, and does not allow the real-time predictions needed for variable-rate control. In contrast, commercial systems that predicts OM on-the-go have been found to be limited in accuracy and repeatability (Chapter 1).

Several prototype on-the-go diffuse reflectance spectroscopy sensors utilizing large portions of the VNIR or NIR spectral regions have been assessed for predicting OC, the primary constituent of OM (Christy, 2008, Bricklemeyer and Brown, 2010; Nawar and Mouazen, 2019). Generally, these studies demonstrated acceptable accuracy, with

some attaining RMSE near 5.0 g OC kg^{-1}. However, these results were generally achieved within a relatively small geography and limited number of fields (<10). Further, accuracy has been found to degrade if local (e.g., field-specific) OC information is not included in the modeling approach. Additional challenges exist with on-the-go measurements, from factors such as dust, soil smearing, light illumination angle, and variable distance between the sensor and the soil that can all introduce measurement error (Sudduth and Hummel, 1993; Mouazen et al., 2009). Collectively, these studies illustrate the complexity that would be required of systems deploying sensors for real-time OC/OM predictions.

In many analyses, VNIR-based OM predictions have been derived from statistical methods such as principal component regression (PCR) or partial least squares regression (PLSR) techniques (Sudduth and Hummel, 1991; Brown et al., 2006). However, recent advancements in statistical and machine learning have allowed for new approaches, such as decision trees, support vector machine regression (SVMR), and artificial neural networks. Several researchers have found similar or improved performance from the advanced techniques compared to traditional methodology on dry, ground soil (Viscarra Rossel and Behrens, 2010; Mouazen et al., 2010). Results reported by Morellos et al. (2016) on field-moist soils determined that Cubist and SVMR approaches outperformed PCR and PLSR modelling in one field in Premslin, Germany. Although these past studies are encouraging, more research is needed to understand how these modeling techniques could be applied to on-the-go sensors across varying soils and soil water contents.

Together, previous research illustrates the complexity and promising utility of OM predictions based on diffuse reflectance spectroscopy. However, investigation is still

needed to determine the optimum methodology for real-time sensing across a wide geography and varying soil water content. Therefore, research was conducted to determine OM prediction accuracy across varying soils and soil volumetric water contents with (i) a commercially-available, planter-mounted sensor and (ii) machine learning techniques applied to multiple combinations of soil reflectance within the VNIR spectrum.

Materials and Methods

Soil Information and Sample Preparation

Surface soils were obtained for the research project from the University of Missouri Soil Health Assessment Center (SHAC; n = 75). The soils ranged in parent material and were obtained in 2020 from throughout 17 counties within Missouri (MO), USA (Fig. 1). At each sampling site, three soil cores were taken to a 7.6 cm depth with a 7.6 cm i.d. tube. Soil from all three cores was composited into a single sample and submitted to the SHAC. They were then air-dried, ground to pass through a 2 mm sieve, and analyzed for texture and OC at the SHAC following established procedures (Burt, 2011; Nelson and Sommers, 1996). Combustion analyses was used to measure OC, and estimates were multiplied by the van Bemmelen factor of 1.72 to convert to OM (Cambardella et al. 2001). Analyses showed OM ranged from 14 to 60 g kg^{-1}, and clay content ranged from 98 to 376 g kg^{-1}.

An additional set of surface soils from Illinois (IL), USA were used as a testing dataset (n=15). These were archived, air-dried soils that were collected in the mid-1980s. They were originally selected to represent Illinois' agricultural soils and varied greatly in OM and clay content. Detailed analyses of the soil samples can be found in Sudduth and

Hummel (1991). In order to ensure consistency among datasets, these soils were re-analyzed for OC using the aforementioned procedures, and these results were used in the study. Similar to the MO set, OC estimates were multiplied by 1.72 to convert to OM. Analyses showed OM ranged from 5 to 59 g kg^{-1}, and clay content ranged from 36 to 315 g kg^{-1}.

Bulk density (BD) was measured on each soil after it had been ground and air-dried. To determine BD, soils were weighed in a container with a known volume (V = 344 cm^3). Established procedures were then used to estimate field capacity and wilting point of each soil utilizing the measured BD (Saxton and Rawls, 2006). Three target volumetric water content (VWC) values were used in the study. The first was that of the original air-dried soil (VWC 1). The second target (VWC 2) was the soil-specific field capacity minus 0.15 cm^3 cm^{-3}, which was near but not exactly equal to the wilting point plus 0.05 cm^3 cm^{-3} (Fig. 2). The third target was soil-specific field capacity minus 0.05 cm^3 cm^{-3} (VWC 3). These VWC levels were chosen to best represent a realistic range in field conditions a proximal soil sensor might encounter.

Data Collection and Processing: SmartFirmer

Data were collected from all soils (MO and IL) with Precision Planting's SmartFirmer at the three target VWC levels. Soils were placed in a section of steel channel that was 5 cm deep, 10 cm wide, and 61 cm long. The SmartFirmer was placed on the soil surface and lightly pressed against the soil during data collection. The sensor was engaged with the soil for 30 seconds to allow for time-series smoothing to occur within the system, and soils were scanned three times at each VWC. After the three scans were completed for a given soil, the steel channel was cleaned using compressed air.

The output from the SmartFirmer was logged at 1 Hz to the Precision Planting 20|20 display. These data consisted of OM, cation exchange capacity, furrow moisture, clean furrow, furrow uniformity, and temperature. The metrics, aside from temperature, were derived from the optical portion of the SmartFirmer that measures reflectance from five wavelength bands, centered at 468, 592, 858, 1198, and 1468 nm. Only the OM metric was used in the present study, and all OM values were converted from percent to mass basis (g kg^{-1}) for ease of comparison among SmartFirmer OM and laboratory data. The manufacturer's calibration relating OM to reflectance was based on OM data derived from the loss on ignition test (Nelson and Sommers, 1996; Precision Planting, 2018). The OM predictions from each of the three scans were averaged from the SmartFirmer. The last three logged observations from each of the three 30 second scans were included in the average (n = 9 observations per soil VWC).

Data Collection and Processing: Bench-top Spectrometer

Similar to the SmartFirmer, data were collected from the MO and IL soils at all three VWC with a FieldSpec Pro FR spectrometer (Analytical Spectral Devices (ASD) Inc., Boulder, CO). Spectral data were collected between 350 and 2500 nm at a 1 nm spacing. The ASD "mug lamp" high intensity light source was used to provide illumination. Measurements were collected through a 33 mm diameter glass-bottomed dish. At each VWC, three spectra were collected from each soil (rotating the dish 90° clockwise between each replication) and were subsequently averaged for analyses. Data were transformed to reflectance using a Spectralon (Labsphere, Inc., North Sutton, N.H.) white reference measurement repeated every fifteen scans (5 soil samples). Reflectance data from 350 to 399 nm were removed from the ASD dataset due to low signal to noise

ratio. Subsequently, the remainder of the spectra were smoothed using a 10 nm average to reduce the dimensionality of data for statistical modeling.

Modeling Procedures for Organic Matter Prediction

SmartFirmer

Linear regression models were examined using R Studio (RStudio Team, 2022) to evaluate the 1:1 relationship of SmartFirmer OM to laboratory measured OM at each of the three VWC levels. An additional regression model explored SmartFirmer OM prediction error as a function of laboratory-measured OM content. Regression models were considered significant at $P \leq 0.05$ and were compared using R^2 and RMSE.

Commercial Wavelength Bands (Targeted Bands)

Two modeling approaches similar to those used in commercially-available sensor systems were evaluated for estimating OM from soil reflectance in the VNIR region. The first approach evaluated data from the bands used by the SmartFirmer. Reflectance values for these wavelength bands were obtained from the 10 nm averaged data collected with the ASD at VWC 2 and VWC 3. These two VWC were chosen to best represent a range in water contents likely to be encountered in a field setting by a proximal soil sensor. To improve prediction capability, reflectance was converted to absorbance (eq. 1). Subsequently, the standard normal variate transformation (SNV) was applied to the absorbance spectra at the previously mentioned wavelengths (Pei et al., 2019). The transformed data were used as explanatory variables in the modeling of laboratory-measured OM.

$$Absorbance = log\left(\frac{1}{Reflectance}\right) \quad (1)$$

Commercial-Range Spectra

A second modeling strategy utilized reflectance data collected with the ASD from 400 to 1500 nm. This wavelength range was selected to encompass the full range of spectra used by commercially-available sensors (e.g., Precision Planting SmartFirmer, Veris iScan). This range is common in commercial sensors due to the affordability of the sensor systems. Extending into longer wavebands (>1500 nm) increases cost of the optical fibers required for instrumentation, and may not be practical for production agriculture equipment. The first derivative of reflectance was used as a preprocessing technique and was calculated from the 10-nm averaged spectra using the 'deriv' function within the 'stats' package in R Studio. This transformation technique has previously been found to be useful when evaluating soils at varying soil water contents (Rienzi et al., 2014; Zhou et al., 2022).

Full VNIR Spectra

The final approach utilized the first derivative of the full VNIR reflectance spectrum (400 to 2500 nm) for predicting OM. The only difference between the Commercial-Range Spectra and Full VNIR Spectra modeling approaches was the inclusion of spectral data from 1510 to 2500 nm. This full-spectrum analysis served as a benchmark of the maximum prediction capability of the dataset. Further, this analysis was included in order to provide insight into whether full spectra, rather than targeted wavelengths or partial spectra, could improve predictive ability.

Machine Learning Approach

A machine learning approach was utilized in all modeling strategies. Several machine learning algorithms were evaluated (e.g., ridge regression, random forest), but

the support vector machine regression (SVMR) algorithm was chosen due to consistent performance in all modeling approaches. The SVMR was fit in all scenarios using the 'caret' package in R Statistical Software (R Core Team, 2022). The SVM is a kernel-based method that was originally developed for binary classification and was later extended to multivariate regression (Drucker et al., 1997). The SVMR is based on the computation of linear regression in a multidimensional feature space. In the present study, the 'Linear' and 'Gaussian Radial Basis Function' kernel functions were evaluated. For our dataset, the 'Linear' kernel function best fit the data. Optimization of model parameters [cost (C) and epsilon(ε)] for each SVMR model were accomplished through a tenfold cross-validation procedure. The optimal C range was determined between 1-10, and the optimal ε was determined within the range of 0.01-0.1. The final, tuned models (optimal C and ε) were selected based upon the lowest RMSE observed from the optimization procedure.

The MO dataset was used for model fitting, with the data normalized and randomly split into training (70%) and testing (30%) datasets in R Studio. Once models were developed, they were tested on the 30% of data withheld from the MO dataset, as well as the entire IL dataset. Thus, the models were tested on data from two geographic areas, one from within the region where the models were trained (MO) and one from a separate geography (IL). Each was evaluated through the R^2 and the RMSE of the models fit on the training datasets.

Variable importance was evaluated for the Commercial-Range Spectra and Full-VNIR Spectra models to determine useful wavebands for prediction. Because all data were normalized, the coefficients at each waveband represented relative significance in

the model. Additionally, the sign of the coefficients represented a positive or negative relationship between predictor and response variables. The absolute value of each coefficient was used for determining waveband significance.

Results and Discussion

Precision Planting SmartFirmer

SmartFirmer OM predictions on the MO soils averaged 32, 28, and 27 g kg^{-1} at VWC 1, 2, and 3, respectively. This suggests that overall, for a given soil, an increase in VWC decreased SmartFirmer predictions of OM. Across all VWC, a positive relationship between SmartFirmer OM predictions and laboratory-measured OM was observed (R^2 = 0.15 to 23; Fig. 3; Table 1). Therefore, the sensor system was able to detect general trends in OM in the dataset. Additionally, the slopes of the regression equations were not significantly different among VWCs, indicating no influence of VWC on the relative response of SmartFirmer OM to laboratory-measured OM (Table 1).

In MO soils, SmartFirmer prediction error increased with VWC. Specifically, RMSE increased by 35% as VWC increased from air-dried to VWC 3 (Table 1). These findings align with field research that found no correlation between SmartFirmer OM and laboratory-measured OM at the wettest of three sensing dates (Conway et al., 2022). That study also suggested that soil texture may influence the repeatability of SmartFirmer OM, especially in sandy soils. In contrast, the present study found no relationship between the prediction error and clay content (data not shown), suggesting instead that differences could be due to other factors such as sensor-to-soil engagement in a field setting that the present study did not capture. A relationship was observed, however, between SmartFirmer prediction error and laboratory-measured OM (Fig. 4). More specifically, as

laboratory-measured OM decreased below 25 g kg^{-1}, SmartFirmer prediction error increased. In general, OM was underpredicted by the SmartFirmer, with greater underprediction occurring at higher levels of OM. In contrast, OM levels were overpredicted at OM < 25 g kg^{-1}. Overall, within the range of the present study (~10-60 g kg^{-1}), the largest error occurred at the highest levels of OM.

The average SmartFirmer OM among VWC was similar for the IL soils, averaging 34 g kg^{-1}. Further, a positive relationship between SmartFirmer OM and laboratory-measured OM was also observed across VWC (R^2 = 0.52), with no significant differences between the slope or intercept of the regression equations (Table 1; Fig 3). Interestingly, the SmartFirmer OM prediction was more accurate (lower RMSE and greater R^2) with the IL than the MO dataset, despite the similar ranges in OM. This could be due to the geography of the soils used to develop the SmartFirmer OM algorithm. If those soils were more similar to the IL soils than the MO soils, then the SmartFirmer might be expected to perform better on the IL soils compared with the MO soils. Research has found that including local or field-specific calibration data improves VNIR-based OM predictions, which is likely due to other soil characteristics (e.g., mineralogy) influencing spectral features (Christy, 2008; Lee et al., 2009; Nawar and Mouazen, 2019).

Similar to the MO soils, a negative relationship was observed between SmartFirmer prediction error and laboratory-measured OM in the IL soils (Fig. 4). However, the response was more centered around zero, with about an equal amount of over- and under-prediction. These results also suggest that the SmartFirmer may be better

calibrated to the IL soils, with the error deviating equally in positive and negative directions.

Spectrometer-Based Data Analyses

Commercial Sensor Wavebands

The primary goal of this analysis was to compare the SmartFirmer OM predictions with models developed using the same 5 targeted wavebands, but with the application of advanced modelling techniques and regionally-based calibration models. When utilizing the SNV-transformed reflectance from the five targeted wavebands used by the SmartFirmer, the SVMR prediction capability was mediocre (Table 2; Fig. 5). A positive correlation was observed in the 1 to 1 comparison in both MO datasets, with no clear influence of VWC on OM prediction. In each scenario, lower laboratory-measured OM values (<38 g kg^{-1}) were overpredicted while higher values were underpredicted. The error, however, was larger in the testing than the training dataset. Further, when the model was tested on the IL soils, no relationship was observed between laboratory-measured and predicted OM. Collectively, the testing results show poor predictive capability for soils outside of the training dataset.

The RMSE values observed in the Commercial Sensor Waveband (i.e., targeted waveband) approach were only slightly lower than those observed with the SmartFirmer data. The main difference between these two approaches was the calibration of the targeted wavebands. The Commercial Sensor Waveband set was calibrated to a subset of the regional data, whereas the SmartFirmer results relied on the internal calibration algorithm. These results suggest that a targeted waveband approach could be slightly improved if the model was exposed to soils from throughout the region where the sensor

was deployed (i.e., soil-specific algorithm). Additionally, findings demonstrated that when only using five wavebands within the VNIR region, little improvement in prediction performance was achieved even with advanced modelling techniques. In contrast, other researchers have successfully predicted OC through a discrete waveband approach (Henderson et al, 1992; Lee et al., 2009). However, the discrete bands chosen in those studies were generally at longer wavelengths than those utilized by the SmartFirmer. Therefore, a discrete approach may be improved with the addition of data from longer wavelengths.

Commercial-Range Spectra

The Commercial-Range Spectra approach, utilizing the 400-1500 nm range commonly found in commercial sensors, showed a strong relationship between predicted and laboratory-measured OM in the training and testing MO datasets (Fig. 6). Additionally, the R^2 and RMSE of the cross-validated training and testing MO datasets were very similar (Table 2), suggesting the model was robust and not overfit. No distinction was observed between the OM predictions at the varying VWC (Fig. 6). This suggests that the approach was able to compensate for the bimodal distribution of VWC present in the dataset. Similar results at varying VWC have been observed, where gravimetric water content, ranging from 150 to 250 g kg^{-1}, did not greatly affect OC predictions (Rienzi et al., 2014). Similar to our approach, their study also used the first derivative of reflectance as a preprocessing technique.

When the model was applied to the IL testing set, deviation from the 1 to 1 relationship and the RMSE increased relative to the MO testing set (Table 2; Fig 6). However, considering that the IL soils came from a separate geography and were not

represented in the model training dataset, these results could be considered successful. Accuracies (i.e., RMSE) in the testing datasets were within similar ranges to studies evaluating OC across a range of water contents within a cross-validation dataset (Nocita et al., 2011; Chaudhary et al., 2012; Rienzi et al., 2014). Additionally, these previous studies utilized reflectance at longer wavelength bands (e.g., 1500-2500 nm) than used in this analysis.

The results from the testing datasets improved considerably (higher R^2 and lower RMSE) in this analysis over the Commercial Sensor Waveband approach using only targeted wavebands. This suggests that information additional to that in the five targeted bands added significant predictive capability to the model. Peak wavelength bands similar to those used in commercial systems were influential in prediction (Fig. 7). For example, 450, 990, 1230, and 1450 nm were within the top ten of 110 most important variables for prediction in the Commercial Spectra approach (Fig. 7). These are at or near wavelength bands used in commercial systems (e.g., SmartFirmer, iScan) and were important for OC prediction in previous studies (Vohland et al., 2014; Ribeiro et al., 2021). The top five wavelengths for prediction were (in order from higher to lower importance) 1160, 1230, 610, 990, and 1450 nm. Wavelengths 1160 and 1450 nm are associated with carbon-oxygen bonds, such as carbonyl groups and wavelengths 990 and 1230 nm are associated with carbon-hydrogen bonds common to organic compounds. (Workman and Weyer, 2008; Rienzi et al, 2014). Collectively, the wavebands found useful for prediction in the present study, as well as those used by commercial sensors, have all been shown to relate to OC or be significant in predicting OC.

However, results from this study suggest that the targeted bands alone are not sufficient for robust prediction of OM, as illustrated by the Commercial Waveband analysis. To investigate targeted wavelength analysis further, the top five wavelengths selected in the Commercial-Range Spectra model were evaluated. Little improvement was observed over the Commercial Waveband approach (data not shown). This was attributed to consistencies between wavelengths used in the analysis and those utilized by the SmartFirmer (e.g., 1450 nm).

Full VNIR Spectra

The Full VNIR Spectra (400 to 2500 nm) modeling approach was evaluated as a benchmark to determine the maximum prediction capability present in the spectral dataset. Similar to the commercial approaches, VWC 2 and 3 were used in the model to represent field conditions. The results from the SVMR found excellent prediction capability for the MO training and testing datasets (Table 2; Fig. 8). The RMSE values for both datasets were much lower than those observed with the SmartFirmer or the Commercial Waveband and Commercial-Range Spectra approaches. For example, in the MO testing dataset, the RMSE was less than half of the Commercial-Range Spectra model RMSE (Table 2). This high level of performance has also been observed in other studies utilizing full-spectrum VNIR sensing and machine learning approaches (Brown et al., 2006; Cho et al., 2017; Liu et al., 2020). Interestingly, accuracy declined on the IL testing set, where RMSE increased to levels similar to the Commercial-Range Spectra model (~8 g kg^{-1}; Table 2). This suggests that the model may have been overfit on the MO training dataset, and therefore was not robust enough to predict a similar range of OM on soils from a different geography.

Some similarities in peak waveband significance were found between the Commercial-Range and Full VNIR Spectra analyses (Fig 7; Fig 9). For example, wavelengths 610, 1160, and 1450 nm were within the top 10 variables for prediction in both modeling scenarios. This supports the utility of collecting spectra from throughout the Full VNIR Spectra range used in the analysis for maximum predictive capability. For example, wavelengths 450, 1160, and 1450 were all within the top 5 most useful variables for the Full VNIR Spectra model within the aforementioned range. This suggests that despite the spectral range used in the modeling approach, significant spectral features within 400 to 1500 nm remained consistent.

These results suggest that the implementation of full-spectrum sensing could result in more accurate predictions in a globally-calibrated, on-the-go OM sensing system. However, the improved prediction capability comes, at least in part, due to information obtained from longer wavelengths (Fig. 9). These longer wavebands (e.g., 1600 and 2200 nm) have also been found to be highly significant in other studies (Stenberg et al., 2010; Cho et al., 2017; Zhou et al., 2022) and organic bonds are known to produce spectral features at these wavebands (e.g., Rienzi et al., 2014). However, the cost and complexity of sensing would increase when compared to systems including only shorter wavelength bands (< 1500 nm).

Conclusions

Results from this study showed that the commercial sensor system (SmartFirmer) detected general trends in OM from low to high across a wide range of soils from MO and IL. Depending on the application, this performance level may be sufficient, for example for determining relative differences in soil productivity or soil health. However,

OM predictions and accuracy were influenced by VWC. Thus, practitioners must realize that predictions could be temporally variable. If more consistent and accurate predictions are required (e.g., for carbon stock monitoring), additional spectral or soil information may be required. This could include full or partial spectra, local calibration samples, and/or publicly available soil information to improve OM prediction.

Results were not greatly improved when the five SmartFirmer wavebands were used to train and evaluate a model (Commercial Sensor Waveband analysis) on soils within a given region (i.e., MO.) Like the SmartFirmer algorithm, the model could detect relative differences between low and high OM. However, accuracy was mediocre. One notable benefit of the Commercial Sensor Waveband approach was that predicted OM did not vary with VWC.

Results from the Commercial-Range Spectra approach, which implemented wavelengths from 400 to 1500 nm, spectral pre-processing, and machine learning resulted in a significant increase in prediction capability. These results were considered robust due to the performance on both testing sets (MO and IL) and indicate that this approach likely would deliver the best combination of accuracy and practicality. Although this type of sensor system is more complex and costly than a discrete waveband approach, it is cheaper than a full spectrum system and provides a balance between performance and cost. Further research will be needed to determine how this approach performs under real world, in-field sensing conditions.

Bibliography

Bricklemyer, R. S., and D.J. Brown. 2010. On-the-go VisNIR: Potential and limitations for mapping soil clay and organic carbon. Computers and Electronics in Agriculture, 701: 209-216. https://doi.org/10.1016/j.compag.2009.10.006

Brown, D.J., K.D. Shepherd, M.G. Walsh, M.D. Mays, and T.G. Reinsch. 2006. Global soil characterization with VNIR diffuse reflectance spectroscopy. Geoderma 132: 273-290.

Burt, R. 2011. Soil Survey Laboratory Information Manual. Soil Survey Investigations Report No. 45. Version 2.0. USDA-NRCS.

Cambardella, C. A., A.M. Gajda, J.W. Doran, B.J. Wienhold, and T.A. Kettler. 2001. Estimation of particulate and total organic matter by weight loss-on-ignition. In R. Lal, J. M. Kimble, R. J. Follett, & B. A. Stewart (Eds.), Assessment methods for soil carbon (pp. 349–359). Lewis Publishers/CRC Press.

Christy, C. D. 2008. Real-time measurement of soil attributes using on-the-go near infrared reflectance spectroscopy. Comp and Elec in Agric. 61:10-19. https://doi.org/10.1016/j.compag.2007.02.010

Cho, Y., Sheridan, A.H., Sudduth, K.A. and Veum, K.S., 2017. Comparison of field and laboratory VNIR spectroscopy for profile soil property estimation. Trans. of the ASABE. 60:1503-1510. https://doi.org/10.13031/trans.12299

Chaudhary, V.P., K.A. Sudduth, N.R. Kitchen, and R.J. Kremer. 2012. Reflectance spectroscopy detects management and landscape differences in soil carbon and nitrogen. Soil Sci. Soc. Am. J. 76:597–606. doi:10.2136/ sssaj2011.0112

Conway, L.S., K.A. Sudduth, N.R. Kitchen, and S.H. Anderson. 2022. Repeatability of commercially available visible and near infrared proximal soil sensors. Precision Agriculture (in submission)

Drucker, C.H., C. Burges, L. Kaufman, A.J. Smola, V.N. Vapnik. 1997. Support vector regression machines. Adv. in Neural Information Processing Systems. 9:155-161.

Henderson, T.L., M.F. Baumgardner, D.P. Franzmeier, D.E. Stott, and D.C. Coster. 1992. High dimensional reflectance analysis of soil organic matter. Soil Sci. Soc. of Amer. J. 56:865-872.

Lee, K.S., D.H. Lee, K.A. Sudduth, S.O. Chung, N.R. Kitchen, S.T. and Drummond. 2009. Wavelength identification and diffuse reflectance estimation for surface and profile soil properties. Trans. of the ASABE. 52:683-695.

Liu, Y., C. Deng, Y. Lu, Q. Shen, H. Zhao, Y. Tao, and X. Pan. 2020. Evaluating the characteristics of soil vis-NIR spectra after the removal of moisture effect using external parameter orthogonalization. Geoderma, 376: 114568. https://doi.org/10.1016/j.geoderma.2020.114568

Lobell, D.B., and G.P. Asner. 2002. Moisture effects on soil reflectance. Soil Sci. Soc. of Amer .J. 66: 722-727.

Lund, E., and C. Maxton. Comparing organic matter estimations using two farm implement mounted proximal sensing technologies. In: Proceedings of the 5th Global Workshop on Proximal Soil Sensing, May 28-31, 2019, Columbia, Missouri. p 35-40.

Minasny, B., A.B. McBratney, V. Bellon-Maurel, J.M. Roger, A. Gobrecht, L. Ferrand, and S. Joalland. 2011. Removing the effect of soil moisture from NIR diffuse reflectance spectra for the prediction of soil organic carbon. Geoderma. 167:118–124. doi:10.1016/j.geoderma.2011.09.008

Mouazen, A.M., B. Kuang, J. De Baerdemaeker, and H. Ramon. 2010. Comparison among principal component, partial least squares and back propagation neural network analyses for accuracy of measurement of selected soil properties with visible and near infrared spectroscopy. Geoderma, 158:23-31. https://doi.org/10.1016/j.geoderma.2010.03.001

Nawar, S., and A.M. Mouazen. 2019. On-line vis-NIR spectroscopy prediction of soil organic carbon using machine learning. Soil and Tillage Research. 190:120-127. https://doi.org/10.1016/j.still.2019.03.006

Nocita, M., A. Stevens, C. Noon, and B. van Wesemael. 2013. Prediction of soil organic carbon for different levels of soil moisture using Vis-NIR spectroscopy. Geoderma 199:37–42. https://doi.org/10.1016/j.geoderma.2012.07.020

Nelson, D. W., and L.E. Sommers. 1996. Total carbon, organic carbon, and organic matter. Methods of soil analysis: Part 3 Chemical methods. 5:961-1010.

Precision Planting. 2018. SmartFirmer: Setup & Operation for Gen 2 20/20 Display. Retrieved from https://s3.amazonaws.com/pp3-products/file-1585250294/SmartFirmer%20Operators%20Guide%20-%20Gen3%20(955714).pdf

Viscarra Rossel, R.A., and T. Behrens. 2010. Using data mining to model and interpret soil diffuse reflectance spectra. Geoderma. 158:46–54. doi:10.1016/j. geoderma.2009.12.025

Workman, J., and L. Weyer. 2008. Practical guide to interpretive near-infrared spectroscopy. CRC Press, Boca Raton, FL.

Rienzi, E. A., B. Mijatovic, T.G. Mueller, C.J. Matocha, F.J. Sikora, and A. Castrignanò. 2014. Prediction of soil organic carbon under varying moisture levels using reflectance spectroscopy. Soil Science Society of America Journal. 78: 958-967.

Saxton, K.E. and W.J. Rawls. 2006. Soil water characteristic predictions by texture and organic matter for hydrologic solutions. Soil science society of America Journal. 70: 1569-1578.

Stenberg, B., R.A.V. Rossel, A.M. Mouazen, and J. Wetterlind. 2010. Visible and near infrared spectroscopy in soil science. In: D.L. Sparks, editor, Advances in agronomy. Vol. 107. Elsevier Academic Press, San Diego. 163–215.

Sudduth, K.A. and J.W. Hummel. 1991. Evaluation of reflectance methods for soil organic matter sensing. Trans. of the ASAE. 34: 1900-1909.

Sudduth, K.A. and J.W. Hummel. 1993. Soil organic matter, CEC, and moisture sensing with a portable NIR spectrophotometer. Transactions of the ASAE. 36:1571-1582.

Zhou, P., K.A. Sudduth, K.S. Veum, and M. Li. 2022. Extraction of reflectance features for estimation of surface, subsurface, and profile soil properties. Comp. and Elec. In Agric. 196: 106845. https://doi.org/10.1016/j.compag.2022.106845

Tables

Table 1. Coefficient of determination (R^2) and root mean squared error (RMSE) from soil organic matter (OM) prediction by the Precision Planting SmartFirmer on soils from Missouri (MO) and Illinois (IL) at three differing volumetric water contents (VWC). Regression relationships (slopes and intercepts) were not significantly different among VWC sets for IL soils, so only results for the aggregate relationship are presented.

	MO Soils		IL Soils	
Soil VWC	R^2	RMSE (g kg^{-1})	R^2	RMSE (g kg^{-1})
VWC 1	0.19	10.22	-	-
VWC 2	0.15	12.42	-	-
VWC 3	0.23	13.80	-	-
All VWC	0.17	12.25	0.52	11.2

Table 2. Prediction results for the three modeling approaches for the Missouri (MO) training, MO testing, and Illinois (IL) testing datasets.

	MO Train Set		MO Test Set		IL Test Set	
Model	R^2	RMSE (g kg^{-1})	R^2	RMSE (g kg^{-1})	R^2	RMSE (g kg^{-1})
Commercial Sensor Wavebands	0.41	7.41	0.25	9.23	N/A	17.2
Commercial-Range Spectra (400-1500 nm)	0.76	4.95	0.69	5.25	0.64	7.92
Full-Spectra (400-2500 nm)	0.98	1.34	0.98	1.42	0.66	7.76

Figures

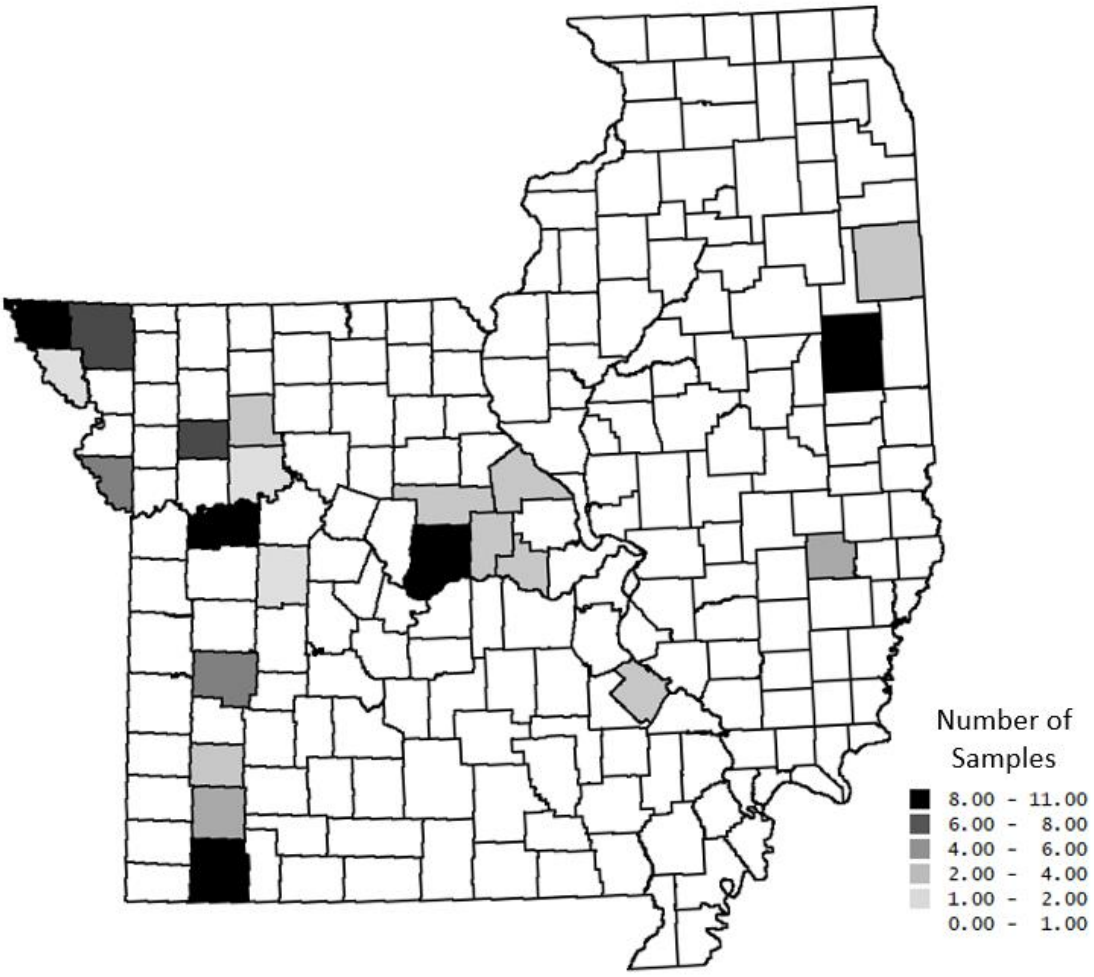

Fig. 1. Map of counties within Missouri and Illinois, USA that were the source of soil samples used in the study.

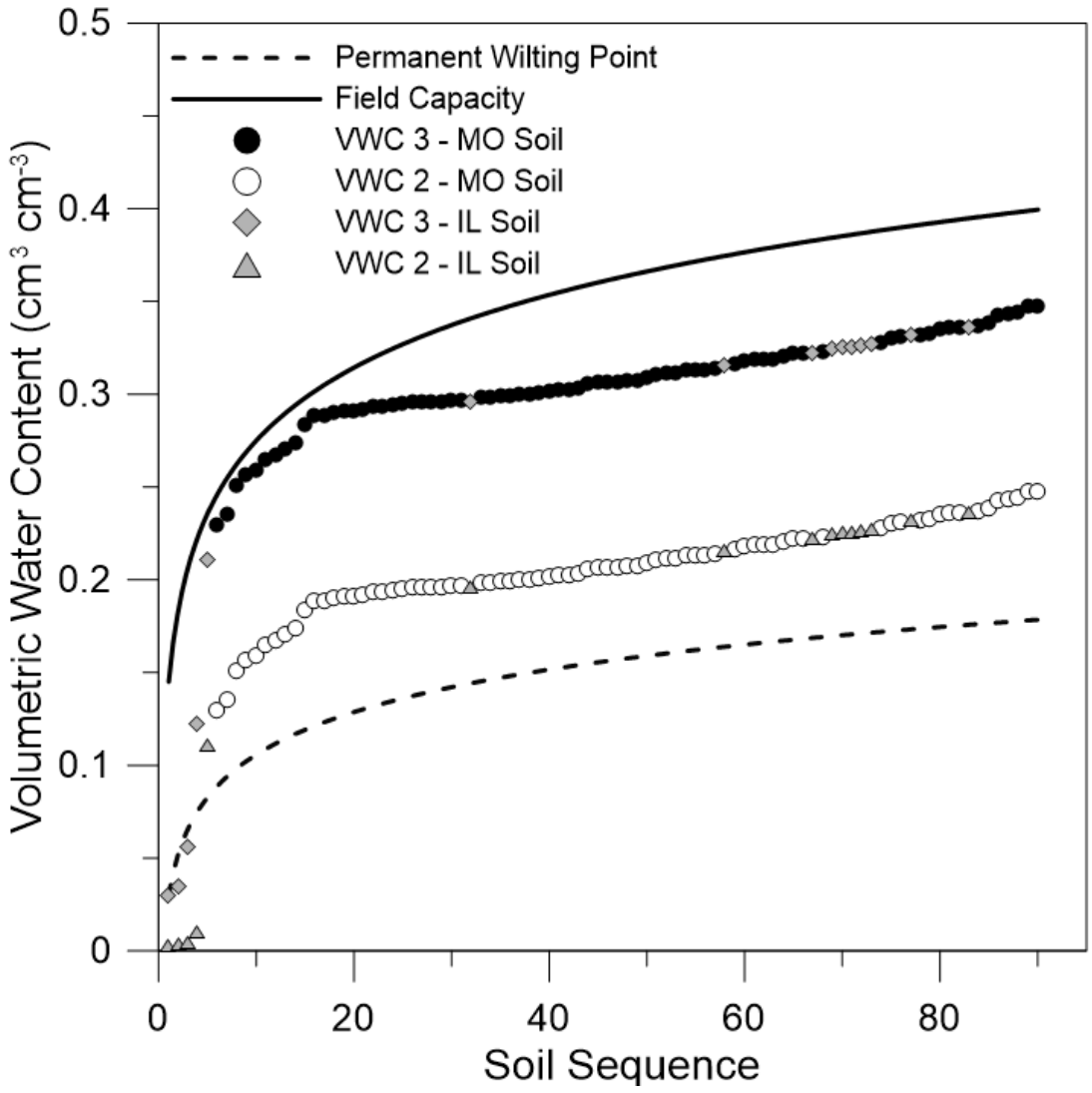

Fig 2. Target volumetric water content (VWC) for the two simulated moist soil conditions used in the study (VWC 2 and VWC 3) from Missouri (MO) and Illinois (IL), USA. Soils were sorted in sequence from smallest to largest VWC 3. For reference, best-fit curves are also shown for estimated field capacity and estimated permanent wilting point.

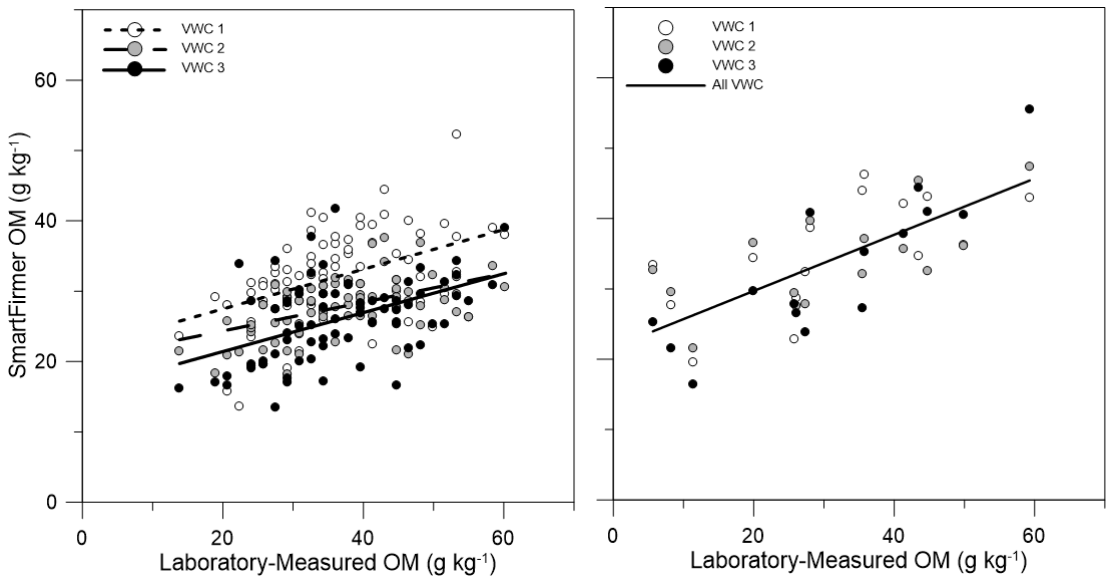

Fig. 3. SmartFirmer soil organic matter (OM) predictions across varying soil volumetric water content (VWC) in relation to laboratory-measured OM on soils obtained from Missouri (MO; left) and Illinois (IL; right). Regression relationships (slopes and intercepts) were not significantly different among VWC sets for IL soils. Therefore, only the aggregate relationship is presented.

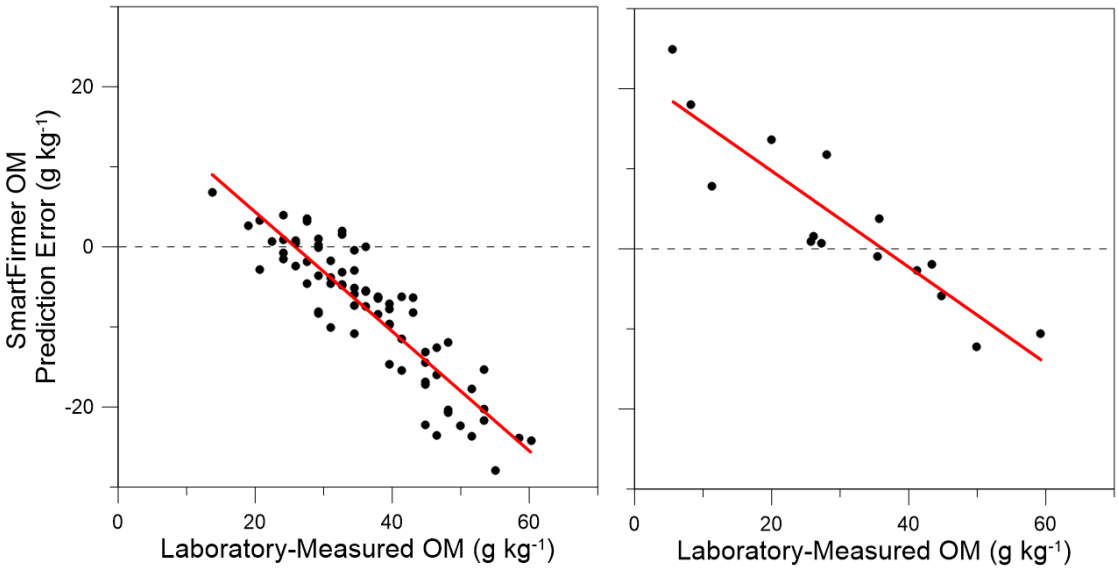

Fig. 4. SmartFirmer prediction error averaged across varying soil volumetric water content (VWC) in relation to laboratory-measured OM on soils obtained from Missouri (MO; left) and Illinois (IL; right).

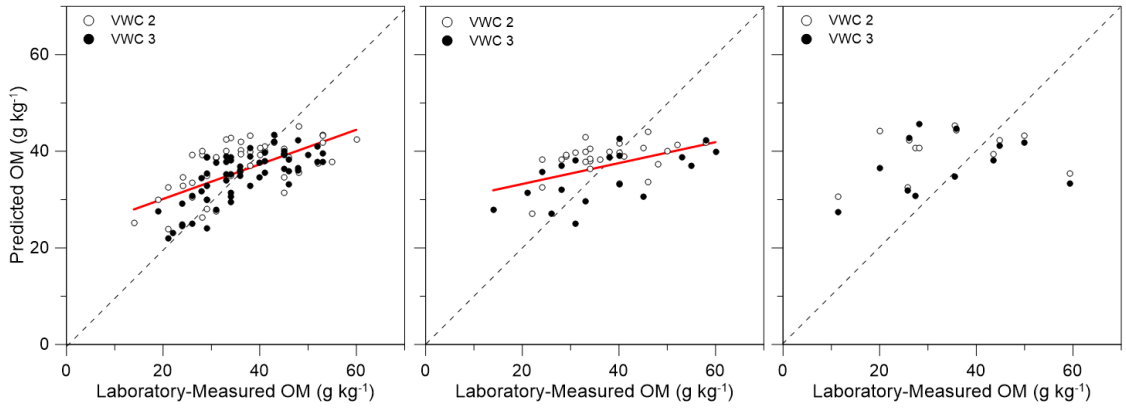

Fig 5. Predicted soil organic matter (OM) in relation to laboratory-measured OM for the Commercial Sensor Waveband approach at varying target soil volumetric water content (VWC) as shown in Fig 2. Results are shown for the Missouri (MO) training (left), MO testing (center), and Illinois (IL) testing (right) datasets.

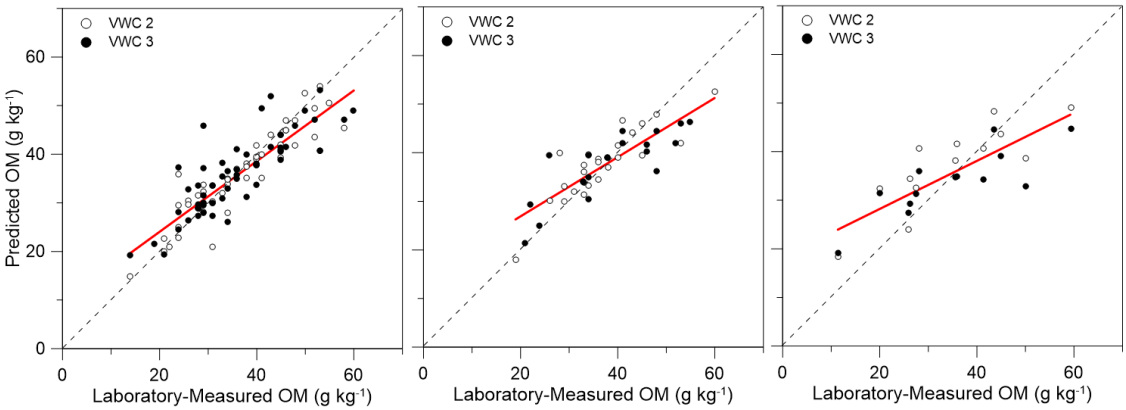

Fig 6. Predicted soil organic matter (OM) in relation to laboratory-measured OM for the Commercial-Range Spectra approach at varying target soil volumetric water content (VWC) as shown in Fig 2. Results are shown for the Missouri (MO) training (left), MO testing (center), and Illinois (IL) testing (right) datasets.

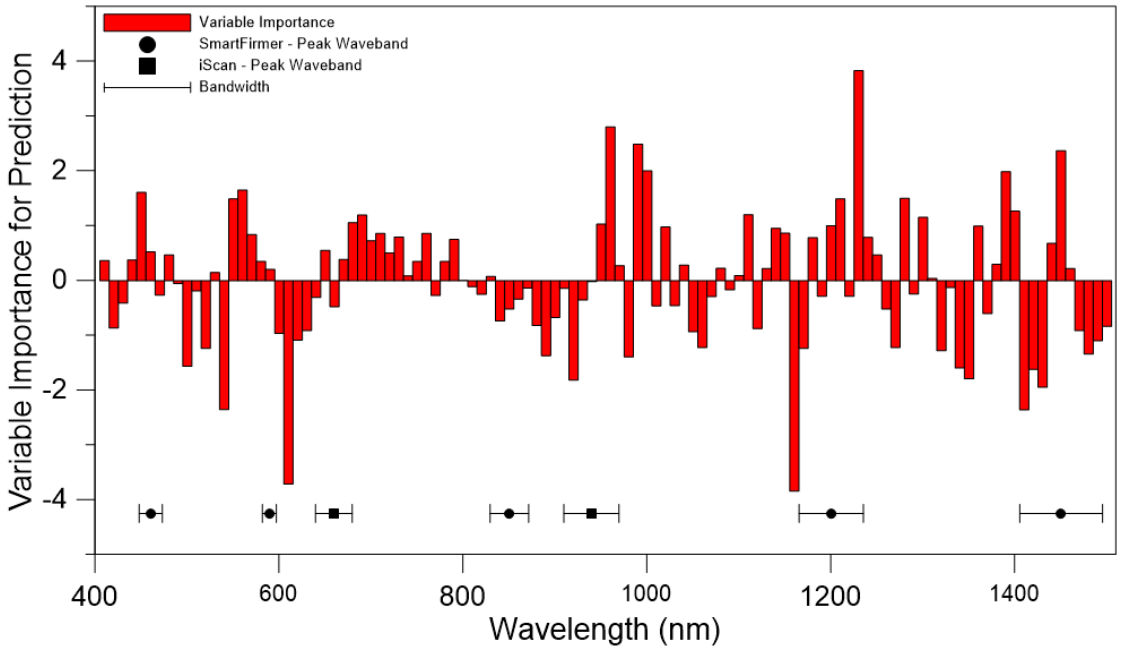

Fig. 7. Variable importance for prediction of organic matter as determined by support vector machine regression implemented in the Commercial-Range Spectra model, which utilized data from 400 to 1500 nm. SmartFirmer and iScan wavebands are indicated at the bottom.

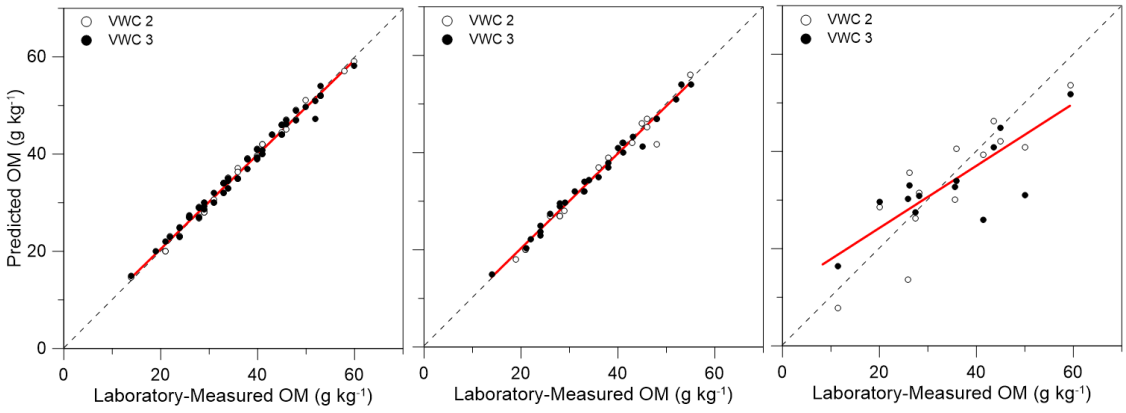

Fig 8. Predicted soil organic matter (OM) in relation to laboratory-measured OM for the Full VNIR Spectra approach at varying target soil volumetric water content (VWC) as shown in Fig 2. Results are shown for the Missouri (MO) training (left), MO testing (center), and Illinois (IL) testing (right) datasets.

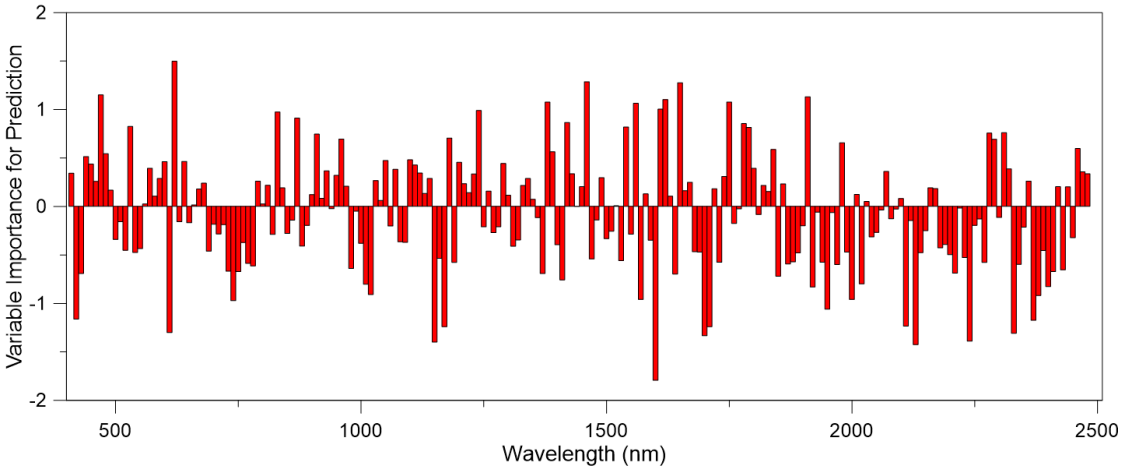

Fig. 9. Variable importance for prediction of organic matter as determined by support vector machine regression implemented in the Full VNIR Spectra model, which utilized data from 400 to 2500 nm.

CHAPTER 4: PREDICTING CORN EMERGENCE RATE WITH TOPOGRAPHIC FEATURES AND ON-THE-GO SENSING TECHNOLOGY

Abstract

Real-time sensor output during row-crop planting operations has the potential to improve control of multiple row-unit functions on-the-go. However, research is lacking on how best to maximize the utility of these new sensor systems across varying landscapes. Therefore, an investigation was conducted to determine if planter and other proximal soil sensor data, in combination with topographic features, could predict within-field variation in corn (*Zea mays* L.) emergence rate (ER) across multiple planting depth treatments. Research was conducted in Missouri, USA on a highly variable claypan soil field in 2020. Corn was planted with a four-row planter equipped with Precision Planting DeltaForce and SmartFirmer systems on each row unit. Four field-length strips of seed planting depth (3.8, 5.1, 6.4, and 7.6 cm) replicated three times were treatments to induce emergence variation. Machine learning approaches were applied to determine the predictive capability of planter sensors, soil apparent electrical conductivity (EC_a), and topographic features (slope, flow direction, and topographic wetness index) in estimating corn ER. Field-scale results from the planting depth treatments showed that planting depth had a marginal influence on corn stands, with stand densities decreasing slightly at 6.4 and 7.6 cm. Additionally, a suite of predictors could effectively estimate ER across the study site, with the highest accuracies observed at the 7.6 cm planting depth. Planter sensor variables representing estimates of inherent soil variability (i.e., OM and texture) were most useful in the ER prediction model, and were superior to estimates of furrow moisture and seed-to-soil contact. These results illustrate the ability to predict ER at a

field scale, and can be used as a framework for further research and development of planter sensor systems targeting uniform corn emergence.

Introduction

Research has found that corn seedling emergence is highly dependent upon seed-to-soil contact, soil moisture, aeration, and soil temperature (Alessi and Power, 1971; Gupta et al., 1988, Elmore et al., 2014). Studies have found optimum corn germination to occur at soil temperatures greater than 20 °C, at field capacity, and with good seed-to-soil contact (Schneider and Gupta, 1985). Generally, operators of row-crop seeding equipment target a planting depth, downforce, row-closing, and residue management strategy that optimizes these parameters. Across landscapes, however, spatial variability in seed zone soil properties often exists due to variations in soil texture, crop residues, and landscape attributes such as slope and aspect (Sudduth et al., 2005). In Missouri, USA (MO), many productive alluvial soils contain large within-field variations of texture, ranging from soils with high sand to high clay content (Miller and Krusekopf, 1918). Similarly, claypan soils in the same region possess landscape attributes and topsoil depth variations that result in complex hydrologic features (Jamison et al., 1968; Sadler et al., 2015).

Agronomic research has evaluated the impact of seeding depth on corn emergence, emergence rate, and yield across landscapes. Studies have aimed to determine whether the optimum planting depth should vary with soil type. Results from these studies are mixed, but have collectively illustrated that the optimal corn planting depth can vary from 2.5 to 7.6 cm based upon soil texture, moisture, temperature, and other factors (Stewart et al., 2021; Coronel et al., 2018; Thomison et al., 2013; Cox and

Cherney, 2015; Thomason et al., 2008). In general, however, research agrees that planting at depths less than 3.8 cm can negatively affect corn emergence due to poor seed-to-soil contact and vulnerability of the seed to moisture and temperature flux. Additionally, poor nodal root development at shallow planting depths can result in yield loss and lodging susceptibility (Elmore and Abendroth, 2007). Further research is needed to determine whether within-field soil moisture or estimations of seed-to-soil contact can give insight to growers to determine the optimum seeding depth for uniform emergence.

In an effort to improve seeding management across variable landscapes, precision agriculture research has explored varying seeding depths within a given field based upon changes in soil moisture (René-Laforest et al., 2015). Soil moisture estimated through a capacitance sensor was used as the guiding parameter because of the influence of soil moisture on germination, as well as the access to on-the-go soil moisture sensors. They found varying planting depth within a field improved corn root development and yield, a result attributed to planting shallower in relatively wet conditions and deeper in relatively dry conditions. Further research is needed to apply these results to more environments in the U.S. Midwest. In addition to sensor technologies, topographic features can give insight into soil water availability, movement, and accumulation across landscapes (Pachepsky et al., 2001). High-resolution elevation is now available through digital elevation models, as well as from machine data collected during field operations. An example often used is combining these landscape features into a calculated topographic wetness index that then can be related to crop performance (Kyveryga et al., 2011).

Many studies have applied machine learning to investigate agronomic questions (Gonzalez-Sanchez et al., 2014, Ransom et al., 2019; Qin et al., 2018). However,

machine learning approaches have not been widely applied for estimating corn emergence parameters. Due to recent technology that allows for dense quantification of soil variability by planter sensor systems, as well as through data collected with unmanned aerial vehicle (UAV) imagery, high-resolution field-scale datasets can now be collected, which subsequently allow for the application of machine learning techniques to help answer agronomic questions related to crop emergence performance.

Commercially-available planting technology now exists that allows for varying seed depth on-the-go during row-crop planting. However, emergence performance information is needed to show how seed zone soil sensors can be best utilized to guide row-unit automation. Therefore, this study was conducted to determine if soil sensor data and topographic features could be used in a machine learning approach to predict corn emergence rate (ER).

Materials and Methods

Study Site and Treatment Layout

Research was conducted in 2020 in central Missouri (38°56’45.7” N 92°07’57.4” W) on a 14-ha production agriculture field. The western portion (2.6 ha) of the field was used for this study. The site was located within the major land resource area 113, also known as the Central Claypan Area. The soil across the site was classified as a Mexico silt loam (fine, smectitic, mesic Vertic Epiaqualf). The field was chosen due to the inherent landscape variability that represented a typical claypan soil toposequence (summit, backslope, and footslope). Specifically, near the center of the field the slope was minimal, representing a more stable soil landscape (summit; Fig. 1). Moving N and S from the center of the field, the slope increased and was more representative of a

backslope position. The N and S facing slopes also supplied aspect variability, which can be visualized through flow direction (Fig. 1c). Lastly, slope decreased and areas of upslope accumulation of soil and water existed at the northernmost and southernmost portions of the field (footslope; Fig. 1b).

Mechanical variability was induced at the study site through three replications of four planting depth treatments (3.8, 5.1, 6.4, and 7.6 cm). All depth treatments were 8 rows wide (two planter widths) and were imposed across the entire transect length. In order to determine depth, closing wheels were tied up for trench inspection, and depth was measured from the top of the seed to the soil surface. The soil surface was determined by laying a flat stake perpendicular to the measuring tape, which stretched from the top of the seed to the soil surface. Subsequently, specific "T" handle settings were determined for each target planting depth. The target seeding rate for the study was 75,820 seeds ha^{-1}, and the corn hybrid used was Pioneer 0589 (Corteva Agriscience, Wilmington, DE, USA). The hybrid had an emergence rating of "7" on Pioneer's scale 1 to 9 scale, where a rating of 9 equated to the highest emergence rating. Corn was no-till planted into soybean stubble on 20 April 2020 with a four-row planter (0.76 m rows).

Seeding Equipment

The planter used in the study was equipped with MaxEmerge XP row units (Deere & Co., Moline, IL, USA). The row units did not include a residue management system (i.e., row cleaners, no-till coulters). The planter was attached to the three-point hitch of a John Deere 6110R tractor. The planter was ground-driven, and equipped with Precision Planting finger-pickup seed meters, an active hydraulic downforce system (DeltaForce®), and SmartFirmers (Precision Planting, LLC., Tremont, IL, USA) on each

row unit. No additional aftermarket components were present on the planter, and OEM rubber closing wheels were used.

The 6110R was equipped with automated machine guidance, where the steering was controlled through Deere's integrated automatic steering system (AutoTrac). This system utilized the StarFire 2 differential correction, which provided ±10 cm pass-to-pass accuracy. The average speed of the tractor during the seeding operation was 1.9 m s^{-1}. The "A-B" method of machine guidance was used, resulting in straight transects with a heading of 184 or 4°.

Planter Sensor Systems

Data from all Precision Planting sensor systems were logged to the Precision Planting 20|20 display (Generation 3) at 1 Hz. The GNSS position was derived from the StarFire 3000 receiver, allowing georeferencing of all data. The two systems providing data for analyses were DeltaForce and SmartFirmer. Data from the DeltaForce system consisted of ground contact (%), gauge wheel load (downforce; N), and downforce margin (N). Downforce margin is described as the minimum gauge wheel load (GWL) observed over a three second period. The hydraulic downforce system automatically adjusted row unit downforce or uplift to maintain a target gauge wheel load of 445 N. This technology improved the consistency of disk-opener operating depth at each of the targeted planting depth treatments.

The Precision Planting SmartFirmer used in the study is designed to mount to a planter row-unit behind the seed tube. This sensor replaces traditional seed firming devices. For this study, they were installed on each row of a 4-row planter. The lens of the SmartFirmer pressed against the sidewall, approximately 0.6 cm above the bottom of

the slot created by the disk-openers. Data layers from the SmartFirmer consisted of by-row furrow moisture (%), temperature (°C), OM (%), CEC (cmol 100 kg^{-1}), clean furrow (%), and uniform furrow (%). These metrics, aside from temperature, were derived from the optical portion of the sensor that measures reflectance from five wavelengths in the visible and near infrared (VNIR) region (468, 592, 858, 1198, and 1468 nm). The furrow moisture metric is defined by Precision Planting as the percent of water weight a corn seed is projected to imbibe over a three-day period (Precision Planting, 2018). As such, it is an index of water availability and is not equivalent to volumetric or gravimetric soil water content. The manufacturer's calibration relating OM to reflectance was based on OM data derived from the loss on ignition test (Nelson and Sommers, 1996; Precision Planting, 2018). SmartFirmer OM values were exported by-row from the 20|20, but row-level estimates were derived through an interpolation method using data from other row units (Strnad, 2018).

Emergence Monitoring

After planting and before corn emergence, emergence monitoring sites were identified and flagged in areas two rows wide by 6.0 m long. Two locations were chosen for each planting depth treatment within each replication (n = 24). In order to capture the maximum amount of variability in landscape attributes and soil moisture at the site, one area of high and one area of low furrow moisture were chosen within each planting depth treatment (8-rows) for the monitoring sites. These were selected based on the as-applied planter data obtained from the 20|20 display that was connected to an iPad (Apple, Cupertino, CA, USA) with the Climate Fieldview Cab application (The Climate Corporation, San Francisco, CA, USA) for data visualization. The locations were

georeferenced and marked by flagging using a handheld Trimble Geo 7x (Trimble, Inc., Sunnyvale, CA, USA). Throughout the emergence period, plants were marked with a unique colored plastic garden stake to differentiate between days of emergence (DOE). This staking occurred throughout the emergence period (12 to 22 days after planting (DAP)). These data were subsequently used to train and validate the unmanned aerial vehicle (UAV) estimated stand density and DOE.

UAV Data Collection

UAV image data were collected on 22 May 2020, which was 32 DAP and 20 d after the first emergence. Plants were between vegetative growth stages V2 and V4 at the time of data collection. The aerial images were collected from a Phantom 4 Advanced UAV imaging system (DJI, Shenzhen, Guangdong, China) with an onboard RGB camera. Images were taken sequentially for the entire study site at 0.5 frames per second, at a flight height of 10 m, and a speed of 2 m s^{-1}. More in-depth detail of the UAV data collection has been provided in Vong et al. (2022).

Stand Density and Day of Emergence

All emergence parameters were estimated based upon a deep learning model (ResNet18) trained with UAV imagery as detailed in Vong et al. (2022). Output from these models was used to create field-scale maps of stand density (plants m^{-1}) and days to imaging from emergence (d). Estimates of stand density and days to imaging from emergence estimates were considered successful with R^2 of >0.95.

The days to imaging from emergence parameter was converted to days from planting, then to growing degree days (GDD; °C) to account for temperature variations throughout the emergence period (Fig. 2). This was performed by summing the GDD

accumulated from planting to DOE. Others have shown that relating emergence to GDD is more helpful than chronological days when assessing agronomics of corn germination and emergence (Nemergut et al., 2021; Gupta et al., 1988).

Daily precipitation and temperature prior to and through the emergence period were obtained from a University of Missouri weather station, located at Bradford Research and Extension center approximately 9 km from the field (http://agebb.missouri.edu/weather). Growing degree days from planting through the emergence period were calculated based on temperature data collected from the aforementioned weather station. The GDD for each day were computed using the following equation:

$$GDD = \frac{Tmin+Tmax}{2} - 10\ °C \quad (1)$$

where GDD = growing degree days (°C); Tmin = daily minimum temperature (°C); Tmax = daily maximum temperature (°C)

Subsequently, the GDD from planting to DOE were summed to determine the required GDD for emergence (GDDE).

Emergence Rate and Uniformity

Field-scale emergence rate relative to planting depth (ER) was derived using UAV-estimated GDDE. The ER was calculated by subtracting the observed GDDE from the mean GDDE at each planting depth. Therefore, positive values represent a delayed ER relative to the mean for a given planting depth. Likewise, negative values represent a quicker-than-average ER. These ER values were calculated for each 1 m length of each row across the entire site.

Soil Sensing and Terrain Features

Soil apparent electrical conductivity (EC_a) from 0 to 0.3 and 0 to 0.9 m depths were measured across the entire site prior to corn planting using a Veris 3100 sensing system (Veris Technologies, Salina, KS, USA). In this study, only the 0 to 0.3 m data were used. The previously mentioned 6110R tractor and guidance system was used to pull the 3100, and data were collected at speeds of 2.2 m s^{-1} on a 9 m transect spacing.

Soil terrain features were calculated from the elevation data collected from the StarFire 3000 receiver and logged to the 20|20 display during planting. The elevation data were interpolated using inverse distance weighting (IDW) to a 6.1 m grid for analysis in Ag Leader's Spatial Management Software (SMS; Ag Leader Technology, Ames, IA, USA). Two metrics were subsequently calculated, and included slope and flow direction. These features were derived from the Spatial Analysis Toolbox in ArcGIS Pro (ESRI, Redlands, CA, USA).

Statistical Analysis

In order to understand the general effects of planting depth across the site, an analysis of variance (ANOVA) test ($\alpha = 0.05$) was performed to evaluate differences in ER at the different planting depths. When ANOVA results were found significant, the Tukey's Honest Significant Difference test was performed to determine differences between depths. These statistical analyses were all performed in RStudio using the "stats" package.

A machine learning approach was applied in all modeling strategies that utilized the field-scale data. The predictor variables for modeling the response variable of ER included all planter sensor metrics listed above (furrow moisture, OM, downforce margin, etc.), as well as soil EC_a, slope, and flow direction.

Predictor and response variables were at varying spatial resolutions and needed to be joined for data analysis. Planter sensor data layers recorded to the 20|20 display were first merged with the gridded EC_a and topographic features using the 'join and relates' feature in ArcGIS Pro. The join retained the row-level resolution of the data from the 20|20, which consisted of a grid cell that was one row wide (0.76 m) by 1 sec of travel (~2 m). Subsequently, the newly merged layer, consisting of all predictor variables, was joined to the to the UAV data layer containing ER. The ER data were in a vector format at a 1-m spacing down each row and were overlaid over the one-row wide grid of predictor variables. The spatially joined data typically resulted in two observations of ER data per one cell of joined predictor variables.

Multiple machine learning algorithms were evaluated (e.g., ridge regression, support vector machine regression, artificial neural network), but the random forest algorithm (RF) was chosen due to consistent performance and the ability for model interpretation. The RF models were fit and interpreted with the 'randomForest', 'randomForestExplainer', and 'ICEbox' packages in R Statistical Software (R Core Team, 2022). The RF algorithm is a supervised ensemble learning technique that can be used for classification or regression problems. It uses a bagging technique, where the data are split and regression trees are created in parallel (Leo et al., 2021). Within each tree, the RF randomly selects features to create a prediction model. In our scenarios, the number of variables evaluated at each split in the decision tree (*mtry*) was set to 3. The final (bagged) model, in our scenario, was an average of 500 separate regression trees. These trees were developed on 80% of the data and tested on the remaining 20%. The Pearson correlation coefficient (r), coefficient of determination (R^2) and root mean

squared error (RMSE) were calculated to interpret performance of the model in the training and testing datasets.

Predictor significance was analyzed using the minimal tree depth distribution from the 'randomForestExplainer' package in R. These values represent the average depth within the ensemble of decision trees that each variable was used to partition the dataset. Therefore, smaller values correlated to more significant variables, as they were used more often at shallow tree depths. In addition to the minimal depth distribution, the individual conditional expectations (ICE) algorithm was applied to covariates of interest, and subsequent plots were created using the 'ICEbox' package in R (Goldstein et al., 2015). This feature allowed for the interpretation of how each variable was used in prediction by the RF model. Specifically, the ICE plots displayed the estimated conditional expectation curves, each of which reflected the predicted response as a function of the covariate of interest, conditional on the distribution of additional covariates. Because the curve intercepts varied, model predictions were "centered" in ICE plots for improved interpretation among the varying intercepts. In the centering process, each curve was "pinched" at the minimum observation of the given predictor variable of interest. In each plot, 10 percent of the entire training dataset was used for visualization.

Results and Discussion

On the day of planting adequate soil moisture was observed for seed germination among the planting depths. This was attributed to a timely planting date and the 1.4 cm of precipitation that occurred in the 10 days prior to planting. On April 20, approximately 25 percent of the corn had been planted in MO according to the National Agricultural

Statistics Service (USDA, 2020). Approximately 48-hr after planting, 0.7 cm of precipitation was received at the study field (Fig. 2). This precipitation event was followed by an additional 5.4 cm of rainfall between 4 and 7 DAP. Other precipitation events also occurred at 9 and 15 DAP. Due to precipitation and moderate temperatures throughout the emergence period, no significant surface soil crusting was observed.

During planting, soil temperatures were measured between 13 and 18 °C by the SmartFirmer. Planting started in the morning, and soil temperatures warmed throughout the operation. For the first seven DAP, daily maximum air temperatures were typically near 20 °C, and minimum temperatures were between 3 and 10 °C. Temperatures moderated starting at about 15 DAP, with minimum temperatures nearing 0 °C. At this point, most of the corn plants had emerged from shallow depths, with some plants still emerging at the deeper planting depths. The decrease in temperature increased the total number of days for the deeper depths to emerge.

Spatial Variability in SmartFirmer Metrics and Soil Apparent Electrical Conductivity

Data collected with the SmartFirmers showed strong spatial structure in several of the metrics, such as OM and furrow moisture (Fig. 3). In general, OM estimates were greatest where the slope was also the greatest (Fig. 1; Fig. 3). The correlation of higher OM to areas of greater slope and erosion aligns with findings from data collected from other similar soil types in the region (Conway et al., 2019). Spatial variability in furrow moisture was observed in the study field, with the highest estimates observed in the northern, central, and southern portions of the field. The largest area of high furrow moisture was observed in the middle of the field, coinciding with high elevation and low slope. In the north portion, high values coincided with areas with of high EC_a (Fig 3).

Some visible N-S striping aligning with the planting depth treatments was apparent in the furrow moisture maps, where deeper planting depths coincided with greater furrow moisture (Fig. 4). Similarly, clear differences in clean furrow and furrow uniformity values were observed between planting depths. In general, both clean furrow and furrow uniformity decreased with increasing planting depth. The response of these metrics was attributed to larger amounts of residue present in the furrow at the shallow planting depths.

Soil EC_a showed similar spatial structure to furrow moisture. In most cases, high EC_a coincided with areas of high furrow moisture (Fig. 3). This was not surprising, as EC_a has been found to correlate to soil texture and water content (Corwin and Lesch, 2003; Sudduth et al., 2005). The two layers did deviate however, in the southwest corner, where a high furrow moisture was observed but a low soil EC_a. The deviations could have been caused by differences in the sensing depth of the systems. In some portions of the field, the EC_a estimates did not align with previous studies that have found EC_a to increase in areas of high propensity of erosion (Kitchen et al., 2005). In our study, areas with the highest slope (south central) corresponded to lower EC_a values. The cause of this phenomena was unknown, but could have been caused by the influence of soil water content and texture on EC_a.

Stand Density and GDDE

The mean number of plants observed at the monitoring sites did not differ by planting depth (mean = 64 plants or 69,200 plants ha^{-1}). Thus, stand densities were 91% of the applied seeding rate. This emergence rate was considered high for no-tillage conditions (Drury et al., 1999), and was attributed in part to adequate soil moisture,

temperature, and the technology present on the planter (i.e., hydraulic downforce). Contrary to the monitoring sites, the UAV-estimated stand density showed a slight decrease at the 6.4 and 7.6 cm seeding depths. When compared to the 3.8 cm depth the decrease was 1,300 and 2,400 plants ha^{-1} for the 6.4 and 7.6 cm depths, respectively. These results suggest that at our study site, seeding at depths greater than 5.1 slightly decreased corn stand densities. However, the effects were considered minimal and did not have a significant impact on corn yield (data not shown).

Visual inspection of the GDDE map (Fig. 5) of the study site showed clear distinctions between planting depths (Fig. 5). Specifically, the results found GDDE to average 60, 62, 64, and 65 °C for the 3.8, 5.1, 64, and 7.6 cm planting depths, respectively (Fig. 6). Thus, more GDD were generally required for deeper planting depths to emerge. This response was similar to results found by Stewart et al. (2021) and Nemergut et al. (2021). At our site, these results support the observation of adequate soil moisture for germination within all the planting depths. For example, no delay in emergence was observed with seeds planted at shallow planting depth. Although average GDDE was delayed with depth, some overlap still existed among planting depths (Fig. 5). This suggests that some seed zone soil variability of factors such as surface residue or soil moisture also affected DOE.

Emergence Rate

The clear effect of planting depth that was observed in GDDE was not as prevalent in the ER (Fig. 6). This was expected, as the ER calculation was performed to mask the effect of planting depth for analysis across the site. Additionally, the ER maps also aid in visualizing spatial variability across the site. For example, the southern portion

of the field had generally smaller ER than the central and northern portions, a feature that is not clear in the map of GDDE. Additionally, a cluster of high ER was observed in the north-central and north-western portions of the field, which coincided with areas of high furrow moisture, OM, and EC_a. This zone was also north-facing and at a low-lying position in the landscape (Fig 1, Fig. 3). These results do not align with those presented by Stewart et al. (2021) on a similar soil type, who found more rapid emergence at footslope positions (higher soil moisture environment). The difference may have been caused by drier and warmer condition observations at planting in the years evaluated in their study. Collectively, these studies highlight the complex dynamic of soil, weather, and landscape effects on corn ER of a given soil type.

Additional mechanical variability was also observed through N-S "striping" of ER (Fig. 6). However, the striping did not align directly with row-level data collected by the planter sensor systems, suggesting that prior field operations were likely the cause. Throughout the field's history, field operations have typically occurred N-S. Because of this, and because the field has been in no-tillage, these effects were likely caused by the influence of historical field traffic and residue distribution. These operations potentially caused variability in compaction and residue distribution across the field.

Field-scale Results

The field-scale modeling of ER was performed to evaluate the impact of soil, machine, and landscape across the study site. The results from the ER model developed across planting depths showed positive relationships between predicted and UAV-estimated ER in the testing datasets (Table 1; Fig 7). At all depths, results from the testing datasets were similar (RMSE = 1.25to 1.38°C). This suggests that despite

differences in planter-based metrics, such as clean furrow, the random forest algorithm was able to decipher between areas of smaller (quicker) and larger (longer) ER at each planting depth.

Variable Significance

Not surprisingly, the most important variables for prediction varied among planting depth (Fig. 8). This was attributed to differences in seed zone properties at each depth, which influenced sensor metrics (e.g., clean furrow; Fig 8). Despite the variation, several variables were consistently useful in the models. At each planting depth, flow direction was one of the top four predictors. This was likely due to the N-S aspect of the field. The response of ER to aspect as discussed above is noted, where clusters of smaller ER were observed on the southern portion and higher ER observed on the northern portion of the field. In addition to flow direction, slope, OM and, soil EC_a were also consistently top variables for prediction. This was likely due to these metrics capturing inherent soil spatial variation at the site, and can be observed in Figure 3.

Interestingly, metrics such as clean furrow (indication of seed-to-soil contact) or furrow moisture were useful at some depths, but were not typically the most important variables for prediction. This indicates that furrow moisture was likely adequate to initiate germination at all planting depths. Additionally, although more residue was present in the furrow at the shallow planting depths, it did not have a large impact on ER when compared to terrain features and other soil sensor data (e.g., SmartFimer OM and EC_a). Collectively, the results suggest that inherent soil variability associated with landscape variation was the driving factor for ER. These results are promising, because many of these inherent variables could be estimated prior to planting, allowing for a

depth, residue management, or GWL prescription prior to the actual planting operation. Subsequently, these prescriptions could then be “fine-tuned” by real-time sensing of seed zone soil properties.

Variable Use in Random Forest Models

Temporally Variable Predictors

The ICE plots allowed for an interpretation of how specific variables were used by the model. Three planter sensor-based metrics were assessed (furrow moisture, clean furrow, downforce margin; Fig. 9). Furrow moisture was evaluated due to the known impact of soil moisture on germination, and because commercially available equipment controls planting depth based upon furrow moisture (e.g., Precision Planting SmartDepth). Clean furrow was evaluated because it was a proxy for seed-to-soil contact, another important factor for seed germination. Additionally, potential exists to guide residue management in real-time with this or a similar estimate of furrow residue. Lastly, downforce margin was assessed because in our study, downforce margin was the most useful metric from the DeltaForce system for estimation of ER. Further, a significant percentage of planters are equipped with active or static downforce systems that can sense GWL, allowing for high resolution quantification of variability in soil resistance.

Results found that, at all depths except 7.6 cm, estimates of emergence rate increased with furrow moisture. An example of the 3.8 and 7.6 cm depth can be found in Fig. 9. The lack of clear response observed at 7.6 cm was attributed to smaller amounts of variability in furrow moisture present at the 7.6 cm depth. These results suggest that targeting a lower furrow moisture generally decreased ER at our study site. These results would likely invert under drier conditions (e.g., late planting date). Therefore, a soil

moisture-driven variable depth system likely should have a dynamic target that incorporates a low and high soil moisture threshold.

The ICE for clean furrow at varying ER predictions showed a negative response at shallow and deep planting depths, illustrating that ER predictions decreased as clean furrow increased irrespective of depth. These results would align with recommendations from Precision Planting, which suggest targeting a clean furrow value of greater than 95%, which would result in an estimate of less than 5% residue in the furrow. Therefore, these results suggest that clean furrow estimates could be used to guide residue management systems to optimize seed-to-soil contact at shallow planting depths in no-tillage conditions.

In our study, downforce margin (minimum GWL) was the most useful metric from the DeltaForce system in estimating ER. However, the significance in the model was low compared to the other predictor variables. At the shallowest depth, a negative correlation was observed between downforce margin and model predictions (Fig. 9). This may indicate that seeds planted in areas with low margin may not have been at the target planting depth, were dropped during row-unit bounce, and/or were placed in soil with high amounts of resistance (Badua et al., 2021; Brune et al., 2018). Collectively, these factors could result in seeds planted at a depth less than the target of 3.8 cm, in little contact with the soil, and/or into compacted soils. A similar, negative relationship was observed at the deeper planting depth although the magnitude of the response decreased. This could have been due to seeds planted in areas of low margin emerging quicker in some cases because they were closer to the soil surface. At shallow depths, lower margin values may have correlated to areas where the row-unit was bouncing out of the soil, and

subsequently misplacing seed. On the contrary, at deeper planting depths, low margin values may have simply been caused by planter row-units not reaching the target depth (i.e., no GWL).

Temporally Stable Predictors

In addition to planter-sensor metrics, ICE plots of three inherent soil properties were also evaluated (flow direction, EC_a, and SmartFirmer OM). Each of these variables were highly significant in all ER planting depth models, with the exception of OM at the 6.4 cm planting depth. In general, the relative relationship of ER to these three inherent soil properties were similar among depths. Thus, for simplicity, ICE plots were created from predictor variables at the 7.6 cm depth. This depth was chosen because the temporally variable metrics (e.g., furrow moisture and clean furrow) were low in significance, which was attributed to the lack of variability in these metrics at the deeper depth. Therefore, the responses to the temporally stable variables were more clearly defined.

The lowest ER was estimated in areas with high flow direction values (Fig. 10), which generally corresponded to south-facing slopes at the site (Fig. 3). Thus, the southern aspect of the field may have stayed warmer throughout the emergence period, resulting in a quicker emergence. The use of EC_a in modeling showed smaller ER estimates in areas of low EC_a (Fig. 10). On the contrary, higher OM was associated with a decrease in estimated ER. Collectively, these responses show that corn emerged quickest on soils that were south-facing, high in OM, and exhibited low EC_a. However, significant variability still existed in these responses, suggesting there were complex interactions and potential areas to improve row-unit management to minimize corn ER.

Conclusions

Results from the planting depth analyses illustrated that planting depth influenced corn emergence parameters, such as stand density and GDDE. Interestingly, planting at the deepest depth (7.6 cm) had little to no effect on corn stand density. This further illustrates the resiliency of corn to emerge from a range of planting depths. Additionally, planting at deeper depths resulted in less variability in ER, suggesting it may be more advantageous to plant corn slightly deeper than traditional recommendations to avoid seed zone variability of moisture, temperature, and residue. However, this conclusion is based on this one no-till case study field; verifying this in other environments is needed. Although deeper planting has been advocated for coarser textured soils, our results found it also to be advantageous on a fine textured claypan soil. This may have been caused by the lack of bare soil present over the seed trench (due to no residue management system) to help reduce soil crusting.

Outcomes from the ER analysis show the potential for combining multiple spatial data layers, both sensor and terrain-based, to predict corn ER. Factors important for predicting ER varied with depth, but these findings showed that a variety of layers were often useful in prediction, including SmartFirmer and DeltaForce metrics, as well as topographic features like surface water flow direction. Therefore, further work is needed to determine whether automated row-unit control could utilize these parameters to adjust in real-time and improve ER, and likely increase emergence uniformity.

Although this research was only conducted on one soil type in one year, it provides a framework for future research evaluating precision seeding technologies at the field scale. Additionally, the results give insight into potential significant and dynamic

planter and soil landscape variables that influence emergence performance. As these are better understood and predicted, they can more reliably be used in planting operations to optimize corn emergence uniformity.

Bibliography

Alessi, J. and Power, J.F., 1971. Corn emergence in relation to soil temperature and seeding depth 1. Agronomy Journal. 63:717-719.

Badua, S. A., Sharda, A., Strasser, R., & Ciampitti, I. 2021. Ground speed and planter downforce influence on corn seed spacing and depth. Precision Agricultre. 22:1154-1170.

Conway, L.S., N.R. Kitchen, K.A. Sudduth, D.B. Myers, A.J. Lindsey, and P.R. Carter. Comparing organic matter estimations using two farm implement mounted proximal sensing technologies. In: Proceedings of the 5th Global Workshop on Proximal Soil Sensing, May 28-31, 2019, Columbia, Missouri. p 47-52.

Coronel, E. G., Alesso, C. A., Bollero, G. A., Armstrong, K. L., & Martin, N. F. 2020. Field-specific yield response to variable seeding depth of corn in the Midwest. Agrosystems, Geosciences & Environment, 3, e20034. https://doi.org/10.1002/agg2.20034

Corwin, D.L. and Lesch, S.M., 2003. Application of soil electrical conductivity to precision agriculture: theory, principles, and guidelines. Agronomy Journal. 95:455-471.

Cox, W. J., & Cherney, J. H. 2015. Field-scale studies show site-specific corn population and yield responses to seeding depths. Agronomy Journal. 107:2475–2481. https://doi.org/10.2134/agronj15.0308

Elmore, R., M. Al-Kaisi, and M. Hanna. 2014. Corn seeding depth: Back to the basics. Integrated Crop Management News. Ames: Iowa State University Extension. Retrieved from https://extension.umd.edu/sites/default/files/_docs/Agronomy%20News%20May%201%202014.pdf

Elmore, R. W. and L. J. Abendroth. 2007. Allelopathy: a cause for yield penalties in corn following corn? Integrated crop management newsletter. Iowa State University. 25 Oct 2010.

Goldstein, A., A. Kapelner, J. Bleich, and E. Pitkin. 2015. Peeking inside the black box: Visualizing statistical learning with plots of individual conditional expectation. Journal of Computational and Graphical Statistics. 24: 44-65.

Gonzalez-Sanchez, A., J. Frausto-Solis, and W. Ojeda-Bustamante. 2014. Predictive ability of machine learning methods for massive crop yield prediction. Spanish. Journalof Agriculture Research. 12:313–328. doi:10.5424/ sjar/2014122-4439

Gupta, S.C., E.C. Schneider, and W.B. Swan. 1988. Planting depth and tillage interactions on corn emergence. Soil Science Society of America Journal. 52:1120–1127.

Hummel, J.W., K.A. Sudduth, and S.E. Hollinger. 2001. Soil moisture and organic matter prediction of surface and subsurface soils using an NIR soil sensor. Computers and Electronics in Agriculture. 32: 149-165.

Jamison, V.C., D.D. Smith, and J.F. Thornton. 1968. Soil and water research on a claypan soil. Tech. Bull. 1397. USDA-ARS, Washington, DC.

Kitchen, N.R., K.A. Sudduth, and S.T. Drummond. 1999. Soil electrical conductivity as a crop productivity measure for claypan soils. Journal of Production Agriculture. 12:607–617.

Kyveryga, P. M., T. M. Blackmer, and P. C. Caragea. 2011. Categorical analysis of spatial variability in economic yield response of corn to nitrogen fertilization. Agronomy Journal. 3: 796-804.

Leo, S.; M.D.A. Migliorati, and P.R. Grace. Predicting within-field cotton yields using publicly available dataset and machine learning. Agronomy Journal. 113: 1150–1163

Nelson, D. W., and L.E. Sommers. 1996. Total carbon, organic carbon, and organic matter. Methods of soil analysis: Part 3 Chemical methods. 5:961-1010.

Nemergut, K.T., P. R. Thomison, P.R. Carter, and A.J. Lindsey. 2021. Planting depth affects corn emergence, growth and development, and yield. Agronomy Journal. 113: 3351-3360.

Pachepsky, Y. A., Timlin, D. J., & Rawls, W. J. (2001). Soil water retention as related to topographic variables. Soil Science Society of America Journal, 65(6), 1787–1795. https://doi.org/10.2136/sssaj2001. 1787

Pioneer. (2013). Corn planting and stand establishment (Field Facts). Pioneer.

Precision Planting. 2018. SmartFirmer: Setup & Operation for Gen 2 20/20 Display. Retrieved from https://s3.amazonaws.com/pp3-products/file-1585250294/SmartFirmer%20Operators%20Guide%20-%20Gen3%20(955714).pdf

Qin, Z., Myers, D. B., Ransom, C. J., Kitchen, N. R., Liang, S.-Z., Camberato, J. J., et al. 2018. Application of Machine Learning Methodologies for Predicting Corn Economic Optimal Nitrogen Rate. Agronomy Journal. 110, 2596– 2607. doi: 10.2134/agronj2018.03.0222

R Core Team. 2022. The R project for statistical computing. Retrieved from https://www.r-project.org

René-Laforest, F. F. 2015. Real-time variable control technologies for precision agriculture. (Master's thesis, McGill University, Montreal, QC, Canada). Retrieved from https://escholarship.mcgill.ca/concern/ theses/fx719q20j

Ransom, C. J., Kitchen, N. R., Camberato, J. J., Carter, P. R., Ferguson, R. B., Fernández, F. G., et al. 2019. Statistical and machine learning methods evaluated for incorporating soil and weather into corn nitrogen recommendations. Computers and Electronics in Agriculture. 164:104872. doi: 10.1016/j.compag.2019.104872

Sadler, E.J., K.A. Sudduth, S.T. Drummond, E.D. Vories, and P.E. Guinan. 2015b. Long-term agro-ecosystem research in the Central Mississippi River Basin: Goodwater Creek Experimental Watershed weather data. Journal of Environmental Quality. 44:13–17. doi:10.2134/jeq2013.12.0515

Schneider, E. C., and S.C. Gupta. 1985. Corn emergence as influenced by soil temperature, matric potential, and aggregate size distribution. Soil Science Society of America Journal, 49: 415–422.

Stewart, S., N.R. Kitchen, M.A. Yost, L.S. Conway, and P. Carter. 2021. Planting depth and within-field soil variability impacts on corn stand establishment and yield. Agrosystems, Geosciences & Environment 4:e20186.

Sudduth, K. A., N. R. Kitchen, W. J. Wiebold, W. D. Batchelor, G. A. Bollero, D. G. Bullock, D. E. Clay et al. 2005. Relating apparent electrical conductivity to soil properties across the north-central USA. Computers and Electronics in Agriculture 46: 263-283.

Thomason, W. E., Philips, S. B., Alley, M. M., Davis, P. H., Lewis, M. A., & Johnson, S. M. 2008. In-row subsoil tillage and planting depth influence corn plant population and yield on sandy- textured MidAtlantic Coastal Plain soils. Crop Management, 7, 1–12. https://doi. org/10.1094/CM-2008-0519-01-RS

Vong, C.N., L.S. Conway, A. Feng, J. Zhou, N.R. Kitchen, and K.A. Sudduth. 2022. Corn emergence uniformity estimation and mapping using UAV imagery and deep learning. Computers and Electronics in Agriculture. (*in press*)

USDA. 2020. Agricultural Statistics Service. U.S. Gov. Print. Office, Washington, DC

Tables and Figures

Table 1. Prediction statistics of emergence rate by the soil sensor and terrain data layers at the four planting depths. The results represent model performance on the testing dataset used at each planting depth.

Model	r	R^2	RMSE (°C)
3.8 cm planting depth	0.86	0.75	1.25
5.1 cm planting depth	0.84	0.67	1.36
6.4 cm planting depth	0.85	0.71	1.27
7.6 cm planting depth	0.84	0.74	1.38

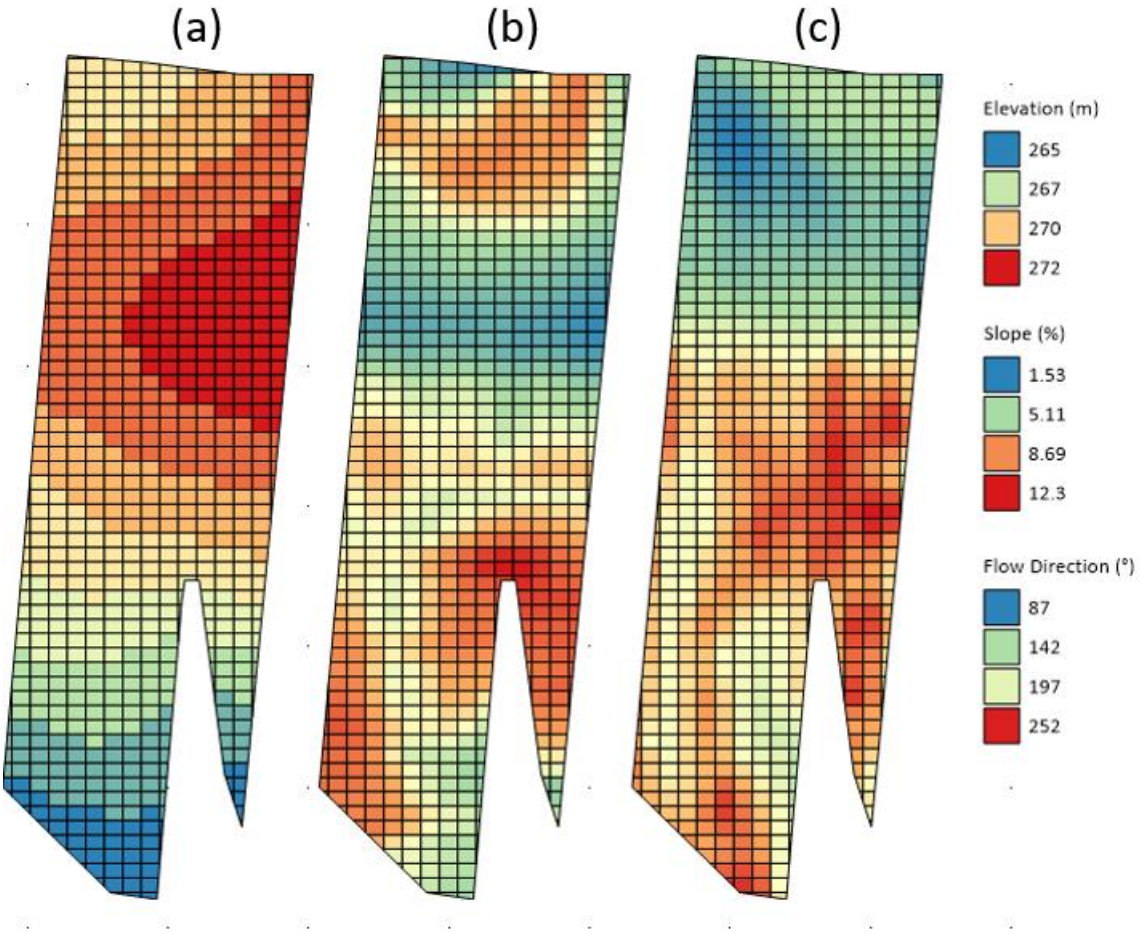

Fig. 1. Elevation (a), slope (b), flow direction (c) for the study site in central Missouri, USA.

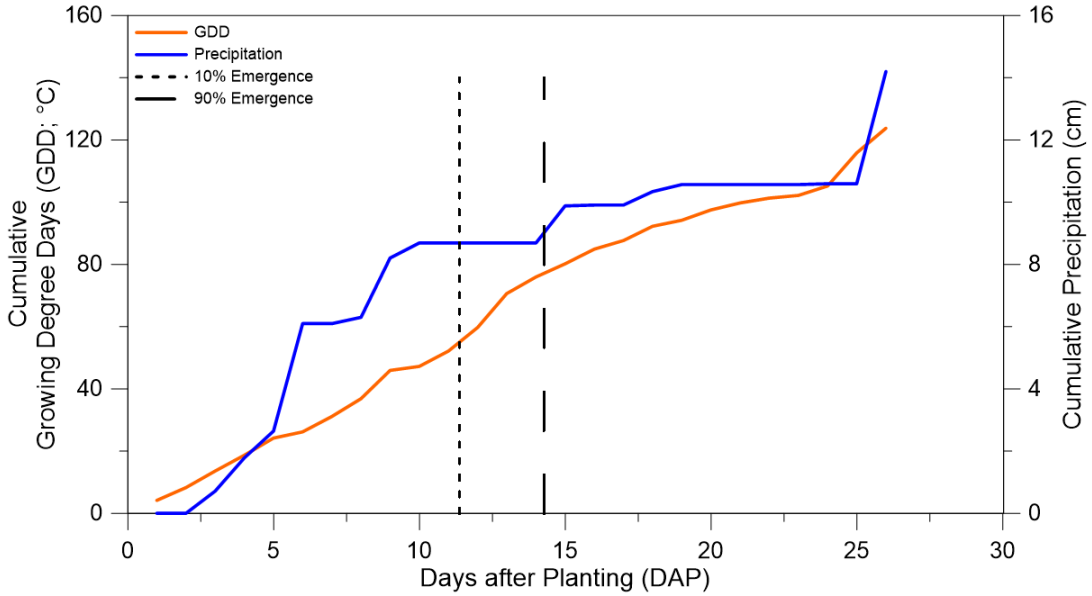

Fig. 2. Cumulative precipitation and growing degree days at the study site in central Missouri, USA from the time of planting through the corn emergence period.

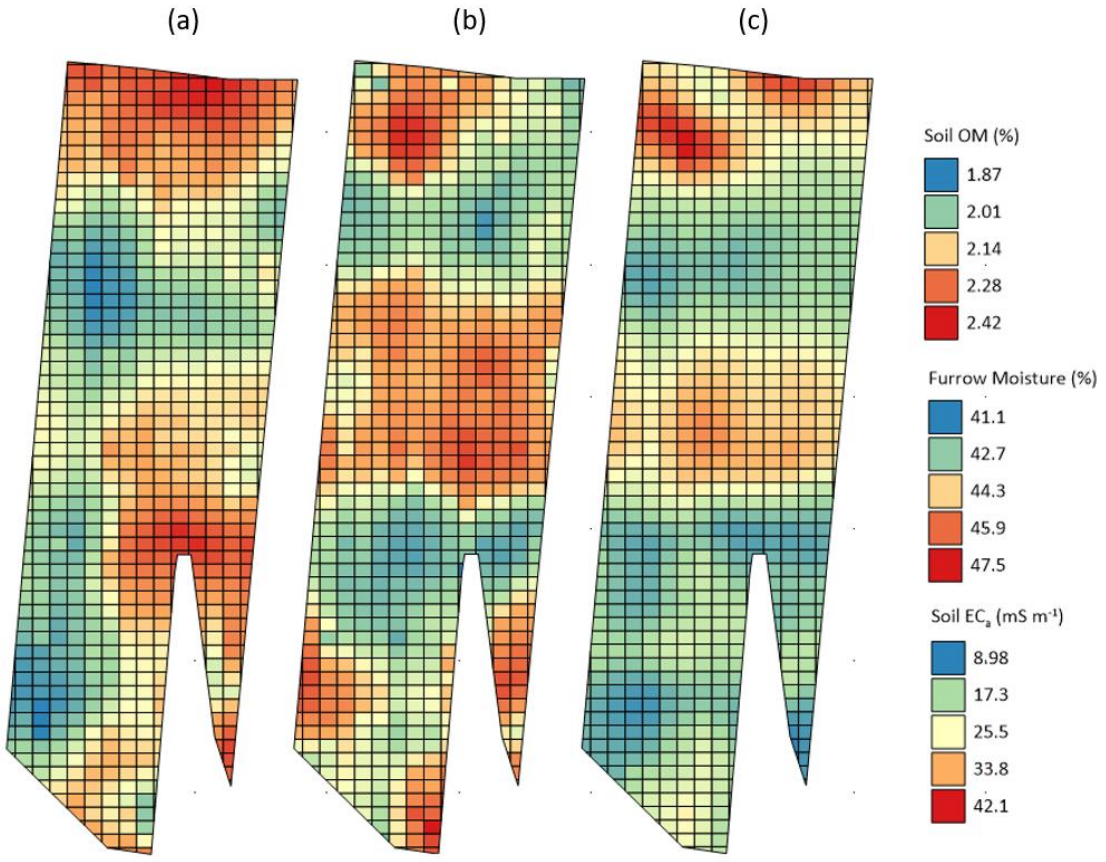

Fig. 3. Interpolated illustrations of Precision Planting SmartFirmer soil organic matter (OM; a), furrow moisture (b), and Veris soil apparent electrical conductivity (0-0.3 m; c) at the study site central Missouri, USA.

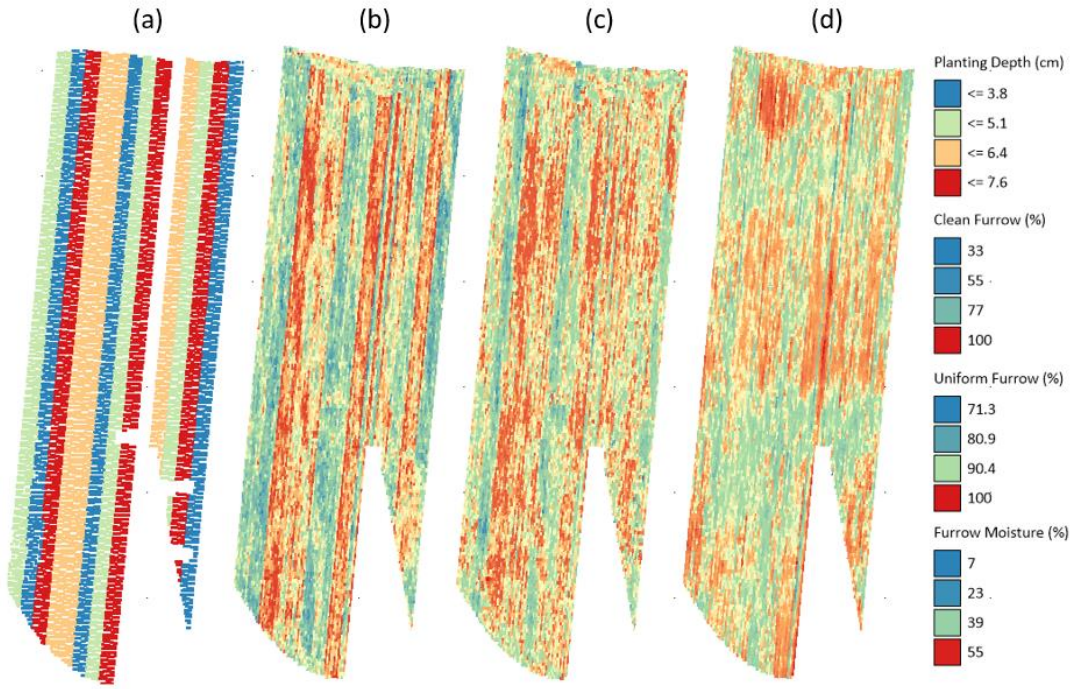

Fig. 4. Row-level illustrations of planting depth (a), Precision Planting SmartFirmer clean furrow (b), uniform furrow (c), and furrow moisture (d) across the study site in central, Missouri, USA.

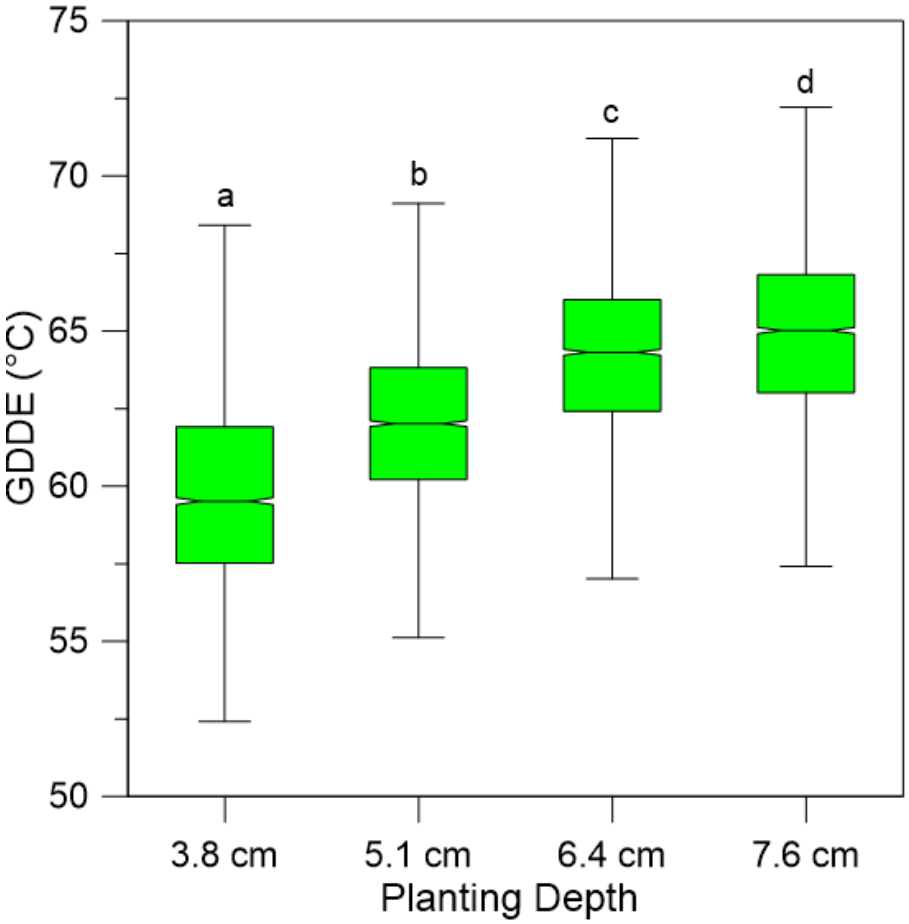

Fig. 5. Field-scale growing degree days from planting to corn emergence (GDDE) by planting depth at the study site in central Missouri, USA.

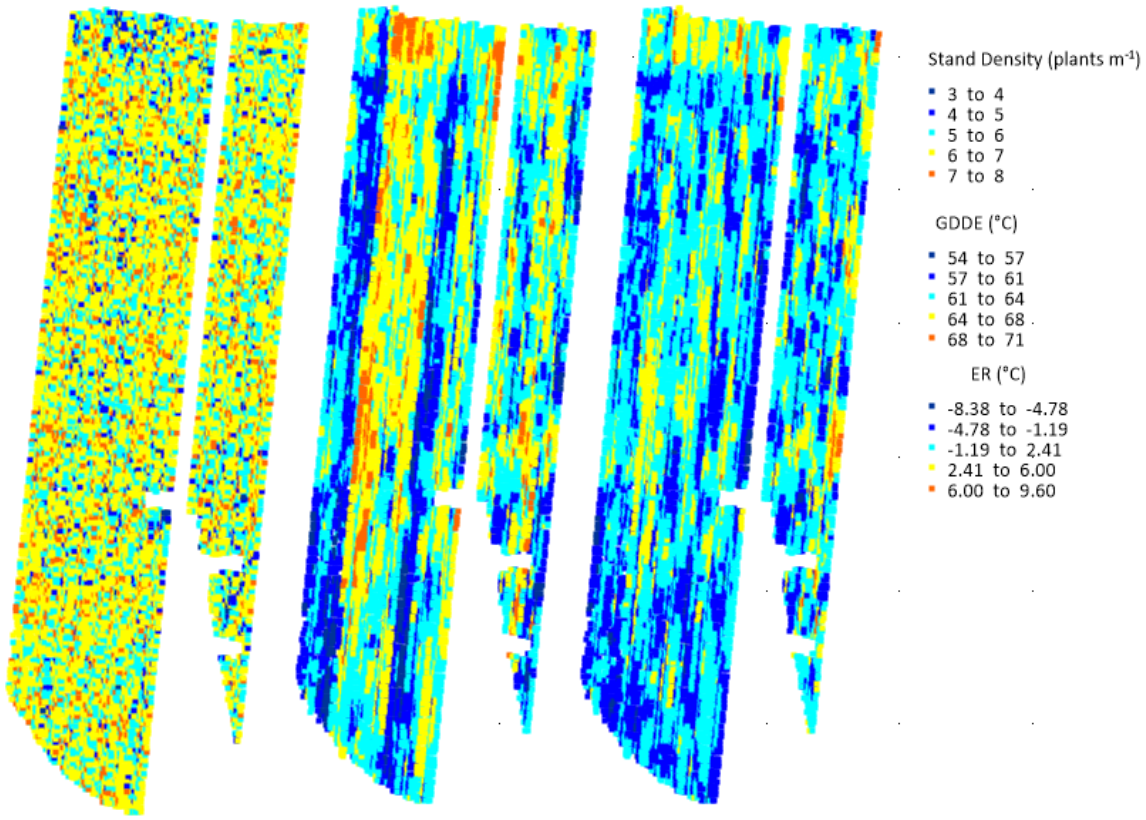

Fig 6. Corn stand density (a), growing degree days from planting to emergence (GDDE; b), and emergence rate (ER; c) estimated through unmanned aerial imagery at the study site in central Missouri, USA.

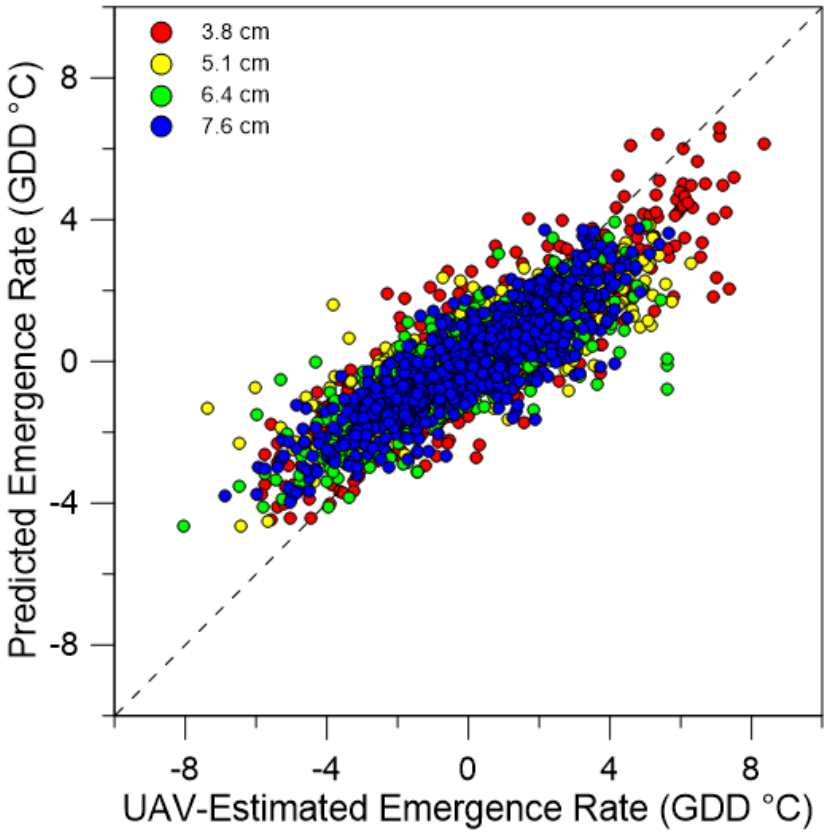

Fig. 7. The UAV-estimated emergence rate in relation to predicted emergence rate for the testing data sets at each planting depth in central Missouri, USA. Model predictions were calculated independently for each planting depth.

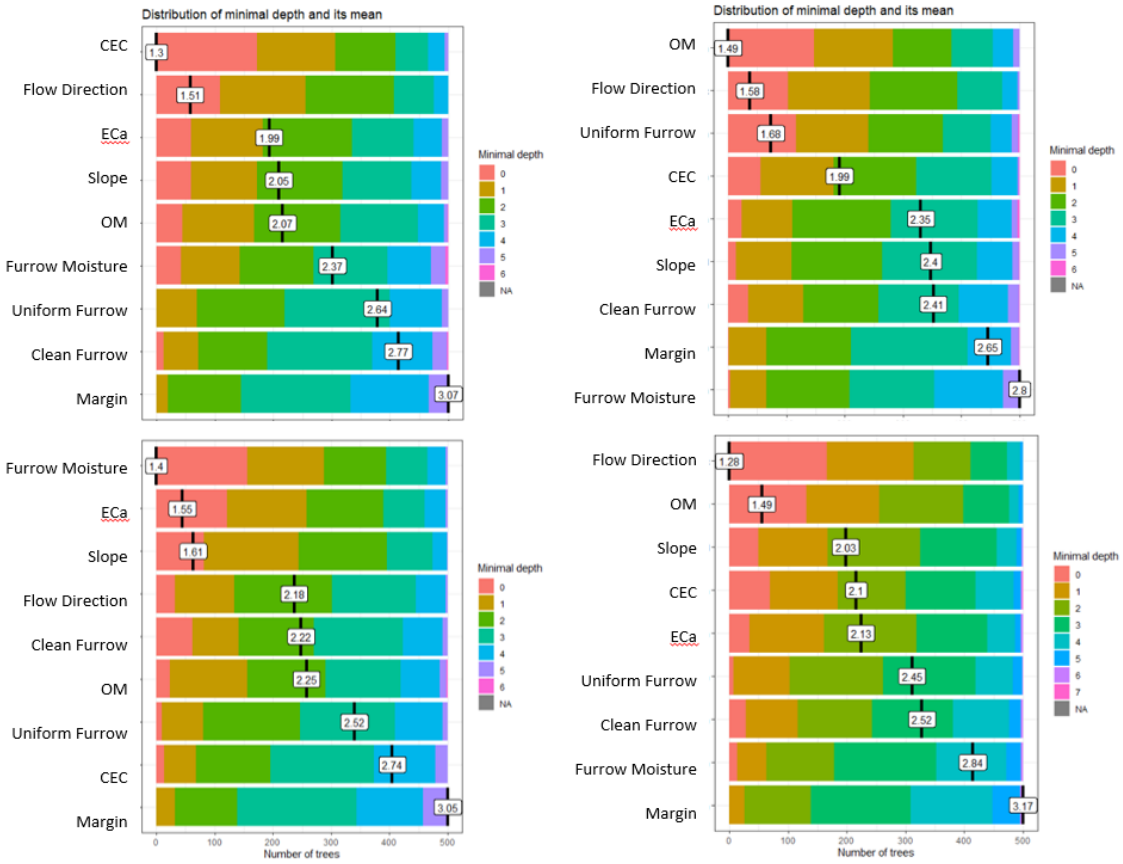

Fig. 8. Distribution of minimal depth for each predictor variable at the 3.8 cm (top left), 5.1 cm (top right), 6.4 cm (bottom left) and 7.6 cm (bottom right) depths in the random forest modeling approaches.

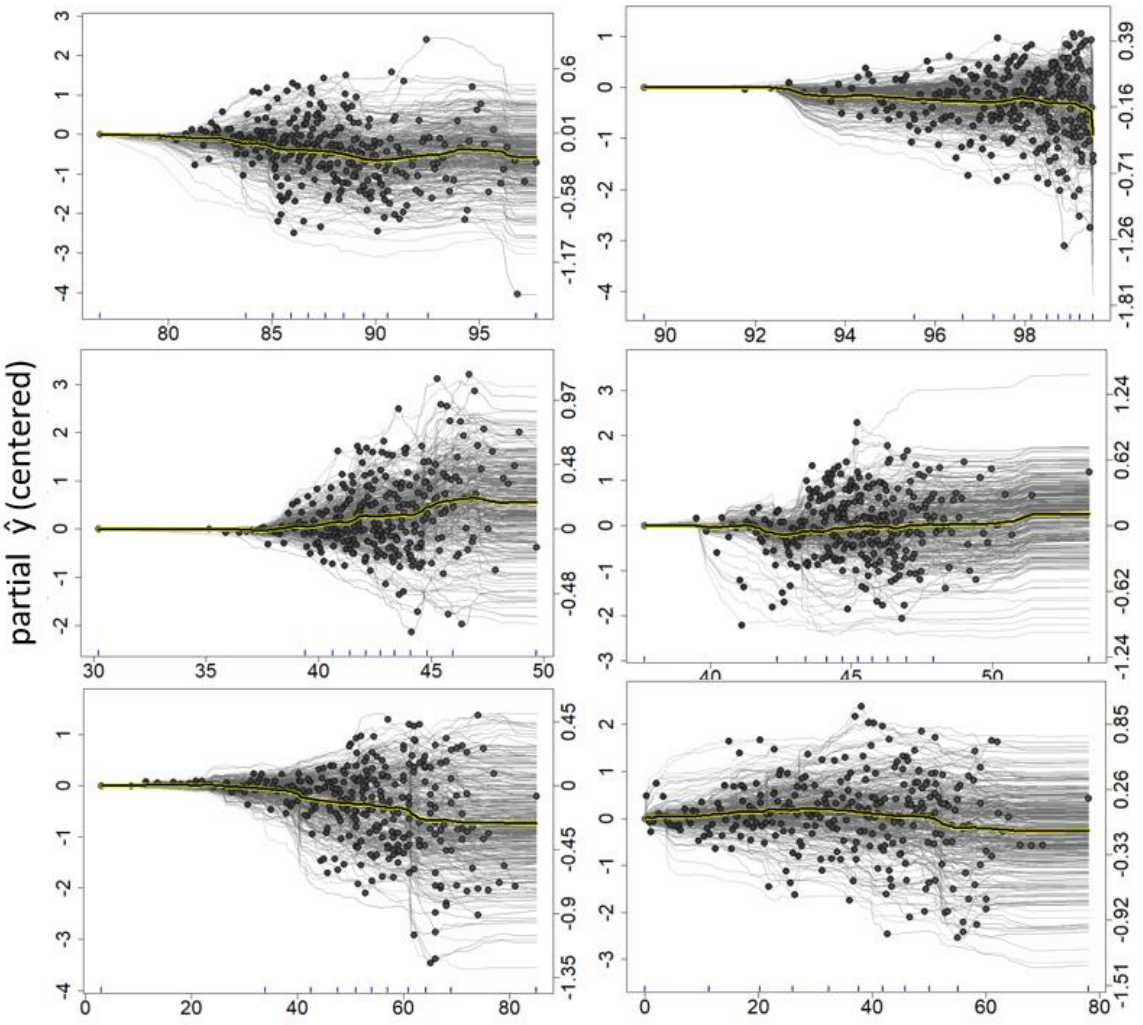

Fig. 9. The individual conditional expectation plot for SmartFirmer clean furrow (%; top), furrow moisture (%; middle), and downforce margin (lb_f; bottom) in the random forest model predicting emergence rate at the 3.8 cm planting depth (left column) and 7.6 cm depth (right column).

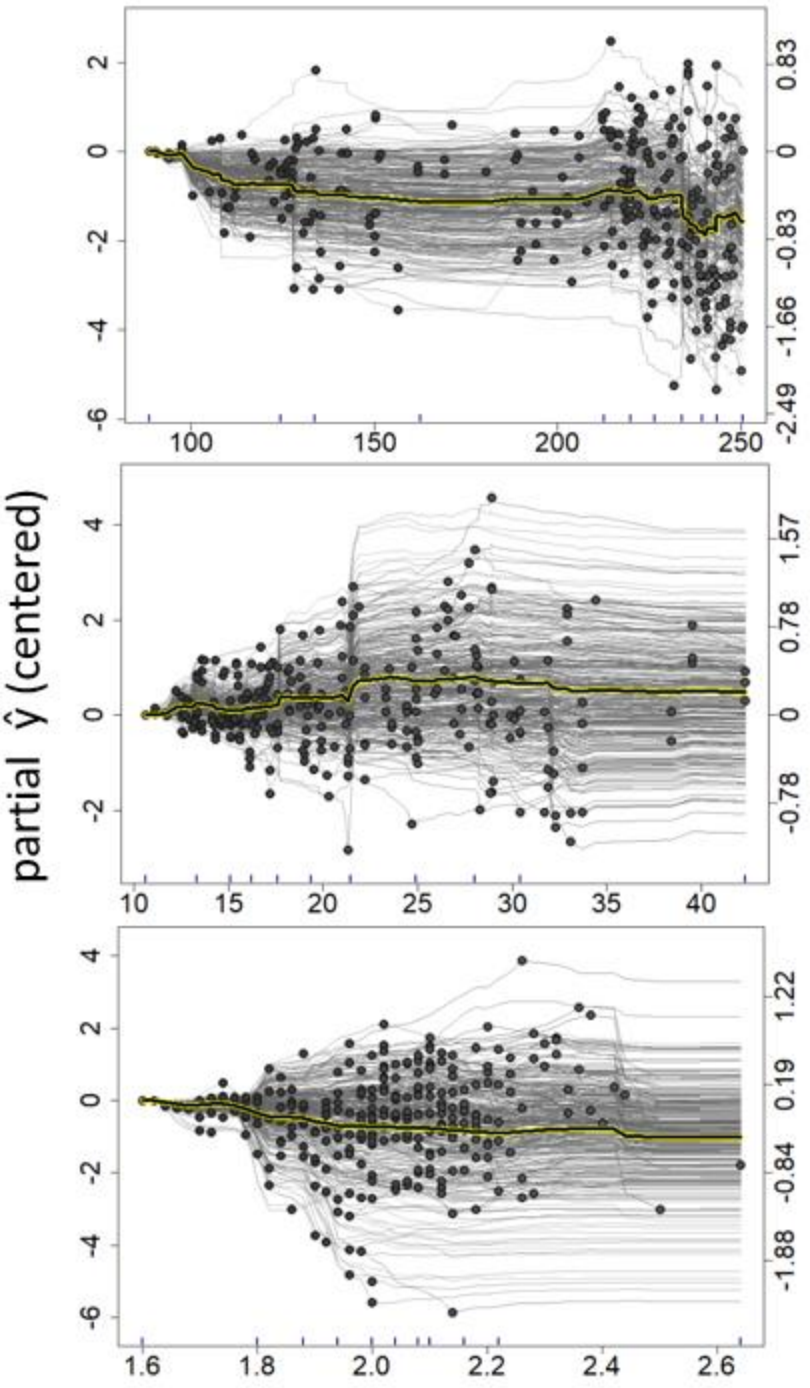

Fig. 10. The individual conditional expectation plot for surface water flow direction (°; top), soil apparent elecetrical conductivity (mS m^{-1}, middle), and SmartFirmer OM (%; bottom) in the random forest model predicting emergence rate at the 7.6 cm planting dept

DISSERTATION CONCLUSIONS

Field-scale research conducted with two commercial sensor systems showed that spatial variability in soil organic matter (OM) could be captured by both systems. However, results showed that inaccuracies with the system employing a "global" calibration occurred due to temporal variations in soil moisture and spatial variability in soil texture. Therefore, my results showed that a field-specific calibration was required for consistent estimates of OM. This outcome highlights the tradeoff between accuracy and the ability to use sensor data for real-time control.

Assessment performed in a controlled environment showed that the commercial sensor system detected general trends in OM from low to high across a wide range of soils. These results aligned with the aforementioned field-scale study. Depending on the application, this performance level may be sufficient, for example for determining relative differences in soil productivity or soil health. However, OM predictions and accuracy were influenced by volumetric water content. Thus, practitioners must realize that estimates could be temporally variable. If more consistent and accurate estimates are required (e.g., for carbon stock monitoring), additional spectral or soil information may be required. This could include full or partial spectra, local calibration samples, and/or publicly available soil information to improve OM prediction.

Results from the planting depth analyses illustrated that planting depth influenced corn emergence parameters, such as stand density and growing degree days from planting to emergence (GDDE). Interestingly, planting at the deepest depth (7.6 cm) had little to no effect on corn stands. This further illustrates the resiliency of corn to emerge from deeper planting depths. Outcomes from the ER analysis showed the potential for

combining multiple spatial data layers, both sensor and terrain-based, to predict corn emergence rate (ER). Factors important for predicting ER varied with depth, but findings showed that a variety of layers were often useful in prediction, including SmartFirmer and DeltaForce metrics, as well as topographic features like surface water flow direction. Therefore, further work is needed to determine whether automated row-unit control could utilize these parameters to adjust in real-time and improve ER, and likely increase emergence uniformity.

Collectively, the work from this dissertation determined:

- Global calibration models of OM will require local information for accurate and consistent implementation due to impacts of factors such as soil texture or water content on spectral features.
- Continuous spectral information in the visible and near infrared spectrum can improve OM estimations across varying soil water contents.
- Topographic features in conjunction with planter-sensor metrics have potential to guide real-time and/or prescriptive management decisions during corn seeding operations.

Further research should be performed to expound upon these findings to determine the maximum utility of commercial proximal soil sensors for row-crop producers.

APPENDIX A:

Supplemental Material for Chapter 2

Fig. 1. Image of Veris iScan attached to a vertical tillage implement.

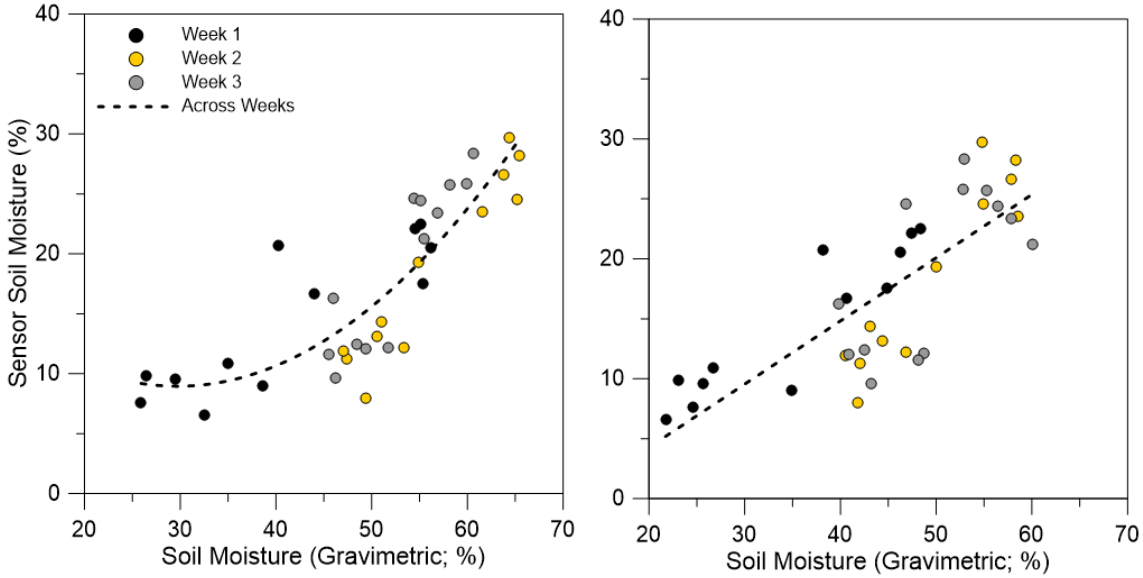

Fig. 2. Soil moisture estimation by the Precision Planting SmartFirmer (left) and the Veris iScan (right) in relation to laboratory measured gravimetric soil moisture.

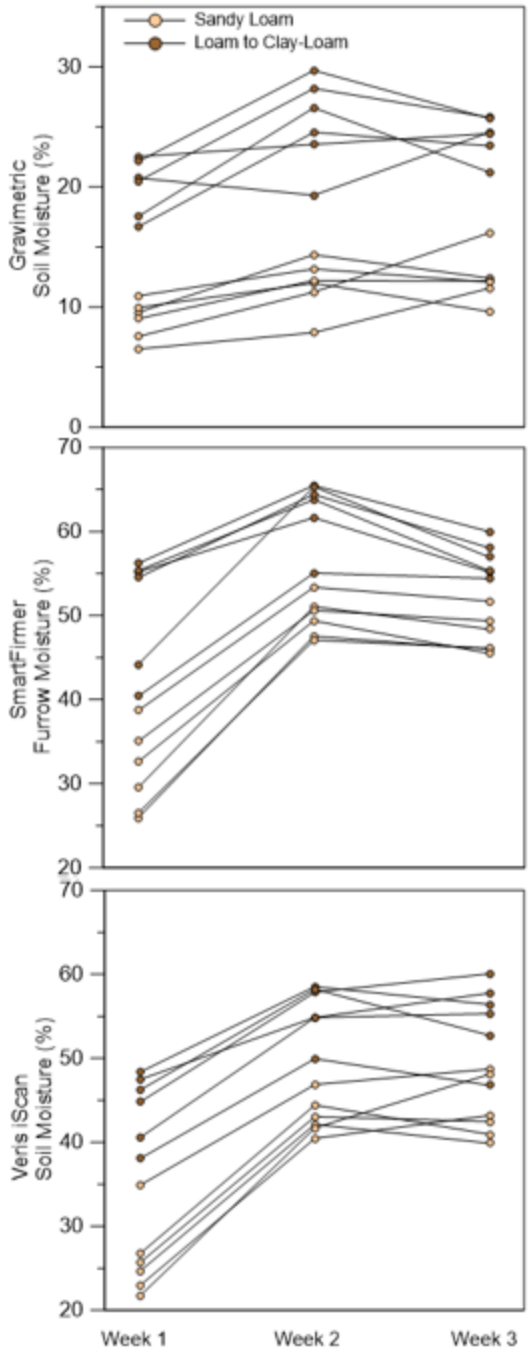

Fig. 3. Laboratory measured gravimetric soil moisture (top), SmartFirmer furrow moisture (center), and Veris iScan soil moisture (bottom) at each of the three sensing dates at the site in Central, MO.

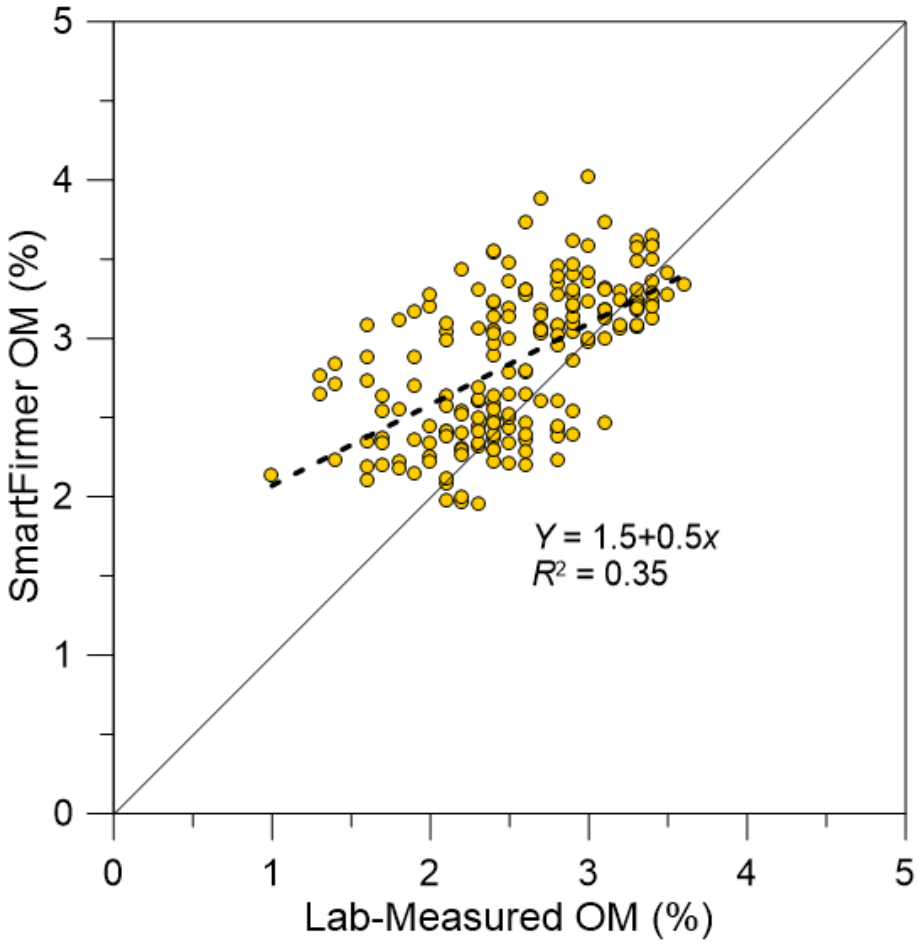

Fig. 4. SmartFirmer organic matter estimation (OM) in relation to laboratory-measured OM (0-15 cm) across 200 ha in west-central Missouri, USA.

APPENDIX B:

Supplemental material for Chapter 3

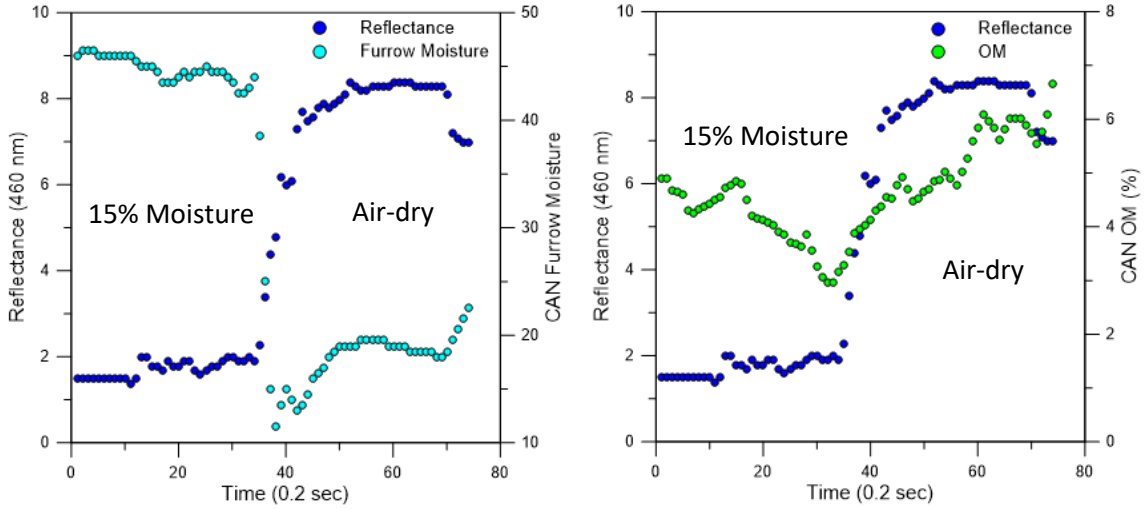

Fig. 1. SmartFirmer reflectance and furrow moisture (left) and reflectance and organic matter (OM; right) response to varying soil moisture levels of a given soil. Results show a clear impact of soil moisture on OM, as well as a smoothing affect present within the system. On the contrary, furrow moisture response was shorter and similar to that of reflectance.

APPENDIX C

Supplemental material for Chapter 4

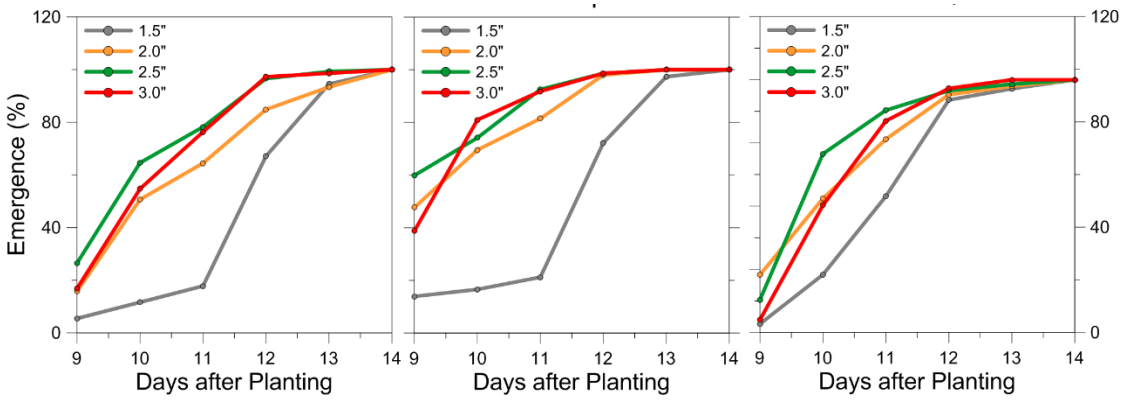

Fig. 1. Corn emergence rate at the summit (left), backslope (center) and footlsope (right) on a claypan soil in 2019 near Columbia, Missouri, USA.

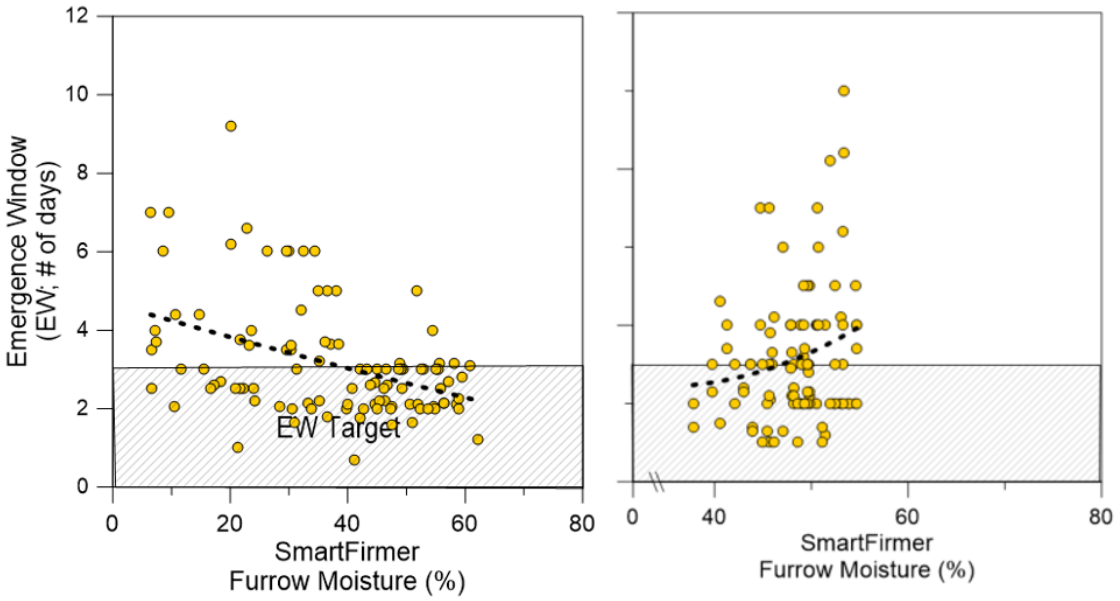

Fig. 2. Emergence window relation to SmartFirmer Furrow Moisture in 2018 (left) and 2019 (right) across riverbottom (alluvial) and upland (claypan) soils.

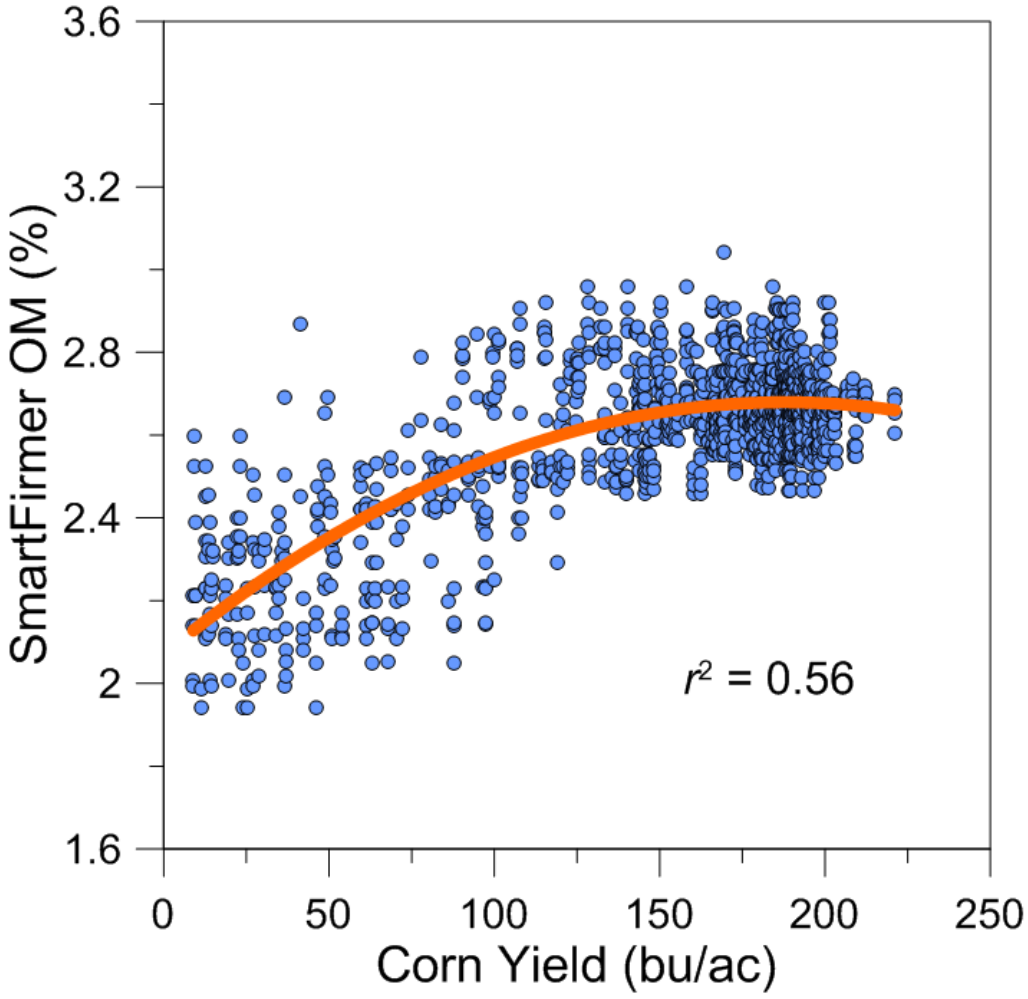

Fig. 3. Corn grain yield response to SmartFirmer OM in 2019 on a claypan soil site in Centralia, Missouri, USA.

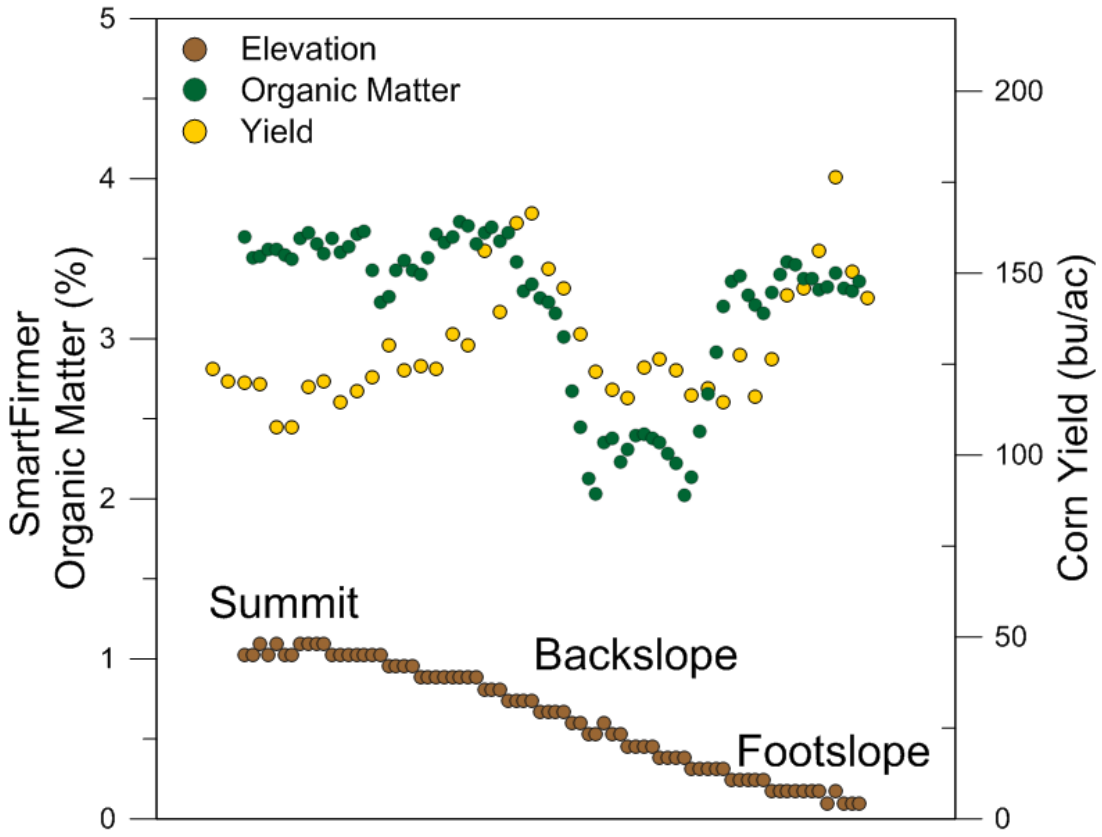

Fig. 4. Transect data of corn grain yield, SmartFirmer organic matter, and elevation across a claypan soil landscape in Centralia, Missouri, USA in 2019.

VITA

Lance S. Conway was born on July 13, 1992 in Washington, MO, USA. He received his Bachelor and Master of Science degrees in Plant Science from the University of Missouri. He then began his pursuit to earn a Doctorate of Philosophy in Soil Science in 2019 under the advisement of Drs. Newell R. Kitchen, Stephen H. Anderson, and Kenneth A. Sudduth.